ADDIS ABABA UNIVERSITY

ADDIS ABABA INSTITUTE OF TECHNOLOGY

SCHOOL OF CIVIL AND ENVIRONMENTAL ENGINEERING

GEODESY AND GEOMATICS PROGRAM

EVALUATION OF SPECTRAL BUILT-UP INDICES FOR IMPERVIOUS SURFACE EXTRACTION USING SENTINEL-2A MSI IMAGERIES: A CASE OF ADDIS ABABA CITY

BY

TSION AYALEW KEBEDE

A Thesis Submitted to the School of Graduate Studies of Addis Ababa University in Partial Fulfillment of the Requirements of the Degree of Master of Science in Geodesy and Geomatics Program (Specialization in Geomatics)

June, 2021

Addis Ababa, Ethiopia

EVALUATION OF SPECTRAL BUILT-UP INDICES FOR IMPERVIOUS SURFACE EXTRACTION USING SENTINEL-2A MSI IMAGERIES: A CASE OF ADDIS ABABA CITY

By

TSION AYALEW KEBEDE GSR/7192/11

Email: tsionayalew16@gmail.com

Approved by the Board of Examiners

ADVISOR	SIGNATURE	DATE
EXTERNAL EXAMINER	SIGNATURE	DATE
INTERNAL EXAMINER	SIGNATURE	DATE
CHAIR PERSON	SIGNATURE	DATE

June, 2021

DECLARATION

I certify that this research work entitled "*Evaluation of Spectral Built-up Indices for Impervious Surface Extraction Using Sentinel-2A MSI Imageries: A Case of Addis Ababa City*" is my own work. The work has not been presented elsewhere for assessment. Where material has been used from other sources, it has been properly acknowledged/referred.

Tsion Ayalew	--------------------------	-----------------------------
Name of Candidate	Signature	Date

As Master research advisor, I hereby certify that I have read and evaluated this MSc thesis prepared under my guidance.

Dr. Binyam Tesfaw	--------------------------	-----------------------------
Advisor	Signature	Date

ACKNOWLEDGEMENTS

First of all, thanks to Almighty God for His unlimited blessings and for giving me the strength to complete this study.

I would like to express my heartful gratitude to my advisor, Binyam Tesfaw (Ph.D.) for his encouragement, great help, considerable effort, and continuous scientific directing along with this study**.** Your office door is always open to me and I appreciate you spending your valuable time meeting with me. Every meeting I spent with you is an improvement for my thesis.

I would like to acknowledge the Regional Center for Mapping of Resources for Development (RCMRD/GMES) for awarding me this opportunity to continue my MSc, and for financial support for the entire study period. Also, I wish to acknowledge the help provided by Ethiopian Geospatial Information Institute (GII).

Finally, my most appreciations are to my parents and friends for their encouragement and support.

TABLE OF CONTENTS

LIST OF FIGURES

LIST OF TABLES

LIST ABBREVIATIONS

ANN	Artificial Neural Network
ABEI	Automated Built-up Extraction Index
AVIRIS	Airborne Visible/Infrared Imaging Spectrometer
BAEM	Built-up Area Extraction Method
BRBA	Band Ratio for Built-up Area
BCI	Biophysical Composition Index
CBI	Combinational Build-up Index
CSI	Combinational Shadow Index
CSA	Central Statistical Agency
DFPS	Double Window Flexible Pace Search
EO	Earth Observation
ECA	Economic Commission for Africa
EBBI	Enhanced Built-Up and Bareness Index
ESA	European Space Agency
ETM	Enhance Thematic Mapper
GIS	Geographic Information Systems
GPS	Global Position System
ISA	Impervious surface area
ISE	Impervious Surface Extraction
IBI	Index Based Built-up Index
LSMA	Linear Spectral Mixture Analysis
LULC	Land Use Land Cover
MESMA	Multiple Endmember Spectral Mixture Analysis
MIR	Mid Infrared
MBI	Modified Built-up Index
MNDWI	Modified Normalized Difference Water Index
MSI	Multispectral Instrument
NDVI	Normalized Difference Vegetation Index
NBI	New Built-up Index

NIR	Near Infrared
NBAI	Normalized Built-up Area Index
NDBai	Normalized Difference Bareness Index
NDBI	Normalized Difference Built-up Index
NDISI	Normalized Difference Impervious Surface Index
NDTI	Normalized Difference Tillage Index
NRUI	Normalized Ratio Urban Index
OLI	Operational Land Imager
OAU	Organization of African Unity
PAN	Panchromatic
PCA	Principal Component Analysis
RF	Random Forest
RS	Remote Sensing
RUI	Ratio Urban Index
ROI	Region of Interest
RMSE	Root Mean Square Error
RO	Runoff
SRS	Satellite Remote Sensing
SEI	Shadow Enhancement Index
SI	Spectral Index
SMA	Spectral Mixture Analysis
SAVI	Soil adjusted vegetation index
SDI	Spectral Discrimination Index
SVM	Support Vector Machine
SWIR	Short Wave Infrared
SAR	Synthetic Aperture Radar
TM	Thematic Mapper
TIRS	Thermal Infrared Sensor
UI	Urban Index
USGS	United States Geological Survey
WGS	World Geodetic System

ABSTRACT

An urban area extraction with a high degree of accuracy is important for a variety of applications, especially urban planning, natural resource management, and disaster prediction. In recent years, extraction of an impervious surface using spectral built-up indices has been extensively explored. However, a comprehensive evaluation of various built-up indices from high-resolution satellite images is still lacking. Hence, this study examines the performance of seven spectral built-up indices in the classification and change detection of impervious surfaces using sentinel-2A MSI imageries in Addis Ababa city. It includes Built-up Area Extraction Index (BAEI), Band Ratio for Built-up Area (BRBA), Modified Built-up Index (MBI), Normalized Built-up Area Index (NBAI), New Built-up Index (NBI), Normalized Difference Built-up Index (NDBI), and Urban Index (UI). All the built-up indices maps were classified into built-up and non-built-up areas and evaluated based on histogram overlap and statistical methods, namely spectral discrimination index (SDI). Simultaneously, a machine learning method called support vector machine (SVM) was employed to classify the imageries into five classes: bare land, built-up, forest, vegetation, and water bodies. The finding of the study indicated that NBAI, NBI, and NDBI have the highest SDI value (1.24, 1.23, and 1.54), (1.06, 1.08, and 1.23), and (1.16, 1.1, and 1.26) for the years 2016, 2018, and 2020, respectively. However, the other spectral built-up indices show unsatisfactory results for the study area. The LULC changes between 2016 and 2020 showed that the built-up area, bare land, and water bodies were increased by 9,084.5 ha, 813 ha, and 2 ha whereas vegetation and forest areas were declined by 9,279.3 ha and 620.2 ha respectively. According to this study, NBAI, NBI, and NDBI were more robust built-up indices with kappa coefficient, (90%, 87%, and 0.81%), (86%, 85%, and 80%) and (92%, 93%, and 86%) for the years 2016, 2018, and 2020, respectively. Also, the overall classification accuracy using SVM is 81%, 86%, and 82% for 2016, 2018, and 2020, respectively and it reveals that this algorism has potential in LULC classification using high-resolution satellite images. Therefore, this study concludes spectral built-up indices show a promising result in the extraction of impervious surfaces.

Keywords: Impervious Surface; Machine Learning Algorithms; Sentinel-2A Imagery; Spectral Built-up Indices; Spectral Discrimination Index; Support Vector Machine

CHAPTER ONE

1. INTRODUCTION

1.1 Background

Over the past few decades, the fast growth of cities has been taking place at a rapid pace around the world (Valdiviezo-N et al., 2018). This Speedy development of building density affects many-dimensional of today's world and increases the interest for different research communities around the globe (Bramhe et al., 2018). In general, Built-up area refers to the regions which are impervious and they are defined as those anthropogenic features which water cannot infiltrate to reach the soil, such as concrete buildings, roads, and parking lots (Sun et al., 2016).

These urban areas are heterogeneous in their spectral characteristics and significant spectral confusion between land cover classes and as a result reduce mapping accuracy (Sinha & Verma, 2016). Extraction of built-up areas has been applied to characterize and quantify impervious surfaces using either ground measurements or remotely sensed data (Weng, 2012a). Each technique has its strength and limitation. Field measurement through GPS can provide reliable information on impervious surfaces, however, it is expensive, labor-intensive, time-consuming, and usually difficult to be applied to large-area assessment (Sun et al., 2016).

Since the late 1990s, the number of remote-sensing satellites has greatly increased and it has triggered numerous efforts to compare the data obtained from the different sensor systems (Xu et al., 2013). Various remotely sensed data with different spatial resolution and spectral values on the land use classes can be applied to map built-up areas and evaluate their dynamics (Ghosh et al., 2018). However, urban land-cover mapping, especially impervious surfaces with high accuracy is still a dilemma (Sun et al., 2016). Pixels in satellite images usually contain mixtures of several land cover types with a variety of spectral information.

Generally, built-up extraction methods can be categorized into three generic groups, namely (i) Spectral Unmixing techniques (Pandey & Tiwari, 2020), (ii) Machine learning algorisms (Mohapatra & Wu, 2007; Lu & Weng, 2009; Salehi et al., 2012; Drzewiecki, 2016; Gong & Wu, 2014), and (iii) Direct segmentation of the imagery through spectral index (SI) methods (Pandey & Tiwari, 2020).

Index-based methods are designed based on spectral bands where specific land covers present their highest and lowest reflectance values among a multispectral dataset (Valdiviezo-N et al., 2018). When compared with per-pixel and sub-pixel image analyses, spectral indices have apparent advantages due to their easy implementation and convenience in practical applications (Deng & Wu, 2012; Sun et al., 2016). Before the launch of the ESA's Sentinel missions, high spatial resolution imagery had been expensive and challenging to access (Valdiviezo-N et al., 2018). These days, the short revisit time of both Sentinel 2A and 2B satellites and the free data availability make them important tools to support urban built-up monitoring. ESA launches these two satellites; namely sentinel-2A and sentinel-2B on 23 June 2015 and on 7 March 2017 respectively.

To quickly and accurately map impervious surfaces from satellite imageries, earlier studies have put forward various spectral built-up indices (Xi et al., 2019). However, despite the continuous development of various spectral built-up indices for the rapid and accurate extraction of impervious surfaces from high-resolution satellite imageries, a comprehensive comparison between these indices as applied to high-resolution satellite imageries is still lacking (Estoque & Murayama, 2015a). Therefore, this study aims to evaluate various spectral built-up indices that have been used previously using high-resolution sentinel 2A Multispectral Instrument (MSI) imagery for impervious surface extraction in Addis Ababa city using time series data. The mapping results have been matched with different remotely sensed indices to ascertain the built-up areas and also provide a clue to determine a more accurate remote sensing index for built-up area growth patterns in the selected study area.

1.2 Problem Statement

Urban areas are dominated by built-up lands with impervious surfaces such as building roofs, paved roads, parking lots, etc. (Xu, 2010). The phenomenon of urban spatial expansion always needs accurate data on urban built-up areas such as the size, shape, and spatial context (Sinha & Verma, 2016). The process of urbanization affects developing countries much more rapidly. Therefore, the need to be able to monitor urbanization based on satellite imagery is quite important (Stathakis et al., 2012). However, extraction of such built-up regions is still challenging due to spatial, spectral, and temporal variability (Sun et al., 2016). Additionally, the high degree intricacy of the spectral distribution between different land use, especially, with the bare land challenges in terms of the pixel amalgamations in areas with heterogeneous substances (Ghosh et al., 2018).

To assist urban built-up area mapping and to evaluate their dynamics, several techniques have been formulated including Spectral Mixture Analysis (SMA), machine learning algorisms, and indices-based classification. SMA is based on an optimal set of reference endmembers, however, this technique is difficult to identify the pure endmembers or the most representative endmembers in heterogeneous urban areas. One alternative to overcome the above mentioned problem is to perform machine learning algorithms. Machine learning algorithms are run by manually selected training samples and they are affected directly by the location, size, and representativeness of training samples (Sun et al., 2016). Although, classification-based algorism may not produce satisfactory accuracy, normally less than 80%, due to spectral confusion of the heterogeneous built-up land class (H. Xu, 2008).

Unlike the above approaches, spectral index-based approaches for the extraction of built-up surfaces have shown some remarkable results in terms of ease of implementation, less execution time, memory efficiency, simplicity, and independence with the training samples (Estoque & Murayama, 2015b; Kawamura, 1996; Sun et al., 2016; Zha et al., 2003). Though, there is problem in extracting the geometry, location, spatial pattern, and magnitude of impervious surfaces and the perviousness–imperviousness ratio due to large spectral similarity and confusion between heterogeneous built-up surfaces and bare soil. Also, quantitative comparison between these spectral built-up indices using different statistical approaches is a quite challenging task. Hence, this study was aimed to evaluate several spectral built-up indices for the rapid and accurate extraction of impervious surfaces from high-resolution satellite imageries, especially using Sentinel-2A MSI imagery. This confusion may reduce to the maximum extent by using a high spatial resolution sentinel 2A MSI image. The use of interferometric synthetic aperture radar (SAR) data provides valuable information in determining the physical characteristics of the urban area through different analysis methods.

1.3 Research Objective

1.3.1 General objective

The general objective of this study is evaluation of spectral built-up indices effectiveness for impervious surfaces extraction using Sentinel-2A MSI imageries in Addis Ababa city.

1.3.2 Specific objectives

The specific objectives of this study is: -

- To show the spectral response curve in between various types of spectral built-up indices.
- To evaluate various spectral built-up indices effectiveness for impervious surface extraction.
- To identify the change in land use land cover for the years 2016, 2018, and 2020 using Sentinel-2A MSI satellite images.

1.4 Research Questions

The research questions, which the thesis aims to address, includes:

- What are the spectral responses of different built-up indices in time series data?
- Which type of indices can effectively extract the impervious surface with Sentinel-2A MSI imageries?
- To what extent does the urban impervious surface change in the years 2016, 2018, and 2020?

1.5 Significance of the Research

The application of remote sensing and spatial information technologies using electromagnetic waves from various parts of the energy spectrum can acutely reflect the physical condition of urban area changes often in little time, thus can be used for built-up area extraction timely and accurately. The spatial distribution and temporal dynamics of built-up land play a significant role in ecosystem services and global environment change. Thus, previous-impervious surface ratio information is required in various applications of land use planning and management. This study focused on cost-effective methods to support asset management through enabling the urban planner and decision-maker to gain a better understanding of the urban built-up area and to make more informed decisions on future planning and resource management. In addition to this, the study focuses on cost-effective remote sensing satellite imagery to evaluate different spectral built-up indices using Sentinel 2A MSI imageries for impervious surface extraction, and also it gives the basis for further study in the future.

1.6 Scope of the Study

In the light of current urban impervious surface extraction practices, this study aims to evaluate the different spectral built-up indices based on the capability of remote sensing satellite technologies, specifically the use of high-resolution sentinel-2A MSI imagery, which has wider implications and advantage in this area. In advance, Sentinel-2A satellite data for the use of built-up extraction, which is a tangible breakthrough in remote sensing technology, allowing for evaluation with high accuracy. The Scope of this research is to evaluate the capacity of different spectral indices for the extraction of the impervious surfaces using Sentinel-2A MSI imageries in Addis Ababa city for the years 2016, 2018, and 2020.

1.7 Limitation of the Study

This study has encountered certain limitations. One of the limitations was the lack of aerial photographs for 2016 and 2018, which enables to validate the result with high accuracy than google earth's image. Also, this study does not include the effectiveness of such methods in different types of sensors like IKONOS and QUICKBIRD imageries due to time and cost limitations. However, all recent efforts are briefly included in the literature review section.

1.8 Organization of Thesis

This thesis is organized into six chapters and a brief description of the chapters is presented below to get a summary of the general composition of the thesis.

Chapter 1 - Introduction:	A general overview of the proposed topic, background information, statements of the problem, objectives, research questions, scope, significances of the study, limitations are presented.
Chapter 2 - Literature Review:	This section includes a theoretical framework and background which include the concept behind the spectral built-up indices and evaluation based on a different approach.
Chapter 3 - Research Design and Methods:	Description of the study area, data and software packages, image processing techniques, classification, various indices computation methods, and accuracy assessment is included to answer the questions raised in the statement of the problem
Chapter 4 – Results:	This section includes the result of the present study.
Chapter 5 – Discussion of Results:	In this chapter discussion and justification based on the finding of the research output are presented.
Chapter 6 - Conclusion and Recommendations:	Based on the result, this thesis concludes and recommends for further studies.

CHAPTER TWO

2. LITERATURE REVIEW

2.1 An Overview of Impervious Surface Extraction

Rapid population agglomeration around the world has given to many environmental consequences which need urgent attention. According to (United Nations, 2018) urbanization is a complex socio-economic process that transforms the built environment, converting formerly rural into urban settlements, while also shifting the spatial distribution of a population from rural to urban areas. Globally over 1 million urban inhabitants are added each week to the world (Kawamura, 1996) and the share of the urban population has risen considerably from 33.61% to 55.27% during 1960–2018 (United Nations, 2018). Currently, over 50% of the population lives in urban areas. By 2045, the world's urban population will increase by 1.5 times to 6 billion. Within this increment of the urban population, new urban infrastructures that provide environmental and social service are required for sustainable development as well as induces increasing needs for lodging, in road networks, services (Bouzekri et al., 2015). Therefore, City leaders must move quickly to plan for growth and provide the basic services, infrastructure, and affordable housing their expanding populations need (United Nations, 2018).

The urban area can be defined as a collection of contiguous urban lands, such as urban settlements, industrial land, commercial land, open space, water bodies, and others (Liu et al., 2014). More recently, impervious surface or built-up area has occurred not only as an indicator of the degree of urbanization, but also a major indicator of environmental quality (Weng, 2012b). As stated by (Carlson & Traci Arthur, 2000) Impervious surface area (ISA) constitutes the fraction of a pixel from and they are the entirety of impermeable surfaces for which the surface can neither evaporate water nor permit rainwater to penetrate such as buildings, roads, driveways, sidewalks, parking lots, rooftops, and so on. The amount of impervious cover would directly be related to the volume, duration, and intensity of urban runoff and alter the hydrologic response of streams and rivers to precipitation and snowmelt events (Weng, 2001).

An increment in the extent of the impervious cover has its effect on watersheds and it may result in an overall decrease of groundwater recharge and base flow and an increase in stormflow and flood frequency (Pellerin, 2004). In addition to this degree and spatial incidence of impervious surfaces may significantly influence urban climate by altering sensible and latent heat fluxes within the urban canopy and boundary layers (Yang et al., 2003).

Urban materials, such as concrete, asphalt, and asbestos can absorb more solar energy, which is then released as heat. The evolution of cities in time and space can bring about progress to the world, but also it results in negative aspects such as the urban heat island phenomenon (Hua et al., 2020; Xu, 2010), surface runoff (RO) change (Carlson & Traci Arthur, 2000), environmental degradation (Thapa & Murayama, 2011) and increased pressure on natural resources (Xu, 2007) which subsidize seriously to global warming (Xu, 2008). As a consequence, a strong positive correlation is found when impervious surface values are plotted against the temperature of the environment (Kawakubo et al., 2019).

Due to these major environmental impacts, considering the extreme influence of urban areas on the surrounding in terms of energy, mass, and resource fluxes combined with the overall growth of the world's population and their Spatio-temporal effects is necessary. Therefore, mapping and estimating impervious surfaces is crucial to a range of issues and themes in environmental science central to global environmental change and human-environment interactions (Weng, 2012a). Generally, the information on impervious surfaces is valuable not only for urban planning and building infrastructure but also for water quality assessment, runoff estimation, urban climate management, and sustainable urban development (Bauer et al., 2007).

2.2 Earlier Impervious Surface Extraction Approaches

Many techniques have been applied to determine the extent and quantify an urban built-up area using either ground measurements or remotely sensed data. Ground measurement using GPS can provide reliable information on impervious surface extraction (Weng, 2012a). However, it is quite expensive, time-consuming, labor-intensive, and usually difficult to be applied to large-area assessments (Sun et al., 2016). Later, aerial photographs have also been used for mapping imperviousness due to their high spatial resolution using manual digitizing techniques and computer-assisted digital processing.

Through manual interpretation, analog photographs are visually interpreted and the results are marked directly on the photographs or on tracing paper placed over them (Zha et al., 2003). Yet, this method has become more severely involved with automation methods such as scanning and the use of feature extraction algorithms (Weng, 2012b). In recent decades, the use of satellite data has replaced the traditional field survey methods for identification of the urban built-up land due to advancements in remote sensing technology and geographic information systems (GIS) (Vigneshwaran & Kumar, 2018). Still, visual interpretation or manual digitizing techniques are used to measure the range of ISA.

2.3 Background to Remote Sensing Technology

The Earth's surface is not homogeneous at all, rather it contains variant objects like built-up, an agricultural area, forest, bare land, water bodies, and others. Remote sensing is a non-destructive technology, which is used to collect information on the earth's surface without contact. The information is sensed and gathered in the form of electromagnetic radiations redirected from the earth's surface. The reflected radiation is formed when the incident radiation and surface elements interact by involving several parameters, such as energy source of luminance, radiation through atmosphere, interaction with target elements, receiving energy by sensor, processing, analysis. The energy source which can illuminate radiations towards the target can be either solar or synthetic aperture radar systems (Schueler, 1987).

The electromagnetic energy passed through the atmosphere and may interact with atmospheric particles. The heterogeneous earth surface interacts with incident radiations and results in reflection, refraction, and absorption of energy in various manners. The reflected part of the energy is sensed by high-definition sensors in the optical or sometimes infrared or microwave bands of the electromagnetic spectrum. The sensed energy is then recorded and transmitted electronically to a processing station which is stored in the form of imagery data for further analysis (Schueler, 1987).

Remote sensing information consist of (a) spectral information is the number and dimension (size) of wavelength intervals (referred to as bands or channels) in the electromagnetic spectrum reflected, emitted, or back-scattered in specific bands or frequencies and the chemical, biological, and physical characteristics of the phenomena under investigation to which a remote sensing instrument is sensitive. The spectral resolution refers to the capability to identify two land cover classes based on their spectral signature. The spectral resolution, therefore, sets the upper limit of the performance of a classifier using spectral information only. It depends on the number and types of spectra measured, the signal-to-noise ratio, and the radiometric precision (pixel depth) of the sensors.

The spectral resolution is quantified based on the separability of an object belonging to a class of interest, the foreground, from a specific background in the spectral domain (Radoux et al., 2016). (b) Spatial Information is a measure of the smallest angular or linear separation between two objects that can be resolved by the remote sensing system. Pixels are normally represented on computer screens and in hard-copy images as rectangles with length and width. If the spatial information about the location of each pixel (x, y) in the image matrix is available, it is also possible to examine the spatial relationship between a pixel and its neighbors. Therefore, the amount of spatial autocorrelation and other spatial geostatistical measurements can be determined based on the spatial information inherent in the imagery. (c) Temporal Information is one of the valuable things about remote sensing science in that it obtains a record of earth landscapes at a unique moment in time.

Multiple records of the same landscape obtained through time can be used to identify processes at work and to make predictions (Jensen, 1996). (d) Radiometric resolution is defined as the sensitivity of a remote sensing detector to differences in signal strength as it records the radiant flux reflected, emitted, or back-scattered from the terrain. It delineates the number of just discriminable signal levels. Therefore, radiometric resolution can have a significant impact on our ability to measure the properties of scene objects. Radiometric resolution is sometimes referred to as the level of quantization. High radiometric resolution generally increases the probability that phenomena will be remotely sensed more accurately (Jensen, 2005).

In general, remote sensing is an attractive source that provides a thematic map-like representation of the earth's surface that is spatially continuous and highly consistent, as well as available at a range of spatial and temporal scales (Foody, 2002). Using satellite data and repeatability of acquisition, analysis of multi-temporal images has broadened the applications of remote sensing to include detection of change in the earth's surface and monitoring dynamics phenomena (Bouzekri et al., 2015). A large number of remote-sensing satellites provide us with continuous remote-sensing imageries for the applications of land use, marine, security, and climate, etc. (XI et al., 2019).

2.4 Remote Sensing Technology for Impervious Surface Extraction

Remote sensing (RS) data, especially from satellite remote sensing (SRS) systems, is an invaluable resource for mapping built-up areas for several reasons (Bhatti & Tripathi, 2014). First, it provides a synoptic view and repeats coverage of a large geographic area (He et al., 2010), which is not possible through ground surveys and it have been applied extensively to analyze urban environments (Deng & Wu, 2012). Secondly, utilizing RS data for urban studies is the availability of historical archives that can help in mapping and understanding urban sprawl over time (H. Xu, 2008). Knowledge about the pattern and extent of built-up lands is important for environmental resources management, risk assessment and disaster management, and landscape and urban development planning. In general urban remote sensing has recently fascinated unprecedented attention (Estoque & Murayama, 2015a).

Remotely sensed data, including both airborne and spaceborne sensor data, vary in spatial, radiometric, spectral, and temporal resolutions are available in the present time. Remote sensing imagery with the high temporal resolution has been applied for monitoring the urban environment. Extraction of urban built-up areas such as the size, shape, and spatial context needs a technique to quickly and timely reveal the information. Fortunately, satellite remote sensing technology offers considerable promise to meet this requirement (Lu & Weng, 2007). The study of urban spatial expansion using several spatial, spectral, and contextual-based algorithms is generated on different remote sensing data. This data helps researchers investigate various urban phenomena in detail, extending their understanding beyond the rather limited knowledge of urban size and shape provided by traditional paper map sources (Weng & Pu, 2013).

In remote sensing data, spatial resolution is one of the basic to be considered, in which the level of spatial detail can be observed on the earth's surface. As the spatial resolution increase, the mixed-pixel problem has greatly reduced which provide a greater potential to extract much more detailed information on urban impervious structures than medium or coarse spatial resolution data. However, there is some problem related with high spatial resolution. The first one is the shadows caused by objects such as tall buildings, trees, and also topography and the high spectral variation within the same land-cover class. The second one is due to purchasing cost (much more expensive) and requires much more time to implement data analysis than medium spatial resolution images. To reduce this problem, select suitable classifiers to effectively handle them and increased spectral variation is common with the high degree of spectral heterogeneity in complex landscapes (Lu & Weng, 2007).

Spatial information may be used in different ways, such as in contextual-based or object-oriented classification approaches, or classifications with textures (Lu & Weng, 2007). Before 2000, there is a limitation in remote sensing research especially in the impervious surface due to lack of high spatial resolution (less than 10 m). The medium spatial resolution images range from (10–100 m), such as Landsat and SPOT, were not readily available and were expensive (Weng, 2012a).

Nowadays, Sentinel 2A MSI imagery which is a high spatial resolution (10m) provides a valuable contribution in urban impervious surface extraction (Copernicus, 2018). Fine spatial resolution data comprise rich spatial information, given that a greater potential to extract much more detailed information such as cartographic features (buildings and roads), and metric information with stereo-images (height and area) (Weng, 2012a).

The spectral resolution is the fundamental principle that determines the accuracy of image classification. The spectral features include the number of spectral bands, spectral coverage, and spectral resolution (or bandwidth). Remote sensing satellite has the different number of spectral bands used for image classification and its range from a limited number of multispectral bands (e.g. SPOT data and Landsat TM with four and seven bands respectively), to a medium number of multispectral bands (e.g. ASTER with 14 bands, Sentinel 2A MSI imagery with 13 bands and MODIS with 36 bands), and hyperspectral data (e.g. AVIRIS and EO-1 Hyperion images with 224 bands) (Copernicus, 2018; Lu & Weng, 2007). To get detailed information and to extract ground information with high classification accuracy, a large number of the spectral band play a great role though it also makes difficulty in image processing and high data redundancy due to high correlation in the adjacent bands. An increase in the number of training samples for image classification can be the solution for high-dimension data.

The combination of spectral and spatial classification is especially valuable for fine land-cover classification systems in areas with complex landscapes (Lu & Weng, 2007). Due to the heterogeneous composition of the urban environment, including artificial materials (i.e., impervious surfaces), soils, rocks and minerals, green and non-photosynthetic vegetation, a large number of the spectral band are needed for accurate classification (Weng, 2012b). For remote sensing applications, image spatial resolution is not the only factor needed to consider. But also temporal resolution refers to the time interval in which a satellite revisits the same location. The higher temporal resolution provides good opportunities to capture high-quality images. This is particularly useful for regions such as moist tropical areas, where hostile atmospheric conditions regularly occur.

More recently, satellite images with frequent revisit times are used widely in urban and environmental monitoring such as Sentinel 2 MSI imagery (Copernicus, 2018). To improve the classification accuracy, effective use of multiple objects of remotely sensed data and the selection of a proper classification method are especially significant (Lu & Weng, 2007). Previously, impervious surface extraction can be modeled using traditional classifications, which assume that the pixel size is smaller than the size of individual urban features, or that most pixels of the imagery only contain one type of urban land cover (Maclachlan et al., 2017). Most studies analyses this pixel into per-pixel and sub-pixel classifier to delineate urban impervious surface in a complex urban environment.

2.5 Per-pixel and Sub-pixel Classifiers

Researchers have also developed per-pixel and sub-pixel-based algorisms i.e. semi-automatic approaches were applied with the integration of supervised and non-supervised classification algorithms to extract the spatial extent of urban areas (urban footprint) (Semenzato et al., 2020). Per-pixel classifiers typically develop a signature by combining the spectra of all training set pixels for a given feature. The resulting signature contains the contributions of all materials present in the training pixels but ignoring the impact of the mixed pixels. Per-pixel classifiers can be either parametric or nonparametric (Weng, 2012a). The parametric classifiers undertake a normally distributed dataset occurs, and that the statistical parameters (e.g. covariance matrix and mean vector) generated from the training samples are representative.

However, the hypothesis of normal spectral distribution is often disrupted, especially with complex landscapes such as urban areas. In addition to this parametric classifiers lies in the difficulty of integrating spectral data with ancillary data. In addition, insufficient, non-representative, or multimode distributed training samples can further introduce uncertainty in the image classification procedure (Lu & Weng, 2007). For a parametric classifier, the maximum likelihood is a known example since its availability in any image processing software. Oppositely, in non-parametric classifiers, the assumption of a normal distribution of the dataset is not required. Additionally, to separate image classes no statistical parameters are needed.

Non-parametric classifiers are thus especially suitable for the incorporation of non-spectral data into a classification procedure. Among the most commonly used non-parametric classification approaches are neural networks, decision trees, support vector machines, and expert systems (Weng, 2012a).

Per-pixel classifiers inaccurately estimate urban surface materials when using moderate to coarse spatial resolution satellite data (spatial resolution > 10 meters), such as Landsat and SPOT imagery (Liao et al., 2021). Per-pixel classifiers have been found too significantly over or underestimate urban areas (X. Zhang et al., 2013). To address this problem sub-pixel classifiers have been modeled for monitoring change in land-use patterns. Sub-pixel classification methodologies such as spectral mixture analysis (SMA) (Yu & Lu, 2014), Vegetation, Impervious and Soil (V-I-S) framework (Roberts et al., 1998). However, the sub-pixel classifier has become insufficient due to endmembers may not fully represent image spectral variability or a pixel may be modeled by endmembers that do not represent materials within its field of view resulting in an inability to adequately portray the high spectral heterogeneity of the urban landscape (Maclachlan et al., 2017).

2.6 General Approaches in Impervious Surface Extraction

More recently, the appearance of finer spatial resolution imagery can support more spectral information than those with low-resolution imagery (Weng & Pu, 2013). Generally, extraction of impervious surface can be grouped into three main groups namely, Spectral unmixing approach (SMA), Machine learning algorisms, and Spectral built up indices (Pandey & Tiwari, 2020).

2.6.1 Spectral Unmixing Approach

Detecting and understanding the dynamics of an urban area is very important for fostering environmental and human sustainability of cities, and also it can be the base for estimating the growth pattern of cities for allocating resources (Bauer et al., 2007). Naturally, the urban landscape is heterogeneous and typically contains features that are smaller than the spatial resolution of the sensors, a complex combination of objects like buildings, roads, trees, soil, grass, water, and so on.

Urban environments are composed of the pixel which is spatially and spectrally heterogeneous at some scale because of the complex mixture of land cover types (Weng & Pu, 2013). Researchers applied per pixel classification algorism to densely populated suburban metropolitan areas, the mixed pixel problem becomes exaggerated (Lu & Weng, 2004). To overcome this problem additional spectral information can be used to extract greater detail by using endmembers using spectral mixture analysis (SMA). This approach has been developed to unmixed images at the sub-pixel scale to estimate the fraction abundance of endmember components within a pixel (Wu & Murray, 2003).

SMA assumes that ideally the spectral signal of a pixel can be modeled by integration of spectra contributed by some endmembers, or pure spectrally individual features, components, or LULC types (Weng & Pu, 2013). This technique is based on (1) selected endmembers should be independent of each other, (2) the number of endmembers should be less than or equal to the spectral bands used, and (3) selected spectral bands should not be highly correlated. (Deng & Wu, 2013) implemented a constrained linear SMA to assess impervious surface distribution in Columbus Ohio, and they conclude that impervious surface fraction can be estimated by a linear model of low and high albedo endmembers.

However, traditional SMA cannot account for the complexity and spectral heterogeneity of urban materials and the variability of spectral contrast between those materials. Therefore, a new approach called the MESMA technique can overcome the limitations of the traditional SMA by allowing the number and type of endmembers to vary for each pixel in the image. The study focuses on a comparative analysis between MESMA and SMA for mapping impervious surface area (ISA) using moderate spatial resolution Landsat TM imagery in the City of Tampa, Florida (Weng & Pu, 2013). MESMA evaluates each possible model (two-, three-, or four-endmember model) based on the criteria of fraction values of each endmember, root mean square error (RMSE), and shadow fraction (Roberts et al., 1998; Shahtahmassebi et al., 2016).

The principle of pixel's spectra with spectra of a set of pure land cover types called endmembers is used in SMA models (Roberts et al., 1998), however, there is a brightness variation in between the spectra of these pure land cover types. (Wu, 2004) propose a model to address the problems associated with brightness variation and shade using Landsat ETM+ imagery in Columbus Ohio. All the above studies are focused on a low or medium-resolution satellite image, which results in mixed pixel problems. Due to this reason, (Lu & Weng, 2009) extract, impervious surfaces from high-resolution IKONOS image based on spectral features using linear spectral mixture analysis (LSMA) and decision tree classifier, and they compared with maximum likelihood classifier and LSMA provided a better result. LSMA approach assumes that the spectrum measured by a sensor is a linear arrangement of the spectra of all components within the pixel (Lu & Weng, 2004). However, SMA-based models are difficult to identify the pure endmembers or the most representative endmembers in heterogeneous urban areas due to spectral characteristics variation of impervious surfaces from high to low albedo (Sun et al., 2016).

2.6.2 Machine Learning Algorithms

Machine learning algorithms are programs (math and logic) that adjust themselves to perform better as they are exposed to more data. The "learning" part of machine learning means that those programs change how they process data over time, much as humans change how they process data by learning. It is an advanced technology in improving the extraction of impervious surfaces by overcoming subjective factors and improve the concrete algorithm automatically in the process of learning (Deng & Wu, 2013). The Artificial Neural Network (ANN), Support Vector Machine (SVM), Random Forest (RF), and Logistic Regression are the most widely used in machine learning algorithms (Pandey & Tiwari, 2020; Weng, 2012a). Most machine learning algorithms are categorized in a non-parametric approach, which able to handle continuous and nominal data, interpretable classification rules, and swift application (Gewali et al., 2018).

2.6.2.1 Artificial Neural Network (ANN)

Artificial Neural Network (ANN) is a non-parametric supervised classification approach and it can estimate the property of data based on training samples. ANN works in the input used to train the neural network is the spectral data of the period of change. A back-propagation algorism is often used to train the multi-layer perceptron neural network model.

Nonetheless, this algorism is time-consuming, sensitive to the amount of training data used, and the hidden layers are poorly known (Jensen, 2005). (Mohapatra & Wu, 2007) estimate the percentage of impervious surfaces by creating activation level maps from high spatial resolution imagery (i.e., IKONOS) using a three-layer feed-forward back propagation neural network. However, this approach has difficulty in determining the initial weight (X. Guo et al., 2020).

2.6.2.2 Support Vector Machines

SVMs use the concept of mathematical planes (maximum-margin hyperplanes) to distinguish between multiple classes based on a decision boundary, or hyperplane, intending to minimize misclassification (Gewali et al., 2018). SVM draws a plane between two classes and maximizes the distance of this plane from both classes to classify accurately (Sukawattanavijit et al., 2017).

In the case of linear classification, this margin is drawn directly. But, when it comes to nonlinear classifications, SVMs use the kernel to convert nonlinear to linear and then find the hyperplane (H. Singh, 2019). SVM minimizes error on unseen data without prior assumptions on the distribution and avoids overfitting (Mountrakis et al., 2011). From all machine learning methodology of global optimization, the SVM algorithm is prior as the classifier because of its improved performance compared to other approaches (H. Guo et al., 2013).

2.6.2.3 Random Forest (RF)

The Random Forest (RF) classifier is an integrated machine learning algorithm based on decision trees. It is non-parametric depending on whether training samples can be represented by a Gaussian probability density function (Gewali et al., 2018). A decision tree relies on a certain statistical threshold, it can determine whether a particular thing belongs to one class or the other (Liao et al., 2021). More recently the application of random forest has been increased to medium spatial resolution data to more accurately represent the complexity of land covers within a pixel.

RF performs well in remote sensing image classification, but it fails to consider the spatial neighborhood information of pixels (Maclachlan et al., 2017). Nevertheless, DTs can be negatively affected by pruning methods, for example, pessimistic error pruning (PEP) introduces a continuity correction value, within error estimation on no theoretical basis, resulting in under or over-pruning (Gewali et al., 2018).

2.6.2.4 Logistic Regression

Logistic regression is one of the most famous algorithms in machine learning. This concept is a modified form of linear regression in which logits are used to determine the probability of an element belonging to a particular class. It gives us an output between zero and one. If the output is greater than 0.5, the element is said to belong to one class; otherwise, it belongs to the other (Singh, 2019).

2.6.3 Spectral Built-up Indices

The results of conventional methods of parametric and non-parametric classification are still subject to the characteristics of the selected training samples. The size, location, and representativeness of all samples have directly managed the reliability of the classified results. Although, the classification is slowed down by select quality training samples that fit the requirement of all those covers to be mapped. Considerable efforts have gone into simplifying the process of automatically mapping land covers, such as using indices that are automatically classified from satellite data (He et al., 2010; Pandey & Tiwari, 2020; Zha et al., 2003).

For extraction of impervious surface, the spectral index-based approaches have shown some remarkable results in terms of ease of implementation, memory efficiency, less execution time, independence with the training samples, and its simplicity (Bouhennache et al., 2019; Estoque & Murayama, 2015b; Kawamura, 1996; Sun et al., 2016; Xu, 2007; Zha et al., 2003). Measurements of impervious surface and additional attributes are used to improve consistent indices of urban expansion (Ghosh et al., 2018). For quick and accurate recognition and classification of impervious surfaces from remote sensing imageries, various spectral built-up indices have been proposed.

In the middle of the 1990s, (Kawamura, 1996) propose Urban Index (UI) using Landsat TM data (Band 7 and Band 4) to update information and assess the condition of rapidly changing urban areas. This index was intended to exploit the inverse relationship between the brightness portion of urban areas in the NIR and the SWIR band of the MIR Channel.

At the beginning of 2000, (Zha et al., 2003) propose a new method based on the Normalized Difference Built-up Index (NDBI) to automate the process of mapping built-up areas and to minimize the lengthy process of manual interpretation and parametric image classification on Landsat TM imagery. NDBI, which takes advantage of the unique spectral response of impervious surface and other land covers. Similarly, NDBI uses NIR and MIR portions of the electromagnetic spectrum to detect variation between the spectral responses of built-up areas. However, NDBI uses the SWIR band of the MIR Channel.

Later, (H. Xu, 2008) proposed an index-based built-up index (IBI) for effective extraction of built-up areas. Unlike previous indices, IBI uses thematic index-derived bands to construct an index rather than by using original image bands. Soil adjusted vegetation index (SAVI), the modified normalized difference water index (MNDWI), and the normalized difference built-up index (NDBI) are the three thematic indices used in constructing the IBI. This approach can reduce plant noise which is common in NDBI because the reflectance of certain types of vegetation increases as the leaf water content decreases.

IBI values are range from -1 to 1, where positive values correspond to the built-up region, while the non-built-up areas (background) have zero or negative ones. (He et al., 2010) improve the NDBI caused by a limitation in urban and bare land heterogeneity using a semiautomatic segmentation approach to delineate built-up regions. It shows that the built-up and barren areas are represented with positive values, while other land covers are outlined with values from 0 to −1 through subtracting the NDVI channel from the NDBI image.

To assist urban residential area mapping, (Jieli et al., 2008) developed New Built-up Index (NBI) on the footprints of Landsat Thematic Mapper (TM) using RED band (visible), near-infrared (NIR), or band 4 (low reflectance in the built-up area) and mid-infrared (MIR), or band 5 (high reflectance in the built-up area). The output shows that the spectral response of barren land is greater than the other land covers in the previous bands. The spectral response of different features is various from region to region due to climatic & topographic changes. However, built-up area and bare soil have a similar spectral response. In 2010, (Xu, 2010) also proposed a new index, normalized difference impervious surface index (NDISI), for estimating impervious surface through integrating thermal band to exploit the radiation emitted from impervious surfaces, decreasing their low reflectance response in the visible, NIR, and SWIR wavelength intervals using Landsat ETM+ image.

Due to mixture of built-up and bare land (Waqar et al., 2012) introduced two new indices; namely, band ratio for the built-up area (BRBA) and normalized built-up area index (NBAI) respectively, to identify the built-up area and bare soil using a unique pattern in the city of Islamabad, Pakistan. (Stathakis et al., 2012) Introduce a new approach, vegetation index built-up index (VIBI) based on the two components, which refers to vegetation content (NDVI), while the other is correlated to soil types and urban materials (NDBI). Mainly, VIBI combines visible (TM band 3) and infrared bands (TM band 4 and TM band 5). In this approach, there is no need to apply a mask or use auxiliary information. VIBI classifies a pixel and the negative value represents urban value while the positive value is other land covers. Although, (Deng & Wu, 2012) develop a method, Biophysical composition index (BCI) to eliminate mixed pixel problems in between impervious surfaces and bare soil.

The formulation of the Biophysical composition index (BCI) was based on Ridd's conceptual vegetation-impervious surface-soil triangle model by a reexamination of the Tasseled Cap (TC) transformation. By the time it was successful due to its simple and convenient derivation of urban biophysical compositions for practical applications. In addition to this, (Liu et al., 2014) proposed Modified Built-up Index (MBI) to improve the contrast between built-up and other land covers using RED band, NIR, and SWIR channel of the electromagnetic spectrum in Landsat TM/ ETM + images in the southern Jiangsu, China. Since the basic ground of indices discussed above is the spectral response of built-up lands in different bands of Landsat Thematic Mapper (TM) and Enhance Thematic Mapper plus (ETM+) data, however, the output based on Landsat-8 Operational Land Imager (OLI) data is supposed to be different as shown in different literature.

Modified Normalized Difference Built-up Index (NDBI) approach developed by (Bhatti & Tripathi, 2014) for built-up area extraction method (BAEM) using newer Landsat-8 Operational Land Imager (OLI) data. Unlike NDBI, this approach uses principal component analysis (PCA) images of the highly correlated bands pertinent to NDBI computation. It integrates the thermal Infrared Sensor (OLI-TIRS) and based on the subtraction of the sum of (NDVI) and (MNDWI) from the NDBI. And the final output was recorded by determining the threshold value through a double window flexible pace search (DFPS) method. Spectral signatures analysis of various land covers indicates the better separation of urban area in band 6 (SWIR 1) compared to others.

Though (Bouzekri et al., 2015) develop an index by combining band 3, band 4, band 6 (SWIR 1), and L which is an arithmetic constant equal to 0.3 and it was applied to a Landsat OLI-TIRS image, which is registered in 2013 from Djelfa city, Algeria. The result obtained by BAEI was compared with other indices such as Band Ratio for Built-up Area (BRBA), Normalized Built-up Area Index (NBAI), New Built-up Index (NBI), and the Normalized Built-up Index (NDBI) and it achieves an accuracy of 92.66 % which is 3-22 % higher than that from previously developed indices.

The New Built-Up Index (NBUI) has been proposed to extract urban built-up area from time-series Landsat Thematic Mapper (TM) and Enhanced Thematic Mapper Plus (ETM+) imageries (Sinha & Verma, 2016). To get NBUI, three indices are integrated; i.e., the Enhanced Built-Up and Bareness Index (EBBI), Soil Adjusted Vegetation Index (SAVI), and Modified Normalized Difference Water Index (MNDWI). Due to the limitation of high similarity in spectral profiles making it a difficult task to distinguish the impervious surface from bare soil areas. So, (Sun et al., 2016) develop a new index, combinational build-up index (CBI), to extract impervious surfaces. Three components are combines to distinguish impervious surfaces, especially from bare soil with a universal and convenient application; namely, principal component analysis (PC1), normalized difference water index (NDWI), and soil-adjusted vegetation index (SAVI), representing high albedo, low albedo, and vegetation, respectively.

Normalized Ratio Urban Index (NRUI) developed by improving the capability of the Biophysical Composition Index (BCI) (Piyoosh & Ghosh, 2018). Panchromatic (PAN) and Band 7 of Landsat 8 image increase the contrast between vegetation and urban areas. To enhance urban built-up areas from barren (bare soil) and vegetation, this study develops Ratio Urban Index (RUI) and compares with NRUI, which is better than RUI in discriminating urban areas from bare soil.

2.7 Perception of Land use Land cover Change

Land is defined as a habitation on which all human movement is being accompanied. Hence, land use is shaped by human needs and environmental features and processes. Land cover is a fundamental variable that impacts and links many parts of the human and physical environments (Cavur et al., 2019). Also, the Land cover is the biophysical state in which it describes the physical state of the land surface; e.g., cropland, mountains or forests, biodiversity, and others (Moser, 1996). Mapping of land-use/land-cover help to understand and examine land-use/land-cover distribution pattern, measure the current conditions or quantity and gather information about landscape change and see the correlation with different intra-urban microclimatic conditions (Gebeyehu, 2018). The cause of changes in the land surface emerges because of both natural and anthropogenic activities (Dessu et al., 2020).

Ethiopia, the second-most populous country in Africa, with an annual population growth rate of 2.3%, has an urban population growth rate of 4.2%. This population growth rate is higher than the average rate (2.2%) for developing countries (United Nations, 2014).

Land use and land cover information are required for policymaking, business, and administrative purposes. Despite the significance of land cover as an environmental variable, our knowledge of land cover and its dynamics are poor. Understanding the significance of land cover and predicting the effects of land cover change is particularly limited by the paucity of accurate land cover data (Rwanga & Ndambuki, 2017).

2.8 Support Vector Machine Algorithm for LULC Classification

Support vector machine (SVM) is a supervised classification algorism in which the user specifies the various pixel values or spectral signatures that must be associated with the specific class. The supervised classification process begins by choosing sample locations of LC types; this is called training area/sites. The computer algorithm then uses the spectral signature of this training area to classify the entire image (Congalton, 1991; Foody, 2004; Smits et al., 1999).

Due to the different capabilities of various algorism in land use land cover separability, the use of the best algorism can increase the classification accuracy. Also, many variables in a classification procedure may decrease classification accuracy (Mukherjee et al., 2021). It is important to select only the variables that are most useful for separating land-cover of vegetation classes. In particular, a good representative dataset for each class is key for implementing a supervised classification (D. Lu & Weng, 2007). In the classification of two land covers, many hyperplanes can be considered but there is only one optimal hyperplane that is projected to generalize better than other hyperplanes can be selected (Ndehedehe, 2014).

The SVM model aims to create a classification hyperplane that divides the data into a predefined number of classes using optimal maximum margin, with points on the margins termed ‘support vectors’ pertains to structural risk minimization (Culberg & Fuhs, 2017). One of the major advantages of this algorism is the broad applicability for land use land cover classification using data from a multitude of sensors such as Sentinel 2 MSI (Ndehedehe, 2014). Also, it has been extensively used for classification purposes, due to its capability to ignore inherent image errors in which there are many more variables than observations, and complexly structured data and to avoid overfitting (Mountrakis et al., 2011).

Kernel methods are commonly used in conjunction with SVM in separating variables that ignore hyperplane outliers and transform data into high dimensional feature spaces. There are three types of kernels for image processing; namely, polynomial, radial basis function, and sigmoid kernels. The best kernel for LULC applications is the radial basis function kernel because it produces the highest overall accuracy and highest overall kappa (Mountrakis et al., 2011). The Regions of Interest (ROI) are used as spectral signatures of LULC categories. Training data help the supervised classification algorithms to learn the pattern and accordingly tune the unknown parameters of the algorithm. Once trained, the supervised classification algorithm is validated further using the testing data (Mukherjee et al., 2021).

2.9 Land use Land Cover Change Detection

Earth's surface is changing rapidly by different factors among which this human-induced are the most dominant. Land use/land cover change detection is a process of identification of the changes or differences of an object by observing it at different times (A. Singh, 1989). Land use and land cover change detection is an important process in current strategies for monitoring and managing natural resources, environmental changes, and urban development because it provides quantitative analysis of the spatial distribution of the population of interest (Dessu et al., 2020).

The technique of remote sensing data performs the change detection matrix using satellite imagery, which becomes powerful in manipulating digital data. The changes in land cover result in changes in radiance values which can be remotely sensed (Parveen et al., 2018). Due to this reason RS technology is highly recommended in mapping the existing situation of the land-use/land-cover phenomena (Gebeyehu, 2018). This process is done after the completion of calculation and analysis of the land use land cover classes from pre and post-monsoon images (Dessu et al., 2020).

2.10 Comparative Analysis of Existing Indices

In the past few years, researchers have made a significant effort to create a good index that reveals the reality of built-up regions. Several built-up indices have been proposed in the extraction of impervious surfaces to work suitably with medium to coarse spatial resolution data such as Landsat imagery. Nevertheless, their performance depends on spatial resolution, climate, acquisition time, and surface relief (Valdiviezo-N et al., 2018).

Therefore, some studies focus on a comprehensive comparison between spectral indices in various satellite imageries for the rapid and accurate classification of built-up lands. This comparison shows that remote sensing of impervious surfaces has become one of the more energetic fields in remote sensing technology (Weng, 2012b). Since a number of the sensors are available, many researchers have compared the performances of different sensors. The comparison ware based on per-band-based, index-based, and classification-based comparisons. Landsat-7 ETM+ and ASTER sensors with index-based Built-up Index (IBI), while the classification algorithm employed is the Support Vector Machine (SVM) for built-up land mapping (Xu et al., 2013).

Recently, the combination of spectral indices with textural features is used to extract built-up areas. In a study conducted by (Bramhe et al., 2018), three spectral indices (Normalized Difference Built-up Index (NDBI), Built-up Area Extraction Index (BAEI), and Normalized Difference Bareness Index (NDBai) are integrated with textural feature such as Contrast, Correlation, Energy and Homogeneity, etc. for each image band to eliminate intermixing of classes observed in the classified image when using spectral channels. Also, an SVM classifier was applied to explore the usefulness of the selected GLCM texture measure to extract built-up area using Landsat-8 multispectral image. (Ali et al., 2019) analyze changes in built-up lands in Short Wave Infrared (SWIR) wavelength, visible Red (R), and Near Infrared (NIR) of multi-temporal Landsat OLI 8 data.

Normalized Difference Built-Up Index (NDBI), Urban Index (UI), and Normalized Difference Vegetation Index (NDVI) are the spectral indices to examine the changes in land use and area cover. Automated Built-up Extraction Index (ABEI) was developed a stable optimum threshold for impervious area extraction and improve the classification accuracy in areas containing bare and sandy surfaces using Landsat 8 OLI imagery (Firozjaei et al., 2019).

(Estoque & Murayama, 2015b) compared different built-up indices from Landsat-7 ETM+ (Enhanced Thematic Mapper Plus) and Landsat-8 OLI/TIRS (Operational Land Imager/Thermal Infrared Sensor) imageries. This study proposes two visible-based indices, i.e. the VrNIR-BI and VgNIR-BI or the visible red/green-based built-up indices.

Where green and NIR are respectively the reflectance of the band 2 and band 4 for the ETM + sensor and the reflectance of the bands 3 and band 5 for the OLI sensor. Additionally, Otsu's method was used to separate the built-up area from the non-built-up area by masking the water part. (XI et al., 2019) investigate the workability spectral indices, VrNIR-BI, VgNIR-BI, UI, NDBI, and IBI on sentinel 2A MSI imagery and Landsat 8 imagery to delineate built-up from non-built-up area and support vector machine (SVM) algorithm was employed to classify the imageries into three classes. However, there are some differences between the two sensors, caused by the differences in the spectral response functions and spatial resolution between the two sensors.

Although, some studies compare two or more machine learning algorism such as support vector machine (SVM) and artificial neural network (ANN) in addition to spectral built-up indices (Mukherjee et al., 2021). They also propose a new spectral index, powered B1 built-up index (PB1BI) using Landsat 7 satellite images based on powered B1 built-up index (PB1BI). The results showed that the proposed index was conceptually simple and computationally inexpensive rather than the machine learning algorism and other indices. Different kinds of literature discuss the advantages, difficulties, and limitations of various built-up indices and they compare the capability between built-up indices with machine learning techniques in a different aspect.

First, Built-up indices do not necessitate a training sample and classification steps to get the output image; second, they rely on spectral differences between some channels (bands) of the electromagnetic spectrum; and thirdly, only an optimal threshold is required to separate urban areas from other land covers from the output of any index method. The above-mentioned reason makes the built-up indices computationally efficient compared to machine learning approaches. Still, the accuracy of built-up indices significantly diminishes by factors such as surface relief, seasonality, and bare soil, among others (Valdiviezo-N et al., 2018).

2.11 Experiments Using Synthetic Aperture Radar Data

Remote sensing satellite images are powerful and up-to-date data for estimation human influence on urban space, which is highly desired by policymakers (Kuc & Chormański, 2019). The accessibility of urban remote sensing satellite imageries is generally used to differentiate built-up areas based on spectral values. Though, the high degree intricacy of the spectral distribution between different urban areas, especially, with the bare soil encounters in terms of the pixel amalgamations in areas with heterogeneous substances (Sun et al., 2016). Objects such as buildings, asphalt roads, runways, concrete, and parking lots, which were difficult to identify images in low and medium spatial resolution such as Landsat imageries, are recognized on the images with a high spatial resolution (Bouzekri et al., 2015). Knowing the strength and dimness of different types of sensor data is crucial for the selection of suitable remotely sensed data for impervious surface extraction (Lu & Weng, 2007).

To characterize and quantify urban impervious surfaces requires considering such factors as the scale and characteristics of a study area, the availability of various image data and their characteristics, cost and time constraints, user's need, and the analyst's experience in using the selected image. Especially, Scale, image resolution, and the user's need are the most important factors affecting the selection of remotely sensed data (Lu & Weng, 2007). Before 2000, the lack of high spatial resolution images is the main reason for scarce research in remote sensing of impervious surfaces (Weng, 2012b). More recently, the appearance of high-resolution remote sensing data increases the potential of built-up dynamics analysis periodically (Valdiviezo-N et al., 2018). They can give better results for impervious surface mapping because of the spatial complexity of components in the urban area (Waqar et al., 2012).

Consequently, to best control urban built-up areas, data sets must have an adequate spatial and temporal resolution to detect the change. However, the usage of very high-spatial-resolution remote sensing data often lacks temporal acquisition consistency (e.g. airborne orthophotos) or they are expensive to purchase (e.g. commercial satellite imagery such as QuickBird, IKONOS, and others) (D. Lu & Weng, 2007).

Unlike optical sensors and aerial photos, SAR (Synthetic Aperture Radar) systems can bring out the potential to provide high quality and free of charge satellites images without being affected by cloud-cover, seasonality, and daytime variations, and can identify urban structures in 5 days revisit time, as well (Kuc & Chormański, 2019). SAR or radar remote sensing can provide new openings, as the target-wave interaction depends on the scattering properties of the features on the ground, based on which backscatter values are generated (S. Sinha et al., 2020b). Multi-temporal Sentinel-2 data released by ESA Copernicus are extensively used to calculate urban sprawl provide imagery data that enable to estimate parameters related to urban structure and imperviousness (Semenzato et al., 2020).

In a study conducted by (S. Sinha et al., 2020b), was in a semi-automated way, space-borne optical data (Resources at-2 LISS III) and synthetic aperture radar (SAR) data (HH/HV dual-polarized L-band ALOS PALSAR) are the two data for designing the built-up indices (BUIs) used for impervious feature detection. For the detection of this area two indices are derived; namely, an Impervious Built-up Index (IBUIopt) and an Impervious Built-up Index (IBUIsar) using spectral-based information from optical sensors and SAR HH/HV backscatter information respectively. Horizontal-Vertical (HV) cross-polarized L-band backscatter coefficient and Horizontal-Horizontal (HH) co-polarized were used in SAR sensors to design BUI. And finally, the result was validated with Ground Truth (GT) data.

Later, the launch of Sentinel 2A and 2B opens a new research approach cause of its free availability and high resolution which enough to delineate urban impervious surfaces. Vertical constructions such as buildings and other anthropic structures act as an indicator, generating a particularly robust radar-echo signal (backscattered) that allows their easy identification (Semenzato et al., 2020). (Sun et al., 2016) propose a combinational shadow index (CSI) to address the frequent occurrence of building shadows in urban areas which challenging task in existing building shadow indices. Therefore, in the creation of CSI, two spectral indices i.e. the shadow enhancement index (SEI), the normalized difference water index (NDWI), and the NIR band (B8), were integrated to separate spectrally similar objects, such as building shadows, water, and low albedo features using Sentinel 2A MSI image.

(Osgouei et al., 2019) introduce a shortwave infrared-based index, the Normalized Difference Tillage Index (NDTI) added to existing indices using Sentinel 2A image. The result obtained by the combinations of spectral indices and the original satellite images were classified using the same training sample in a supervised SVM algorithm, which is a non-parametric, machine-learning-based structure. Nowadays, the arrival of new sensors contributes an imperative application to use multiple types of remote sensing data, especially in long-term dynamic monitoring.

High-resolution satellite images were integrated with other approaches, for example, sentinel 2A MSI imagery with google satellite imagery (Vigneshwaran & Kumar, 2018), textural feature, and spectral indices combined with Support Vector Machine (SVM) classifier (Bramhe et al., 2018).

2.12 Accuracy Assessment

In remote sensing data, the term accuracy is used to express the degree of ‘correctness’ of a map or classification. Accuracy assessment or validation is a substantial step in the processing of remote sensing data for further analysis. It establishes the information value of the resulting data to a user (Rwanga & Ndambuki, 2017). Therefore, the classification accuracy is taken to mean the degree to which the derived image classification agrees with reality or conforms to the ‘truth’ (Foody, 2002). Hence, the classification error is, thus, some discrepancy between the situation depicted on the thematic map and reality. The evaluation of land cover maps is assessed by some ground or other reference data set. Disagreements between the two data sets are typically interpreted as errors in the land cover map derived from the remotely sensed data (Congalton, 1991). Accuracy assessment based on the error matrix is the most commonly employed approach for evaluating per-pixel classification (Lu & Weng, 2007).

The assessment of accuracy is utilized in the computation of confidence intervals for the overall, producer’s and, user’s accuracies. The confusion or error matrices were created as a square array of numbers arranged in rows (classified data) and columns (true or reference data). Indeed, confusion or error matrices refine both classification accuracy and characterize errors by describing the value derived from it. The overall accuracy of the classified image compares how each of the pixels is classified versus the definite land cover conditions obtained from their corresponding ground truth data (Walker et al., 2009). It is calculated as the sum of the major diagonal, i.e. correct classifications, divided by the total number of accuracy assessment samples. Producer's accuracy measures errors of (omission/exclusion), which indicates how well the reality land cover types can be classified by the mapper. The user's accuracy (commission/inclusion error) indicates how often a classified pixel matching the land cover type of its corresponding reality location (Campbell & Wynne, 2011; Congalton, 1991; Jensen, 2005).

In the error matrix the measure of accuracy that uses the information content of the confusion matrix more fully than the basic percentage of correctly allocated cases such as the kappa coefficient of agreement, are frequently derived to express classification accuracy. Kappa is a discrete multivariate technique that measures of overall statistical agreement of an error matrix in accuracy assessment (Abebe & Megento, 2016). Kappa reflects the difference between the actual result and the expected result. Kappa is the percentage of data values in the central diagonal of the table that subsequently adapts these values for several agreements that could be estimated because of the probability itself (Congalton, 1991; Foody, 2004; Smits et al., 1999).

Table 2-1: Category of kappa statistics

Kappa statistics	< 0.00	0.00 - 0.20	0.21 – 0.40	0.41 – 0.60	0.61- 0.80	0.81 - 1
Strength of agreement	Poor	Slight	Fair	Moderate	Substantial	Almost perfect

Source: (Koch et al., 1977)

CHAPTER THREE

3. RESEARCH MATERIALS AND METHODS

3.1 Description of the Study Area

3.1.1 Location

Addis Ababa is the capital and the largest city of the Federal Democratic Republic of Ethiopia is located in the center of the country. Addis Ababa is geographically located on latitude 9° 01' 29.89" N and longitude 38° 44' 48.80" E. As the capital city of the Federal Democratic Republic of Ethiopia, it is located almost at the center of the country. The city has covering a total area of 539. Km^2 and divided into 10 sub-cities as shown in figure 3-1. Since 1963, Addis Ababa has hosted the Organization of African Unity (OAU). It also hosts many other continental and international organizations including the headquarters of the United Nations Economic Commission for Africa (ECA), and therefore often referred to as "the diplomatic capital" of the African continent.

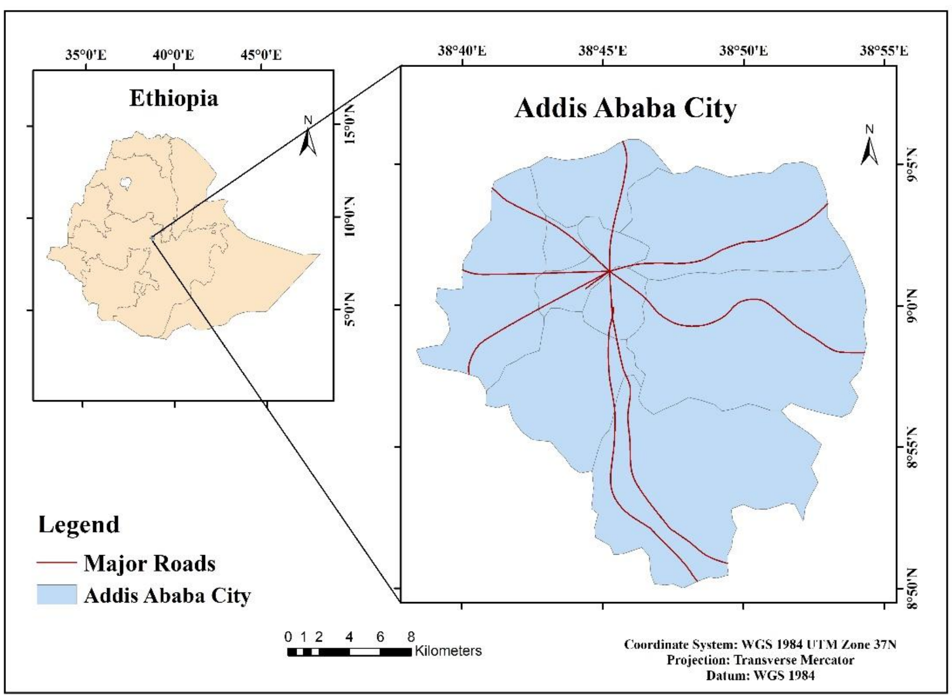

Figure 3-1: Location Map of the study area

3.1.2 Topography

Addis Ababa city lies at a minimum altitude of 2044m to a maximum altitude of 3030m above sea level. Because of having the highest altitudinal position, Addis Ababa ranks the fourth highest capital city in the world and takes the first rank from African cities. There is a great variation of height within the city, so that much of it is built on the slope. The city has experienced spatial spread mostly towards the southern, eastern, and southwestern parts. The northern part of the city, which is the foothills of the Entoto Mountains has a higher elevation while the southern part of the city, which is the Akaki Kality area has a lower elevation. The elevation map of the study area is extracted from ALOS 12m resolution which is downloaded from the Alaska Satellite website (https://asf.alaska.edu/).

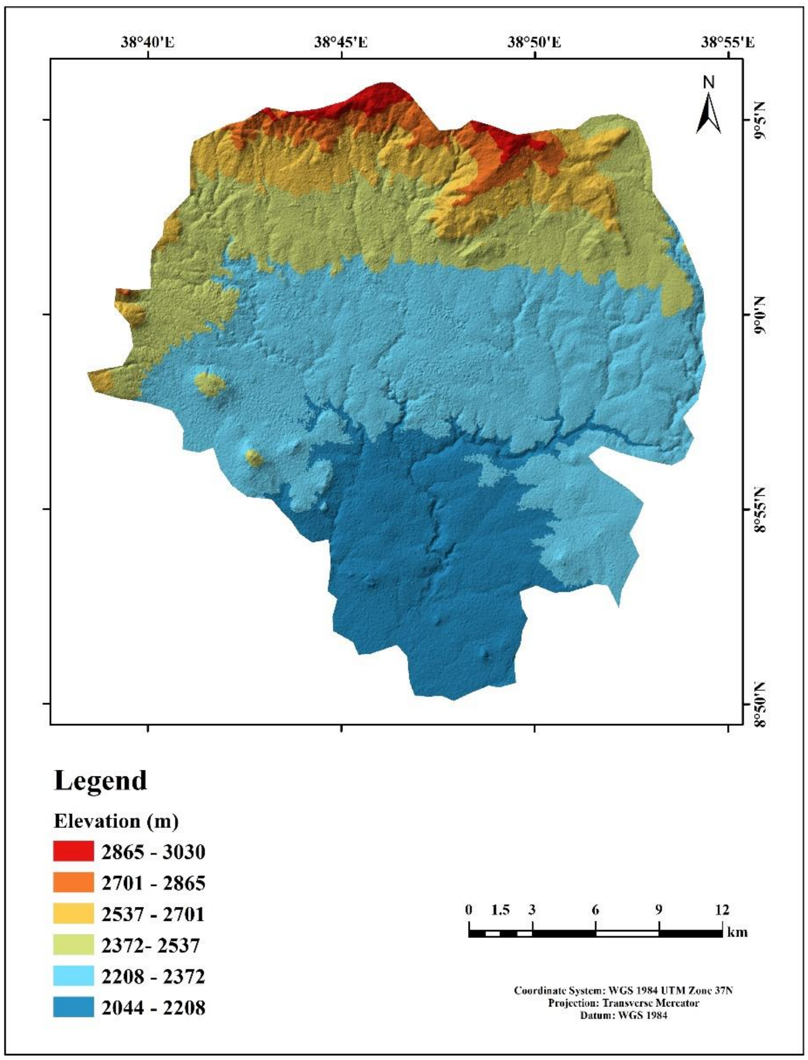

Figure 3-2: Elevation map

3.1.3 Population

According to the Central Statistical Agency of Ethiopia 2007 population census conducted by the Ethiopian national statistics authorities, Addis Ababa has a total population of 2,739,551 urban and rural inhabitants. For the capital city, 662,728 households were counted living in 628,984 housing units, which results in an average of 5.3 persons to a household. After eight years, the population number increased by 81.73% and (3,273,000) in the year 2015 (CSA, 2013). When the time interval covering the working period is considered, because of the migration due to economic and social problems, the population greatly increased in the city.

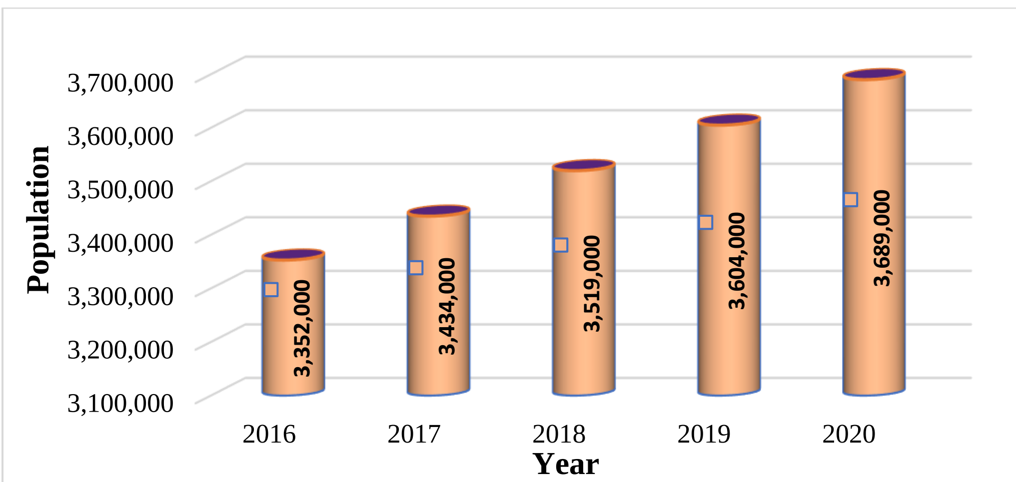

Figure 3-3: Estimated population number of Addis Ababa city

3.1.4 Climate

Addis Ababa experiences average monthly temperature varies between 10 °C and 20 °C implying subtropical climate conditions. Climatically, the maximum temperature recorded in April and May being its hottest months and the lowest average temperature recorded was around 14.4 °C in December, which is the coldest month.

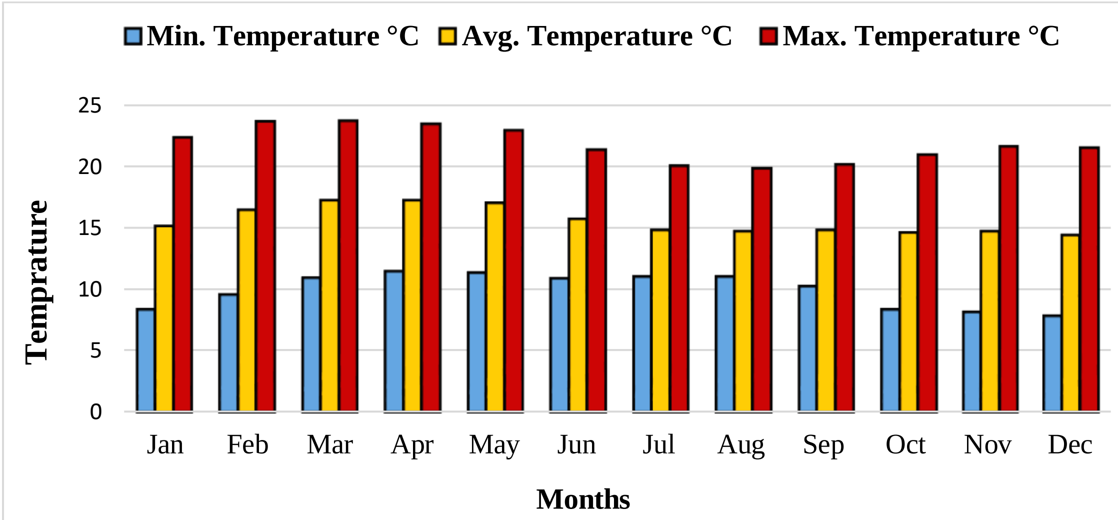

Figure 3-4: Monthly temperature distribution of Addis Ababa city

(Source: https://en.climate-data.org/africa/ethiopia/addis-ababa/addis-abeba-532/)

The city has a rainfall peak between July and August and minimum rainfall (driest month) between December and February. There is 7 mm of rainfall in December. The greatest amount occurs in August, with an average of 419 mm.

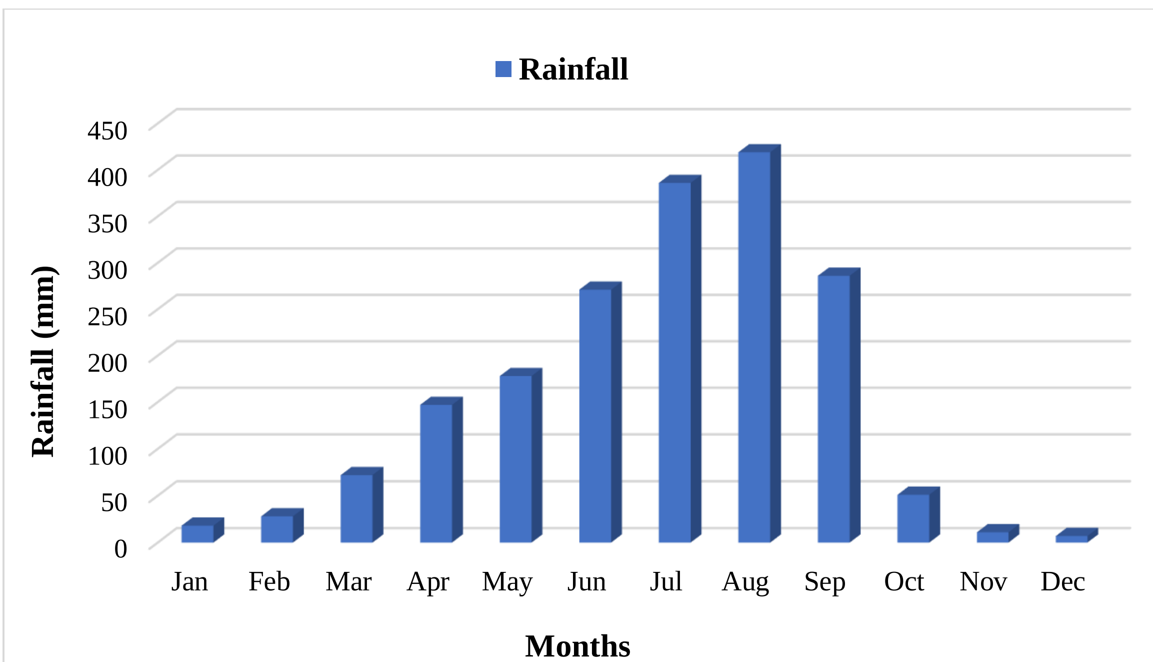

Figure 3-5: Monthly Rainfall distribution of Addis Ababa city

(Source: https://en.climate-data.org/africa/ethiopia/addis-ababa/addis-abeba-532/)

3.2 Data and Data Source

3.2.1 Primary Data Collection

The primary data source was used for the evaluation of different spectral built-up indices from sentinel 2A imagery for the extraction of impervious surfaces. Field surveys were used as a primary data source for the evaluation. During this time field reconnaissance and measurement of sample point through Handheld GPS which provides improved location accuracy, in the range of operations of each system with 3m accuracies were done. The samples were collected for accuracy assessment. Fifty sample points were collected from each land cover type and a total of two hundred fifty sample points were collected from five land-use classes. These data are used for visual interpretation and accuracy assessment.

3.2.2 Secondary Data Collection

Secondary data were collected from different sources including the website of ESA, different books, journals, articles, Google Earth, and Aerial photographs. The aerial photograph was captured in the year 2020 within the boundary of the study area in 30 cm resolution by the Ethiopia Geospatial Information Agency, was applied as a reference to an area that is not suitable for field measurement in handheld GPS.

Table 3-1: Data and data sources

Data Name	Acquisition Date	Spatial Res(m)	Source	Purpose
Sentinel 2A MSI imagery	2016, 2018 and 2020	10	ESA	For Indices calculation and Image classification
Aerial Photograph	2020	0.3	Geospatial Information Institute (GII)	For accuracy Assessment (2020)
Ground Truth data	2016, 2018 and 2020	-	Field data and google earth	For accuracy Assessment
Addis Ababa City Boundary	-	-	Geospatial Information Institute (GII)	To extract/clip data to the study area
ALOS	2009	12	Alaska Satellites	To identify study area topography
Population data	-	-	CSA	To extract population data
Temperature and rainfall data	-	-	World climate	To extract climate data

The European Space Agency (ESA) developed the operational Sentinel-2 mission within the frame of the European Union Copernicus program. The Sentinel-2A and Sentinel-2B satellites were launched on 23 June 2015 and on 7 March 2017, respectively and both maintain a sun-synchronous orbit at 786 km altitude. The Sentinel-2 mission specification is based on a constellation of the twin satellites, Sentinel-2A and Sentinel-2B, flying in the same orbit but phased at 180° and designed to give a high revisit frequency of 5 days at the Equator. The multispectral imager covers 13 spectral bands with a swath width of 290 km and a spatial resolution of 10 m (four visible and near-infrared bands (NIR)), 20 m (six red-edge and shortwave infrared bands (SWIR)), and 60 m (three atmospheric correction bands) (Copernicus, 2018).

Sentinel-2 data provide a viable complementary source to the pre-existing moderate-resolution images, with an increased spectral resolution, and provide a continuity of SPOT and USGS Landsat Thematic Mapper instrument and observation data, by contributing to the current multispectral operational products, such as land-cover maps, land-change detection maps, and geophysical variables. Also, it will ensure that SENTINEL-2 makes a significant contribution to Copernicus themes such as climate change, land monitoring, emergency management, and security (Copernicus, 2018).

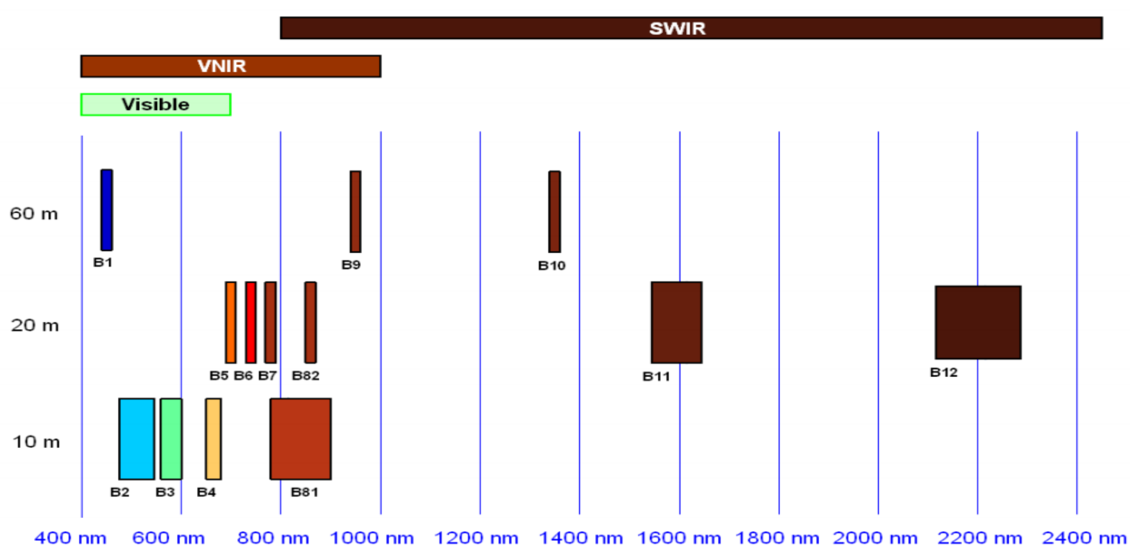

Figure 3-6: Spectral bands of sentinel 2A image

(Source: http://step.esa.int/main/download/)

Sentinel-2 image products are available to the community at the Level-1C (top-of-atmosphere reflectance in cartographic geometry) and Level-2A (bottom-of-atmosphere reflectance in cartographic geometry) processing levels.

The granules or tiles of Sentinel-2A MSI images for these two levels are provided as 100 km×100 km sized ortho-images in the UTM/WGS84 projection, which were downloaded from the ESA website, free of charge. (Copernicus, 2018).

Table 3-2: Spectral bands of sentinel 2A MSI

Sentinel-2A MSI		
Name	**Band (Resolution/m)**	**Range/nm**
Coastal aerosol	B1 (60)	443.9 ± 13.5
Blue	B2 (10)	492.1 ± 49
Green	B3 (10)	559 ± 23
Red	B4 (10)	665 ± 19.5
Pan		
Red_edge 1	B5 (20)	703.8 ± 10
Red_edge 2	B6 (20)	739.1 ± 9
Red_edge 3	B7 (20)	779.7 ± 14
NIR_{wide}	B8 (10)	833 ± 66.5
NIR_{narrow}	B8A (20)	864 ±16
Water Vapor	B9 (60)	943.2 ± 13.5
Cirrus	B10 (60)	1376.9 ± 38
SWIR 1	B11 (20)	1610.4 ± 70.5
SWIR 2	B12 (20)	2185.7 ± 119

3.3 Software's and Instrument Used

To image analysis and interpretation of urban built-up land cover indices using sentinel 2A MSI imagery, such different software's are used.

Table 3-3: Software's and instrument used

Software	Purpose
Quantum GIS 3.1	To Pre-processing sentinel data, for spectral index calculation and to generate different thematic maps
ENVI 5.3	For land use land cover classification in SVM
ARCMAP 10.5	Accuracy assessment and data analysis
Google Earth Pro	For reference in accuracy assessment
Microsoft Word and Microsoft Excel	Data analysis and generation of graphs and charts.
Handheld GPS	To collect the coordinate of sample point for accuracy assessment

3.4 Methodology

The methodology adopted for this study is shown by a flow chart in figure 3-7. Evaluation of the spectral built-up indices for impervious surface extraction using Sentinel 2A MSI imagery comprised four major steps: Initially, satellite data has been examined for pre-processing requirements, which include atmospheric correction, geometric correction, and spatial enhancement through resolution merging and clipping of unwanted features. Subsequently, indices-based calculations of the built-up area extraction were implemented. Based on this, seven spectral built-up indices were computed. Training samples for various land use were demarcated on the image and collected for further classification analysis by a non-parametric classifier (SVM) in different bands. Assessment of performance of these various spectral built-up indices was carried out in various ways. The steps of methodology have been briefly described in the subsequent sub-sections.

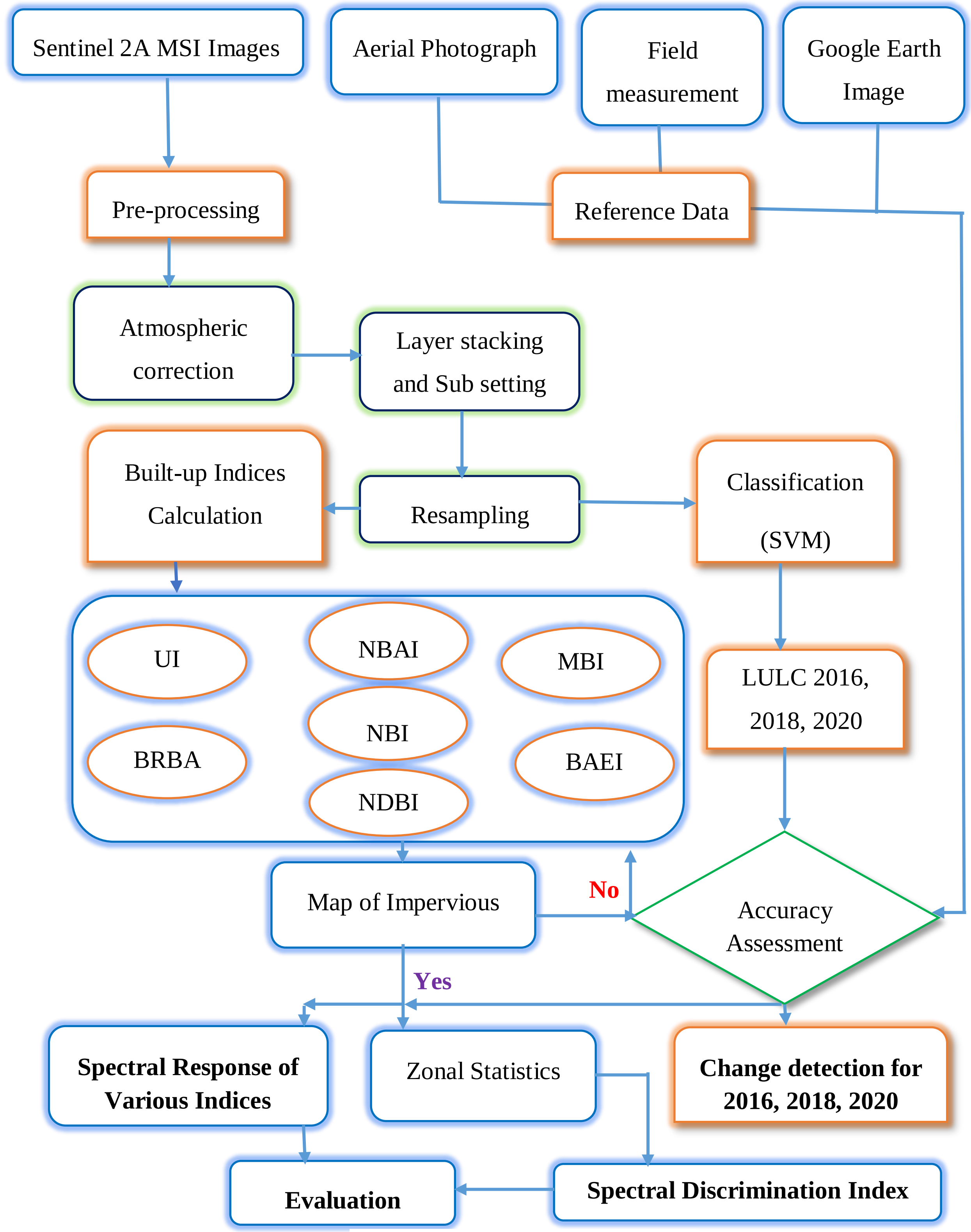

Figure 3-7: Methodology flowchart

3.5 Image Acquisition and Pre-processing

The Sentinel-2 MSI imageries are distributed as Level-1C products, which are ortho-image top of atmosphere (TOA) reflectance in cartographic geometry (Radoux et al., 2016). In this research, processed Level-1C (top-of-atmosphere reflectance in cartographic geometry), cloudless Sentinel images were used to execute the analysis and evaluation of spectral built-up indices. Satellite data from the Sentinel-2A MSI imagery was chosen for this study for two main reasons; the first one is its relatively high 10 m spatial resolution, and the second is its radiometry includes two NIR and two SWIR bands. These two characteristics make the Sentinel-2A data appealing for impervious surface extraction.

The acquisition dates of the images were October 2016, 2018, and 2020 in clear sky conditions, with minimum atmospheric disruptions for Addis Ababa City. The area of the study lays in two tiles, therefore, these tiles were stacked and clipped by the shapefile of the study area. Existing indices have major drawbacks because of their inability to separate urban areas from bare land in the dry season. Due to this reason, wet seasons were selected for study time to get very high separation accuracies in between bare land, vegetation, and urban area.

3.5.1 Atmospheric Correction

According to (XI et al., 2019), atmospheric conditions and aerosols are variable in space and time and have significant impacts on remote sensing images. Since atmospherically corrected images are essential to assess spectral indices with spatial reliability and product comparison, level-1C data have been processed to level-2A (top-of-canopy) taking into account the effects of aerosols and water vapor on reflectance. Therefore, the QGIS tool within the Semi-Automatic Classification plugin realized only 10 bands for atmospheric correction of Sentinel level-1C imagery. The algorism uses only 10 bands and B1 (coastal aerosol), strongly influenced by the atmosphere and band B9 and B10, which were water vapor and cirrus, did not provide spectral information about the Earth’s surface. Due to this reason, they were not included in the pre-processing steps.

3.5.2 Geometric Correction

The ESA provides free geometrically corrected Sentinel 2A data collections and the images were acquired in cartographic geometry (WGS84 UTM 37N) projection from the website of ESA (*http://step.esa.int/main/download/*). Therefore there is no need for geometric correction for this data.

3.5.3 Resampling

Sentinel-2A MSI image bands have different spatial resolutions through the wavelength portions. Thus, there was a need for uniform spatial resolution for analyses such as spectral profile generation, spectral index generation, and multispectral image classification. Previous studies performed a relative analysis to evaluate the effects of downscaling and upscaling to 10 m and 20 m resolution with Sentinel-2 images, respectively. The result shows that downscaling to 10 m resolution yields high classification accuracies rather than upscaling 20m resolution, due to a loss of spatial details and an increase in the number of mixed pixels, by combining four adjacent pixels (Zhang et al., 2018). Therefore, Sentinel-2A imageries with 20 m resolution bands were resampled to 10 m, by using the nearest neighbor method, to preserve the spatial resolution integrity.

The nearest neighbor resampling method is preferable because of its easy implementation and spectral information preservation. After atmospheric corrections, the two scenes will be mosaic and clipped based on the area of interest.

3.6 Spectral Built-up Indices Computation

Spectral indices provide relevant feature information in various remote sensing applications within less computational time (Ghosh et al., 2018). Index-based methods are designed based on spectral bands to enlarge the intensity contrast between a particular land cover and the background, where specific land covers present their maximum and minimum reflectance values among a multispectral dataset. Ideally, the result of normalized difference should in the range from -1 to 1 to produce a new component. Where 1 represents the specific land cover, while -1 indicates background areas.

Mathematically, if Bi and Bj are the ith and jth bands from a multispectral image set respectively, then the expression for computation of a given index is as follows (Valdiviezo-N et al., 2018).

$$ND = \frac{B_i - B_j}{B_i + B_j} \tag{1}$$

The classification of impervious surface assumes different spectral patterns for multiple bands to delineate built-up pixels and non-built-up pixels (barren lands, vegetation, forest, water bodies, and so on) in satellite image (Mukherjee et al., 2021). Blue, Green, Red, near-infrared (NIR), and short-wavelength infrared (SWIR) portions of the electromagnetic spectrum in remote sensing imagery are generally used for the calculation of spectral indices (Pandey & Tiwari, 2020). Red and near-infrared (NIR) bands have a high-level correlation and have significant positive coefficients for the classification with barren pixels and green respectively (Mukherjee et al., 2021). For example, the normalized difference vegetation index (NDVI), which is used for extracting plant, is calculated as the difference between NIR and RED bands such as

$$NDVI = \frac{B_{nir} - B_{red}}{B_{nir} + B_{red}} \tag{2}$$

When compared to barren pixels, urban built-up areas have a lower mean value in RED and NIR bands. Therefore, this concept makes it easy to separate the distribution of built-up pixels from the same green and barren pixels in inverse relationship to RED and NIR bands.

Since the reflectance of built-up areas is higher in SWIR and NIR regions in contrast to other spectral regions. The corresponding band comparison was needed for calculating built-up indices (Pandey & Tiwari, 2020). Recently, the availability of Sentinel 2A data advances the computation of spectral built-up indices by introducing two NIR (band 8 and band 8A) and two SWIR (band 11 and band 12) bands. Band 8 (NIR) has a wider spectral range than Band 8A (NIRnarrow) and is intended for generating outputs in 10 m resolution (XI et al., 2019).

Therefore, only Band 8 was used in the computation by omitting Band 8A. SWIR has higher reflectance than other spectral bands of the electromagnetic spectrum, therefore a multitude of spectral indices designed to extract urban impervious surfaces, have been proposed in the literature. Based on this, seven spectral built-up indices (UI, NDBI, NBI, NBAI, BRBA, MBI, and BAEI) were computed to evaluate their accuracy in the extraction of urban impervious surfaces.

Table 3-4: Sentinel 2A spectral bands employed to compute built-up indices

Band	Wavelength (nm)	Specification
3	559	B_{GREEN}
4	665	B_{RED}
8	833	B_{NIR}
11	1610.4	B_{SWIR1}
12	2185.7	B_{SWIR2}

3.6.1 Urban Index (UI)

The urban index (UI) is first proposed by (Kawamura, 1996) for the extraction of urban built-up areas. It makes use of short wave infrared (SWIR1) or (B11) and NIR channel or (B8). The UI was intended to exploit the inverse relationship between the brightness of urban areas in the NIR and SWIR channels as shown in equation (3)

$$UI = \frac{B_{SWIR1} - B_{NIR}}{B_{SWIR1} + B_{NIR}} \tag{3}$$

Where, B_{SWIR1} and B_{NIR} are the surface reflectance value of the first shortwave-infrared and near-infrared band, respectively.

3.6.2 Normalized Difference Built-up Index (NDBI)

The normalized difference built-up index (NDBI) is proposed by (Zha et al., 2003) for creating a built-up index image. It utilizes the difference and the ratio of short wave infrared (SWIR2) or (B12) and Near Infrared band (NIR) or (B8) to highlight the built-up areas as depicted in equation (4)

$$NDBI = \frac{B_{SWIR2} - B_{NIR}}{B_{SWIR2} + B_{NIR}} \tag{4}$$

Where, B_{SWIR2} and B_{NIR} are the surface reflectance value of the second shortwave-infrared and near-infrared band, respectively.

The difference between NDVI from NDBI result built-up and bare land with positive values ranges from 0 to 1, while background features are marked with negative values ranges from 0 to −1. This index takes improvement in its computation speed and its simplicity.

3.6.3 New Built-up Index (NBI)

The new built-up index (NBI) was proposed by (Jieli et al., 2008) observing the spectral response of different land covers in the RED, NIR, and SWIR bands. Based on the fact that the spectral response of each land cover is most distinctive from one another, especially barren land is greater than the other for each band listed above. The new built-up index (NBI), makes use of the RED (B4), NIR (B8), and SWIR (B12) bands according to the expression:

$$NBI = \frac{B_{RED} * B_{SWIR2}}{B_{NIR}} \tag{5}$$

Where, B_{RED}, B_{SWIR2} and B_{NIR} are the surface reflectance value of visible red band, the first shortwave-infrared and near-infrared band, respectively.

3.6.4 Band Ratio for Built-up Area (BRBA)

(Waqar et al., 2012) developed a new index named, band ratio for the built-up area (BRBA). To effectively discriminate impervious surface areas, the indices make use of RED (4) and

SWIR2 (B12) bands as shown in equation (6). BRBA uses various combinations of bands to extract urban built-up areas more accurately as shown in equation (6).

$$BRBA = \frac{B_{RED}}{B_{SWIR2}} \tag{6}$$

Where, B_{RED} and B_{SWIR2} are the surface reflectance value of the visible red band and the second shortwave-infrared, respectively.

3.6.5 Normalized Built-up Area Index (NBAI)

These indices were also developed by (Waqar et al., 2012) to delineate the impervious surface from previous using the bands, GREEN (B2), SWIR1 (B11), and SWIR2 (B12) as shown in equation (7).

$$NBAI = \frac{B_{SWIR2} - B_{SWIR1}/B_{GREEN}}{B_{SWIR2} + B_{SWIR1}/B_{GREEN}} \tag{7}$$

Where, B_{GREEN}, B_{SWIR1} and B_{SWIR2} are the surface reflectance value of the visible green band, first shortwave-infrared and the second shortwave-infrared, respectively.

3.6.6 Modified Built-up Index (MBI)

Modified Built-up Index (MBI) was proposed by (Liu et al., 2014) to magnify the contrast between built-up and non built-up areas. The MBI index utilizes RED or (B4), Near Infrared band (NIR) or (B8), and short wave infrared (SWIR1) or (B11) to highlight the built-up areas and it is given by the following equation (8).

$$MBI = \frac{B_{SWIR1} * B_{RED} - (B_{NIR} * B_{NIR})}{B_{RED} + B_{NIR} + B_{SWIR1}} \tag{8}$$

Where, B_{RED}, B_{SWIR1} and B_{NIR} are the surface reflectance value of the visible red band, first shortwave-infrared and near-infrared, respectively.

3.6.7 Built-up Area Extraction Index (BAEI)

Built-up area extraction index (BAEI) first introduced by (Bouzekri et al., 2015) made use of RED (B4), GREEN (B2), and short wave infrared (SWIR1) bands, and apart from using spectral channels, this indices uses an arithmetic constant L to enable the extraction according to the expression (9)

$$BAEI = \frac{B_{RED} + 0.3}{B_{GREEN} + B_{SWIR1}} \qquad (9)$$

Where, B_{GREEN}, B_{RED}, B_{SWIR1} and L are the surface reflectance value of the visible green band, red band, first shortwave-infrared and arithmetic constant which is 0.3, respectively.

3.7 Image Classification

Image classification is the process of conveying pixels/objects of the image to the predefined LULC classes. It is mostly used in remote sensing for various purposes. However, its result is affected by many factors which affect the classification accuracy such as the spatial resolution of the remotely sensed data, selection of a suitable classification method, classification software, and the nature of the study area, etc. (Parveen et al., 2018). Therefore, these factors must be considered when selecting a classification method for use. To identify and reduce uncertainties caused by mixed pixels in the image-processing, researchers categorized the image processing into two major classes, namely; parametric classifier and non-parametric classifier (D. Lu & Weng, 2007). In this study non-parametric classifier (support vector machine) was used by selecting the representative region of interest for each land use land cover class.

3.8 Urban Land Cover Classification Based on SVM classifier

In this study, five major land covers are automatically mapped using a support vector machine classifier. SVM is a supervised classification that received a lot of attention from the research community because of its fair classification results and in quantifying remote sensing data (Bramhe et al., 2018). It rests upon machine learning algorism to label the pixels in an RS image as representing a particular class or land cover types. In supervising classification two information is considered, which is ‘features’ in multiple bands of satellite image and ‘label’ the class to which each pixel belongs (built-up or non-built-up) (Mukherjee et al., 2021).

Among from non-parametric binary statistical learning methodology, SVM is one of it, which separate a dataset into classes (training data) based on a decision boundary or hyperplane to reduce misclassification on unseen data without prior assumptions made on the probability distribution of the data (Mountrakis et al., 2011) as shown below in figure 3-8.

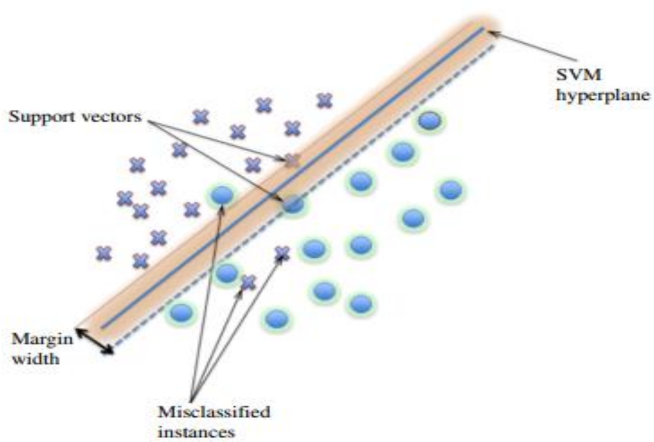

Figure 3-8: Linear support vector machine example

Source: adapted from (Burges, 1998)

In this study, the SVM machine learning classification approach is applied to Sentinel-2A MSI data for the years 2016, 2018, and 2020. In addition, ten bands of Sentinel-2A image were classified using the training samples, defined by the region of interest (ROI). The performance of SVM’s is dependent on the selection of the appropriate kernel type

(Ndehedehe, 2014). Therefore, for this study, a radial basis function kernel is selected as it is found to be more suitable for LULC applications.

The classification process was performed using the ENVI software, which requires a set of parameter definitions. The gamma is the most critical parameter and was the only parameter changed in this research, which is 0.01 to minimize the computation time and increase the quality of image classification. The penalty parameter is set to 100 to reduce misclassification in the training step. To guarantee each pixel is assigning to the correct class, the classification probability threshold should be set to zero. When the pyramid level is assigned to zero, the classification of each land cover to be performed directly on the original image pixels, instead of the first-pass classification on low-resolution pyramid layers. The Region of Interest (ROI) is used as a spectral signature for five land use and land cover categories namely built-up, barren, vegetation, forest, and water.

Table 3-5: Description of LULC Classification

Class name	Description
Built-up	Land covered by buildings and other man-made structures such as residential, commercial, industrial area, parking lots, railways, and road networks
Bare land	Lands with exposed soil, sand, or rocks, and never have more than 10% vegetated cover during any time of the year. Bare ground, barely exposed rocks, strip mines, quarries, and gravel pits
Vegetation	Rain feed arable lands, cultivated field, irrigated cropland and farming lands
Forest	Lands dominated by manmade and natural forests trees with a percent cover >60% and height exceeding 2 meters, Deciduous forest land, and evergreen forest land
Water bodies	Lakes, reservoirs, ponds, marshes, rivers, stream, and swamps

Source: (Latham et al., 2002)

LULC classification in SVM consists of three stages; the first is selecting the training area which is created by creating a polygon for each class and the area selection is performed manually, the second, creating the region of interest. The training area is stored as a region of interest that is generated in spatial space (only based on pixel values). Lastly, classify the image based on the region of interest as shown in Figure 3.9.

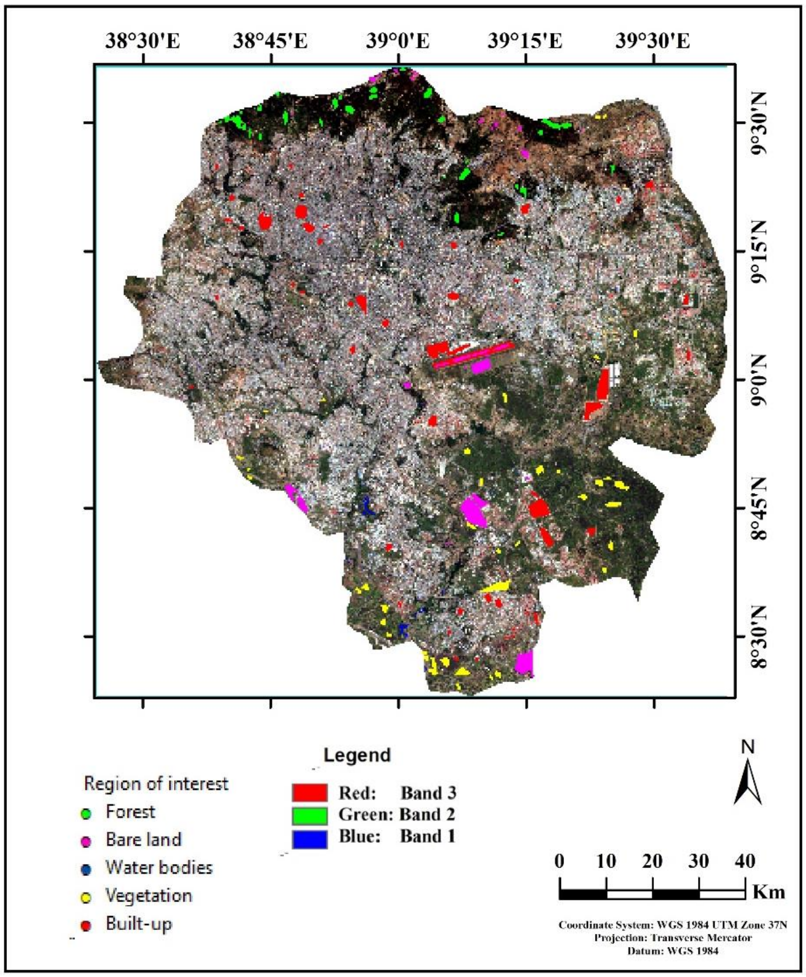

Figure 3-9: Region of interest for 2020

3.9 Land Use Land Cover Change Detection

The LULC changes were detected between two pairs of LULC maps between 2016 and 2020. The detections were held between the years (2016 – 2018, 2018 – 2020, and 2016 - 2020). Using post-classification comparison techniques the area of each LULC class changed to all other LULC classes were identified. The area coverage of the change in each

LULC category can be identified in a change detection matrix. This matrix is a square matrix containing all LULC categories in rows and columns. The values were presented in terms of hectares and percentages. The percentage LULC changes were calculated using the following equation:

$$\text{LULC change (\%)} = \frac{(A_2 - A_1)}{(A_1)} * 100 \qquad (10)$$

Where,

LULC change – change of land use land cover

A1 - Area of each LULC classes for the initial image

A2 - Area of each LULC classes for the later image

The LULC change rate was computed using the formula suggested by (Puyravaud, 2003):

$$R = (1/\Delta t) \ln (A2/A1)*100 \qquad (11)$$

Where,

R - Annual rate of change in %;

Δt - Time interval in years during the LULC change being assessed;

ln - The base of the natural logarithm function;

A1 - Area of each LULC classes for the initial image

A2 - Area of each LULC classes for the later image

The matrix shows the number of changes in hectare and the percentage of which LULC class changed to other classes. The values of the rate of changes can be negative or positive to show either the LULC class has decreased or increased between the two years. The LULC categories decreased between two different years showed a negative rate of change values. The persistence values were the diagonal values which mean unchanged amount. The gain values are computed by subtracting the persistence value from the total area of the final year and the loss value is also computed by negative of subtracting the persistence value from the total area of the initial year.

3.10 Spectral Discrimination Index

The accuracy of the extracted impervious surface through spectral built-up indices varies from one index to another. However, to quantify the degree of separation between such land covers, spectral discrimination index (SDI) was employed, based on the means and Standard Deviations (SD) of the classes (Kaufman & Remer, 1994). SDI is the difference of the mean value of two classes divided by the sum of their standard deviations. To avoid the negative value in the difference in means value it is replaced by the absolute value (Y. Deng et al., 2015). SDI with a value larger than 1 means that the two classes are well separable, while values smaller than one indicate a large degree of histogram overlap between the two classes (Pereira, 1999). In this study, the two-sample class distributions refer to the distributions of built-up index computed for built-up pixels and non-built-up pixels.

$$SDI = \frac{|\mu_1 - \mu_2|}{\sigma_1 + \sigma_2} \qquad (12)$$

Where,

SDI- Spectral discrimination index

μ_1 and μ_2 - mean index values of classes 1 and 2

σ_1 and σ_2 - standard deviations of classes 1 and 2

Here, the supervised classification result obtained by machine learning algorism (SVM) and impervious surface abundance achieved by various spectral built indices were taken for generating mean and standard deviation of the two classes. The result of these two statistical values was summarized using the zonal statistics tool of the Arc GIS10.5.

3.11 Accuracy Assessment

Accuracy assessment is an integral part of an image classification procedure. To evaluate the accuracy of the classification results and robustness of the seven spectral built-up indices (UI, NDBI, NBI, NBAI, MBI, BAEI, and BRBA), omission error (OE), commission error (CE), overall accuracy (OA) and overall kappa index of agreement (KIA) were derived from the confusion matrix. A suitable classification system and a sufficient number of training samples are prerequisites for successful classification. Accuracy assessment is to quantitatively assess how effectively the pixels were assigned to the correct land use land cover classes (Rwanga & Ndambuki, 2017).

The accuracy assessment of the classification results was performed with random sample points. Ground truth data collected from the field, aerial photographs, and google earth imagery were used as the reference data to assess the accuracy of classification. A random point distribution was designed, according to the heterogeneity potential and areal coverage of the classes. At least 50 points per LULC class must be collected for areas less than 4000 km2 and having fewer than 12 classes (MacLean & Congalton, 2012; H. Zhang et al., 2009). For this study 50 points per class were collected, a total of 250 points were collected for five land-use classes i.e. Built-up, Bare land, Forest, Vegetation, and Waterbodies for the validation of LULC classification.

Also, 200 sample points were collected for built-up and non-built-up LULC type to validate the results from each spectral built-up indices. Field data and aerial photographs were used to validate the classification output both for LULC classification by SVM and by spectral built-up indices for the year 2020 and google earth for 2016 and 2018. A qualitative assessment through visual comparison between the index-derived LUC maps and the reference images was also done. The training sample distribution and the number of points used in the accuracy assessment are provided with the reference in figure 3-10.

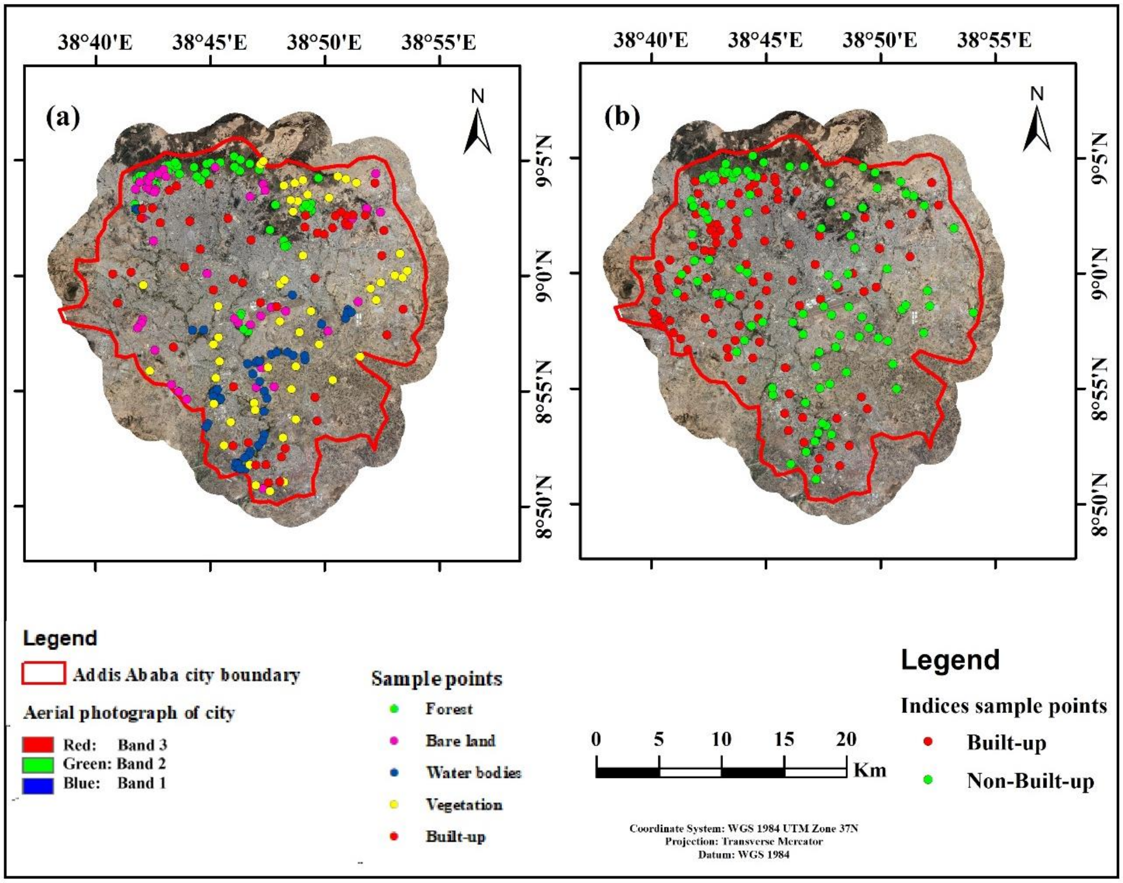

Figure 3-10: The sample points (a) for five LULC types by SVM, (b) for two LULC type by spectral built-up indices for 2020

CHAPTER FOUR

4. RESULTS

4.1 Impervious Surface Indices Results

4.1.1 Built-up Area Extraction Index (BAEI)

Figure 4-1 indicates the built-up area extraction index (BAEI) map of Addis Ababa city for the years 2016, 2018, and 2020. In 2016, 0.31 were recorded which is the lowest value and in 2020, 11.8 which is the highest BAEI value. In general the values of BAEI ranges from (0.31 – 3.81), (0.41 – 6.1), and (1.4 – 11.8) in 2016, 2018, and 2020, respectively.

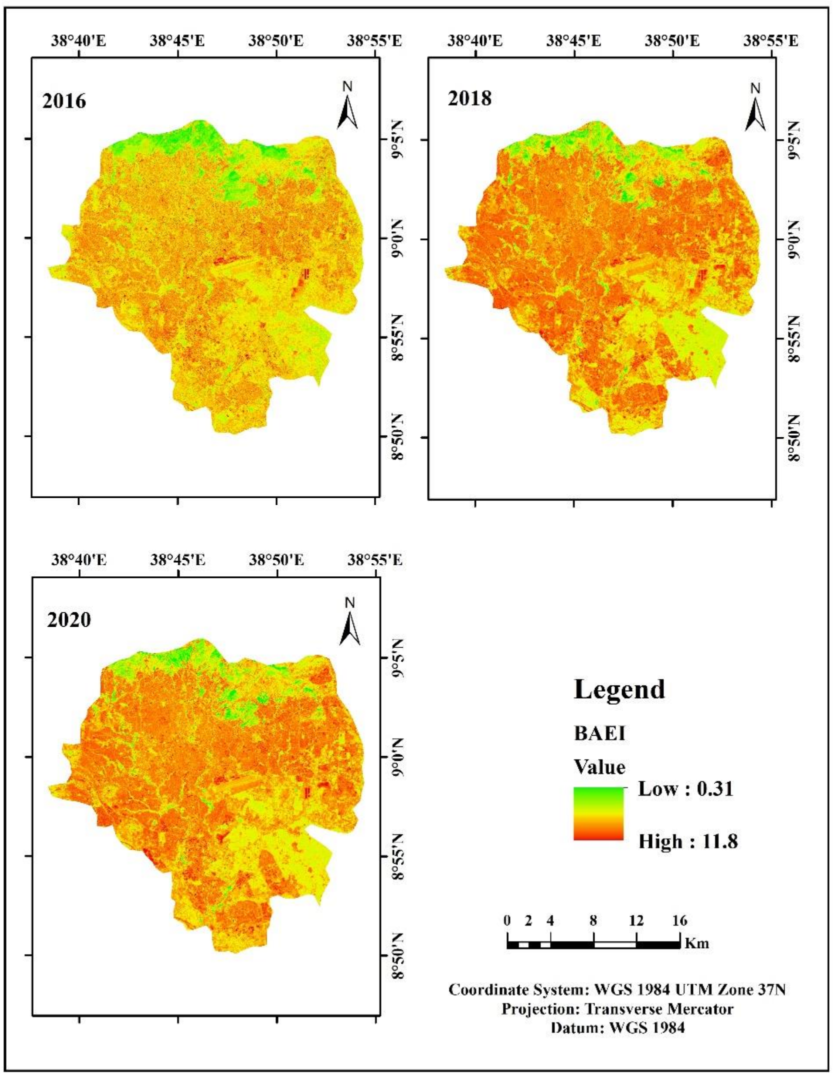

Figure 4-1: Built-up Area Extraction Index Maps

4.1.2 Band Ratio for Built-up Area (BRBA)

Band ratio for built-up area (BRBA) is one of the built-up extraction index in this study. BRBA demonstrates built-up area maps for 2016, 2018, and 2020. In this index 0.03 were recorded as the lowest value in 2016 and 4.64 were the highest value in 2018 as shown in figure 4-2 BRBA ranges from (0.03 - 4.05), (0.14 - 4.64), and (0.13 – 4.48) for the years 2016, 2018 and, 2020, respectively.

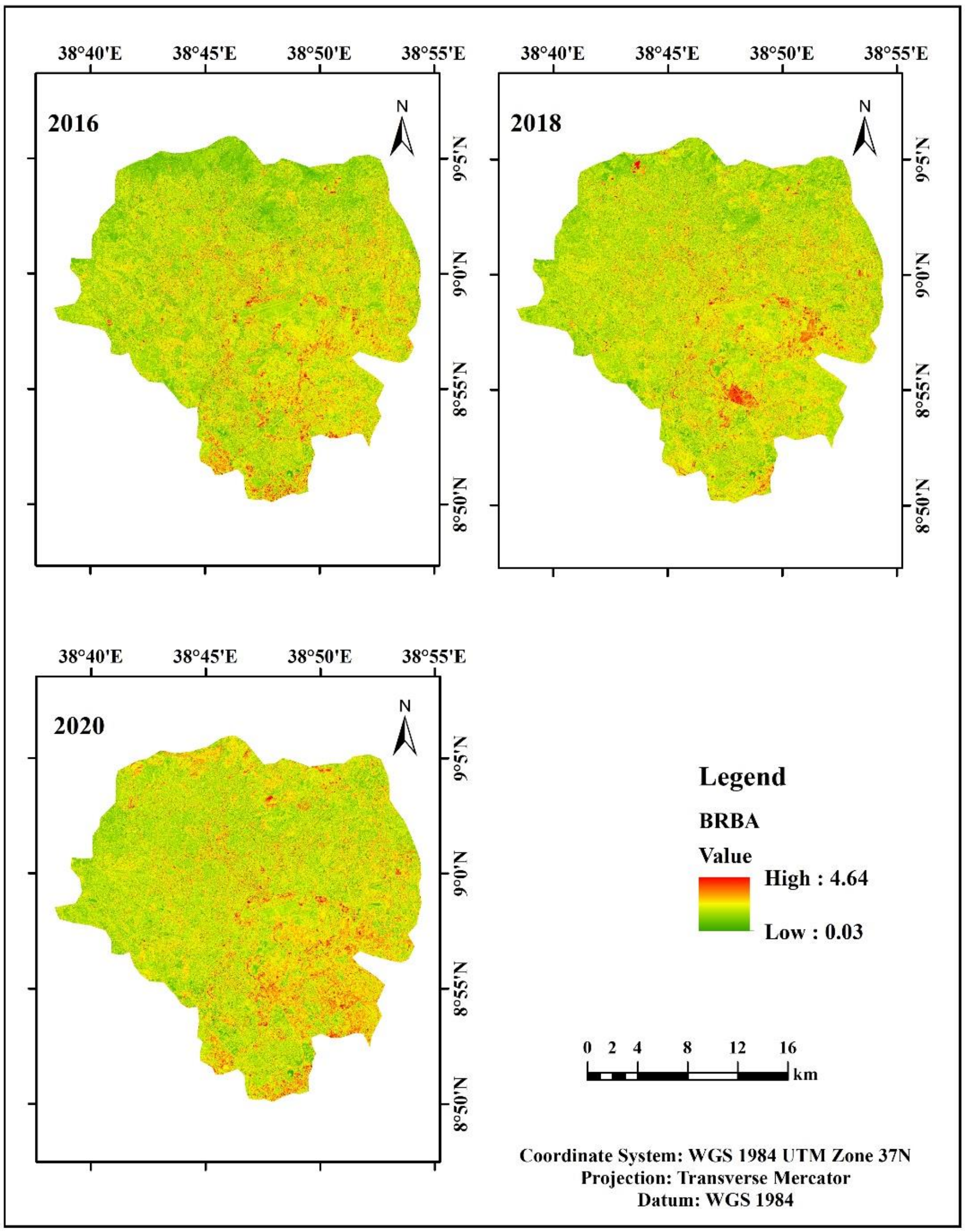

Figure 4-2: Band Ratio for Built-up Area Maps

4.1.3 Modified Built-up Index (MBI)

Figure 4-3 shows the MBI maps for the years 2016, 2018, and 2020. MBI recorded the lowest value (-4.18) in 2016 and the highest value (2) in 2020 as shown below. Based on the result of MBI value ranges from (-4.18 – 1.28), (-0.32 – 0.16), and (-3.44 – 2) in the years 2016, 2018, and 2020, respectively.

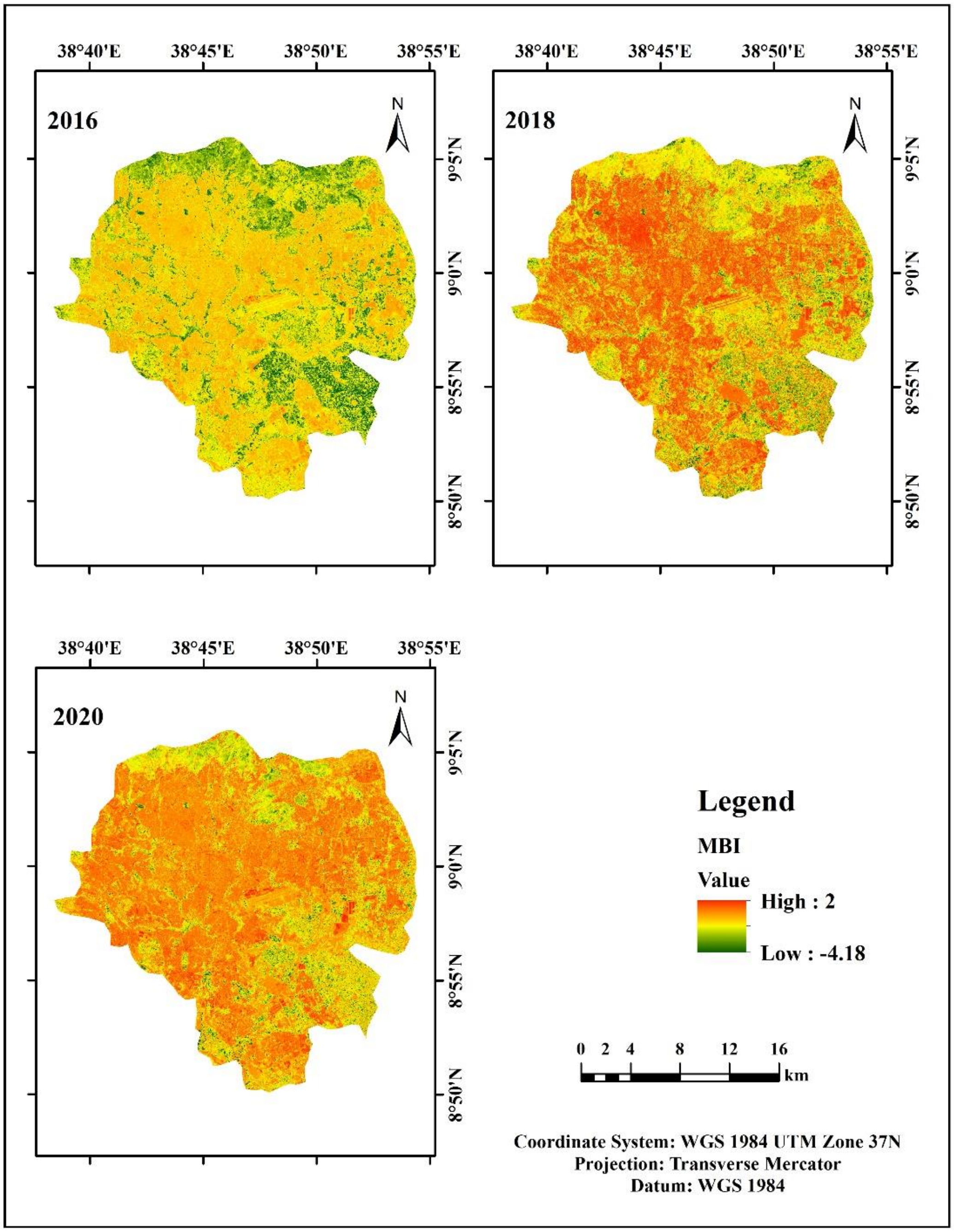

Figure 4-3: Modified Built-up Index Maps

4.1.4 Normalized Built-up Area Index (NBAI)

Figure 4-4 shows a normalized built-up area index (NBAI) map of the built-up area for 2016, 2018, and 2020. In this index -0.47 was recorded as the lowest value in 2016 indicated by the green one and 0.45 was the highest value in 2020 marked by the red as shown below. NBAI ranges (-0.47 – 0.33), (-0.37 – 0.41), and (-0.44 – 0.45) for the year of 2016, 2018 and, 2020, respectively.

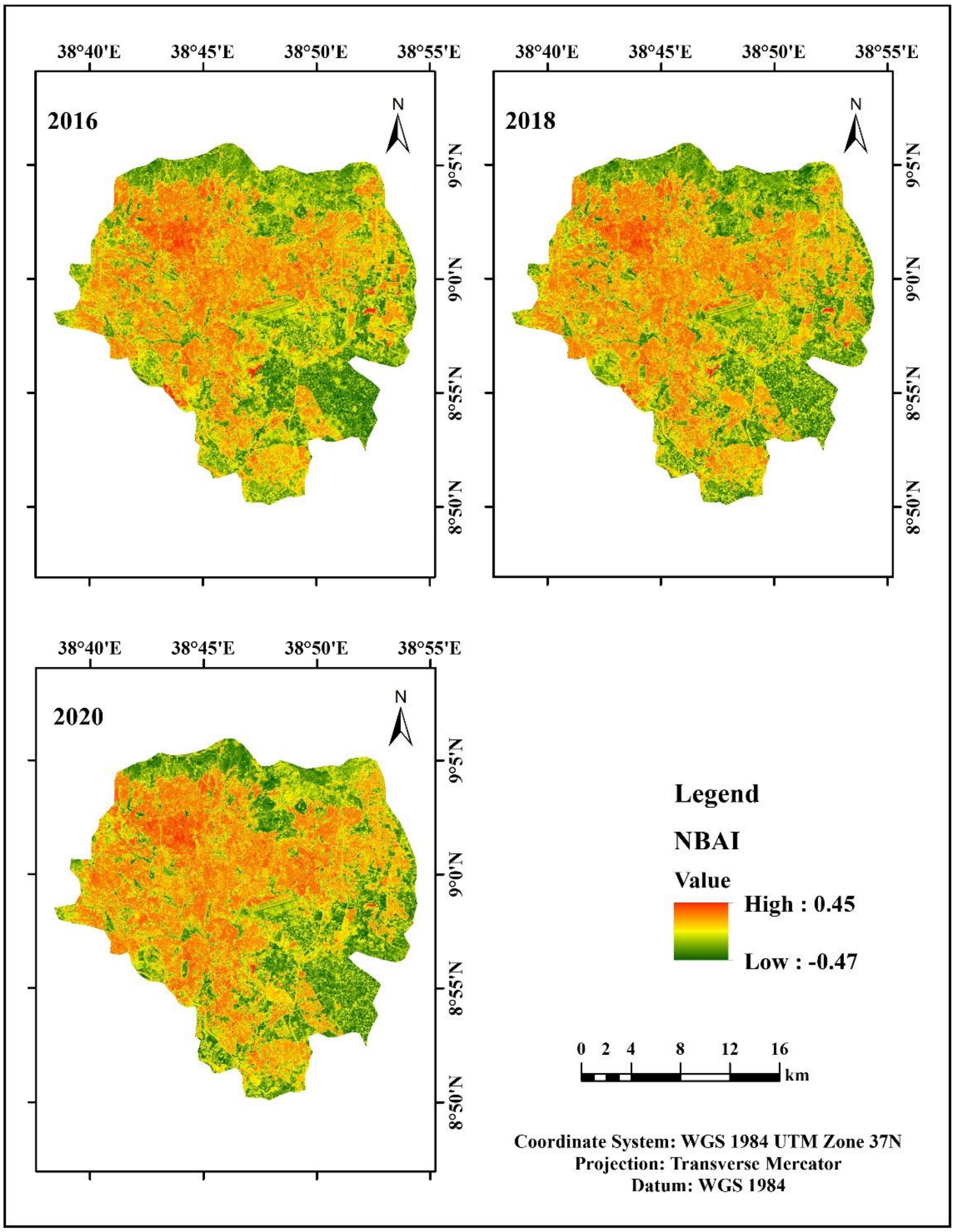

Figure 4-4: Normalized Built-up Area Index Maps

4.1.5 New Built-up Index (NBI)

Figure 4-5 shows the NBI maps for 2016, 2018, and 2020. The year 2020 has the highest NBI value (1.16). In this result, the lowest value (0.01) recorded for the three years is similar. The value of NBI ranges (0.01 – 0.59), (0.01 – 1.15), and (0.01 – 1.16) for the years 2016, 2018, and, 2020, respectively.

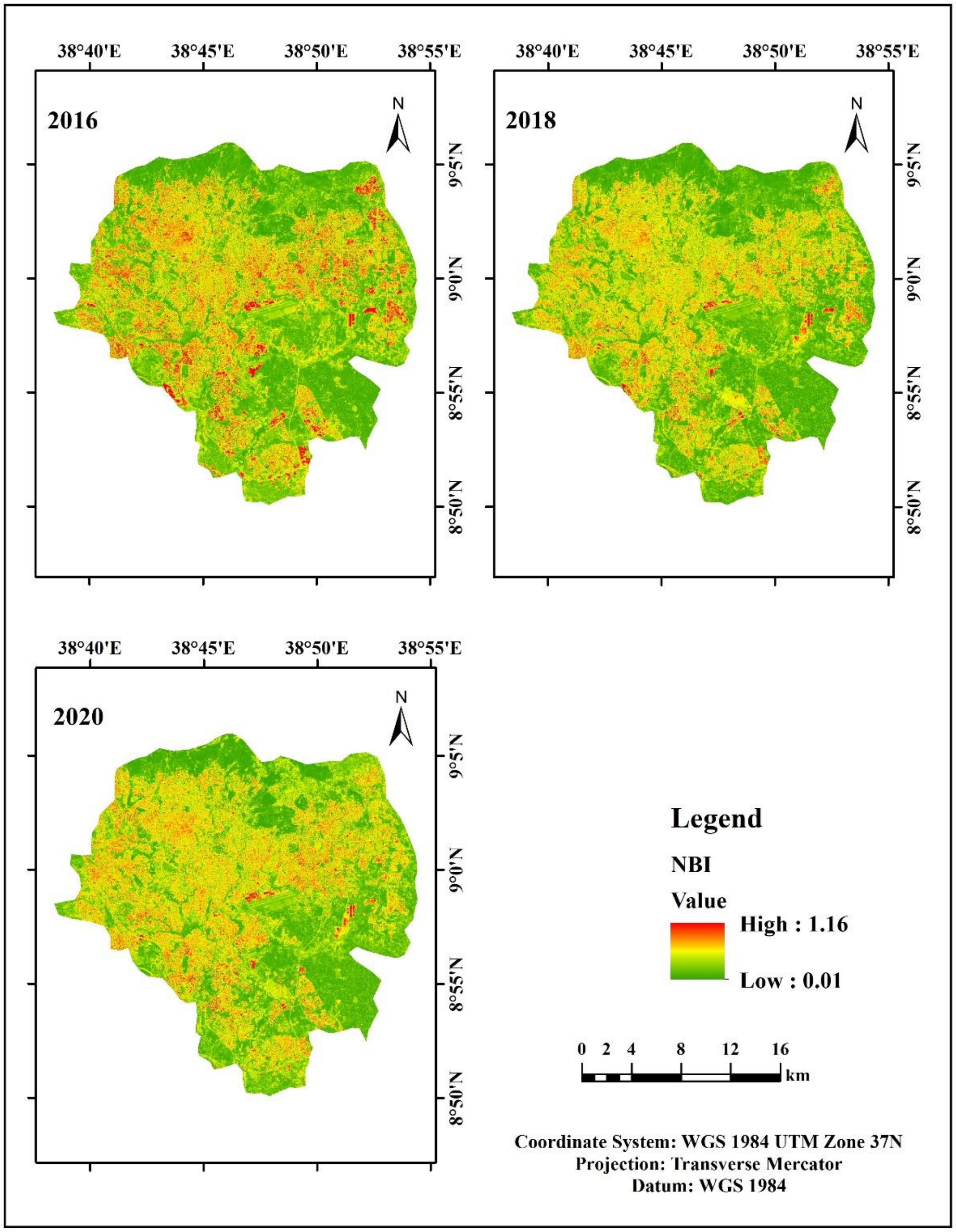

Figure 4-5: New Built-up Index Maps

4.1.6 Normalized Difference Built-up Index

Figure 4-6 shows NDBI maps for 2016, 2018, and 2020. The highest value of NDBI was (0.73) and the lowest value of NDBI was (-0.78), both values were recorded in 2016. The value of NDBI was ranges (-0.78 – 0.73), (-0.71 – 0.68) and (-0.76 – 0.71) for the years 2016, 2018, and 2020, respectively.

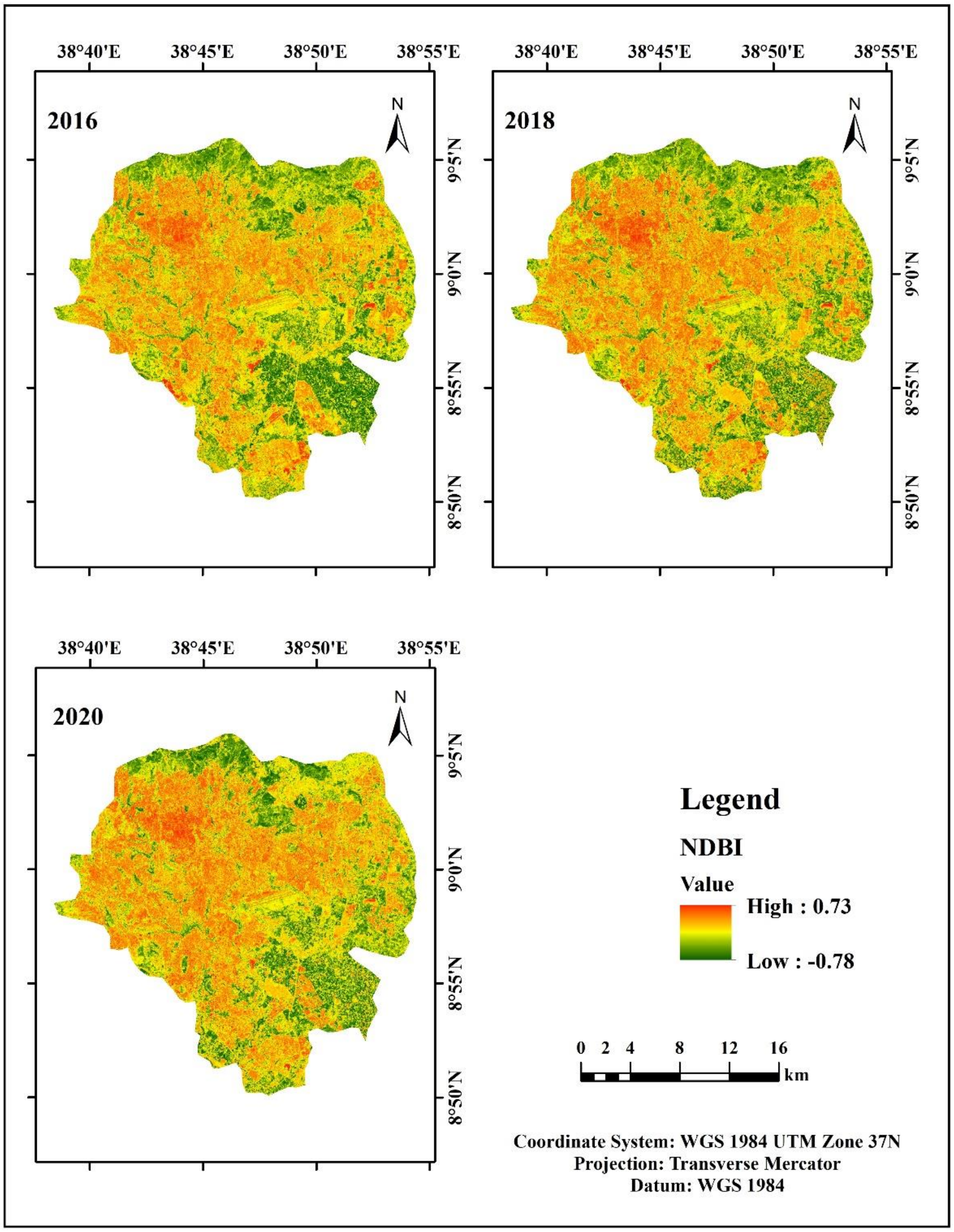

Figure 4-6: Normalized Difference Built-up Index Maps

4.1.7 Urban Index (UI)

Figure 4-7 shows UI maps for 2016, 2018, and 2020. The highest value of UI was (0.69) and the lowest value of UI was (-0.57), both values were recorded in 2018. The value of UI was ranges (-0.53 – 0.65), (-0.57 – 0.69), and (-0.54 – 0.59) for the years 2016, 2018, and 2020, respectively.

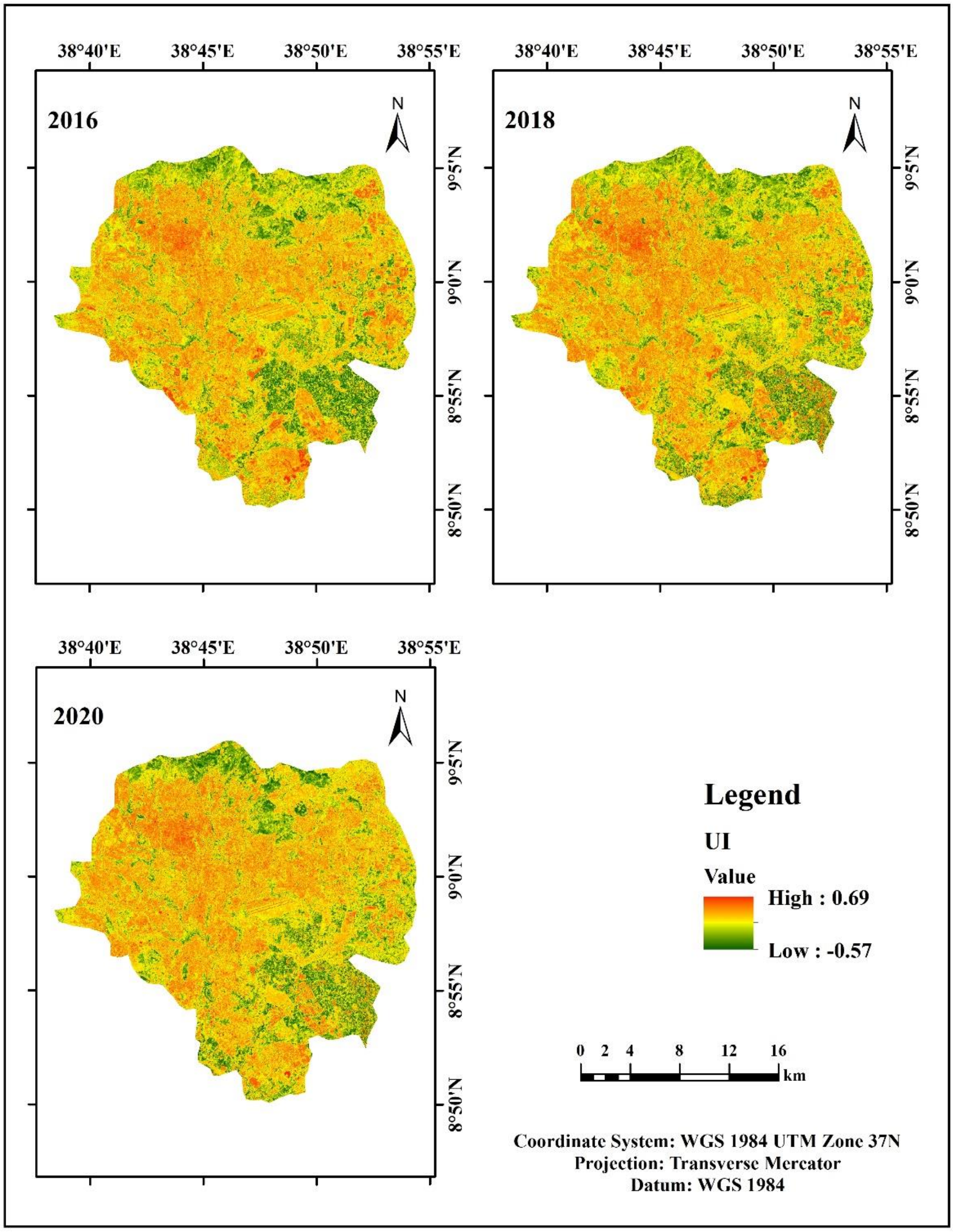

Figure 4-7: Urban Index Maps

4.2 Urban Land Use Land Cover Classification

In this study, five LULC classification maps were produced for the years 2016, 2018, and 2020 as shown in figures 4-8, and Spatio-temporal area coverage was analyzed in table 4-1. In 2016 the total area was covered by bare land (22.8%), forestland (6.1%), vegetation (37.2%), and water bodies were covered 0.3%. and the remaining parts of the area were covered with built-up (33.6%). In 2018, bare land, forestland, vegetation, and water were covered 24.7%, 6%, 23.1%, and 0.5% of the total area respectively. The rest of the areas were covered with built-up (45.6%). In 2020, bare land (24.3%), built-up (50.4%), forestland (5%), vegetation (20%) and water (0.3%) were covered the total area. To some extent in the classification, the vegetation LULC type was generalized to other classes, but as evident in the field observation, vegetation is highly diminished due to urbanization. The vegetation cover has been declining since the year 2016 in the order of 37.2% for 2016, 23.1% for 2018, and 20% for 2020. However, the built-up coverage has been increased by these years, in 2016 (33.6%), in 2018 (45.6%), and 2020 (50.4%).

As shown in table 4-2 the change in bare land, built-up area, and water bodies from 2016 to 2018 were increased by 1031.5 ha, 6499.8 ha, and 143.5 ha respectively while forest and vegetation were decreased by 87.3 ha and 7587.5 ha. The change from 2018 to 2020 showed that the built-up area was highly increased by 2584.7 ha while bare land, forestland, vegetation, and water bodies were decreased by 218.4 ha, 533 ha, 1691.8 ha, and 141.5 ha respectively. From 2016 to 2020, built-up area, bare land, and water bodies were increased, especially the built-up area are radically changed by 9084.5 ha, 813 ha, and 2 ha respectively. Initially, the vegetation coverage was more than the other land cover types but later it shifts to bare land and built-up area.

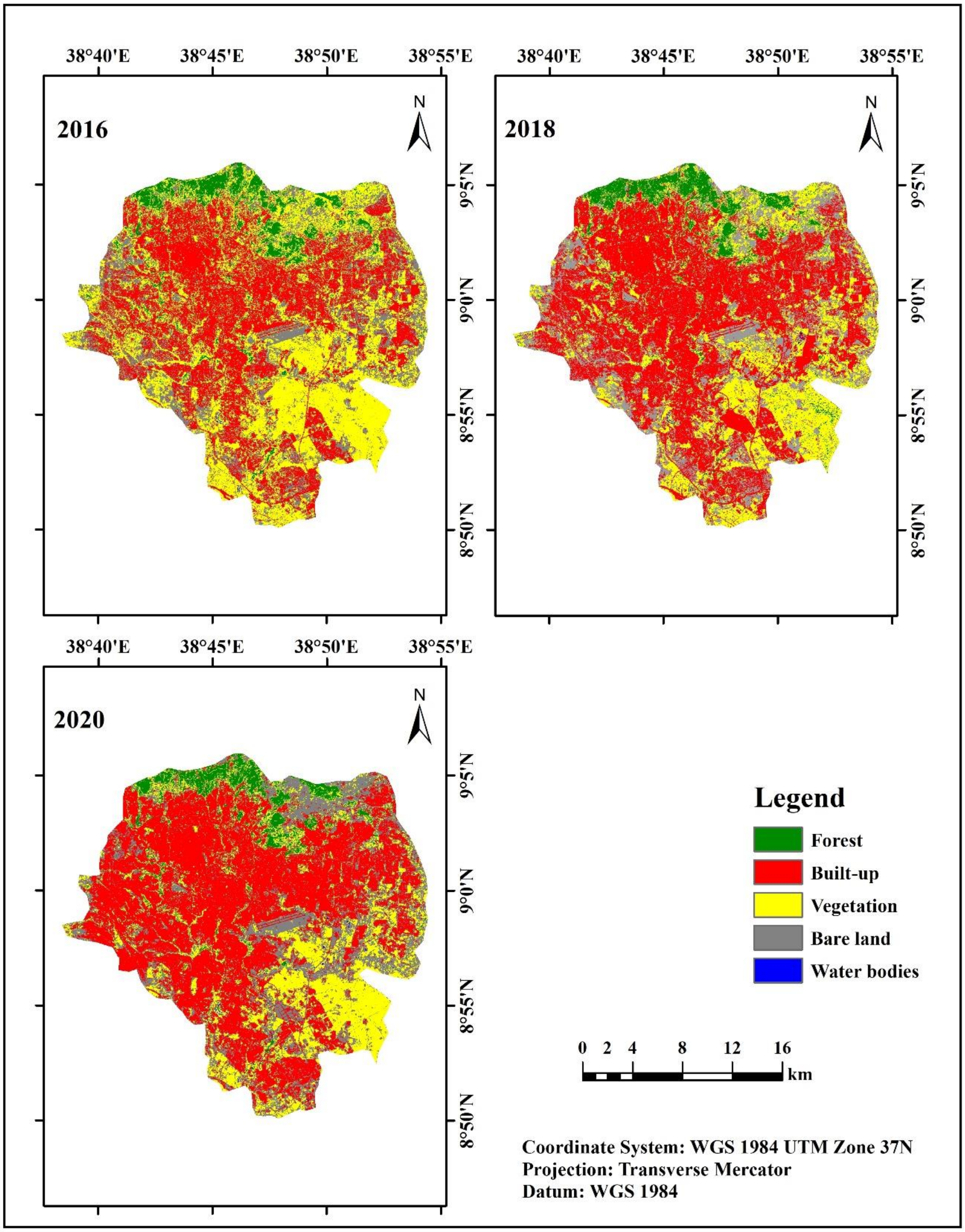

Figure 4-8: Land Use Land Cover Maps

Table 4-1: Area coverage of LULC

Area coverage in (2016, 2018 and 2020)						
	2016		2018		2020	
LULC Type	Ha.	%	Ha.	%	Ha.	%
Bare land	12287.5	22.8	13319.0	24.7	13100.5	24.3
Built-up	18101.9	33.6	24601.7	45.6	27186.4	50.4
Forest	3303.2	6.1	3216.0	6.0	2683.0	5.0
Vegetation	20054.8	37.2	12467.3	23.1	10775.5	20.0
Water	152.7	0.3	296.2	0.5	154.7	0.3
Total	53900.1	100	53900.1	100	53900.1	100

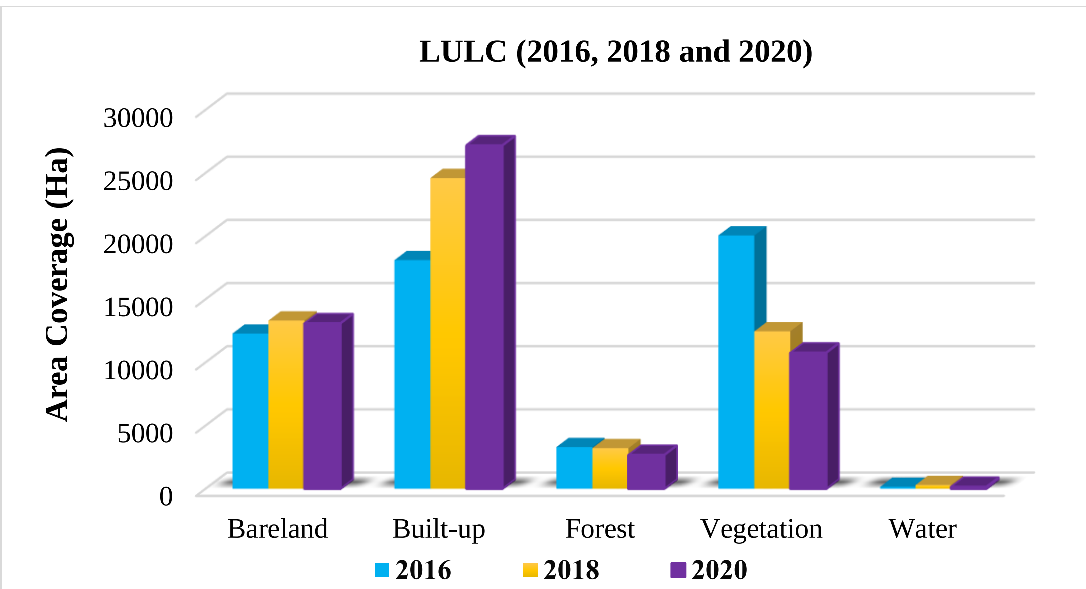

Figure 4-9: Area coverage of LULC type between 2016 and 2020

Based on table 4-2 the rate of LULC change in the urban area in between 2016-2018, 2018-2020, and 2016-2020. Built-up area (15.3%) and water bodies (33.1%) changed with the highest rate from 2016 to 2018. Similarly bare land (4%) shows some rate of change while forest and vegetation values were declined by (-1.3) and (-23.8%) respectively. In the period 2018 to 2020, except the built-up area (5%) all other land covers were decline by (-0.8%)

for bare land, (-9.1%) for forest, (-7.3%) for vegetation and (-32.5%) for water bodies. In general, from the period of 2016-2020, there was a high rate of change in a built-up area (20.3%). Likewise, bare land (3.2%) and water bodies (0.7%) show some rate of change, however, forest and vegetation were decreased by (-10.4%) and (-31.1%) respectively.

Table 4-2: LULC transformation between 2016, 2018 and 2020

LULC transformation between 2016, 2018 and 2020									
	Change 2016-2018			**Change 2018-2020**			**Change 2016-2020**		
LULC Type	Ha	%	Rate (%)	Ha	%	Rate (%)	Ha	%	Rate (%)
Bare land	1031.5	8.4	4.0	-218.4	-1.6	-0.8	813.0	6.6	3.2
Built-up	6499.8	35.9	15.3	2584.7	10.5	5.0	9084.5	50.2	20.3
Forest	-87.3	-2.6	-1.3	-533.0	-16.6	-9.1	-620.2	-18.8	-10.4
Vegetation	-7587.5	-37.8	-23.8	-1691.8	-13.6	-7.3	-9279.3	-46.3	-31.1
Water	143.5	94.0	33.1	-141.5	-47.8	-32.5	2.0	1.3	0.7

4.3 Accuracy Assessment for Classified LULC Map

Classified LULC maps from remotely sensed imageries may contain some errors. Therefore, accuracy assessment was employed to find out those errors to ensure the reliability of the produced LULC maps. The classification results in figure 4-8 shows, five main urban land use land cover types that are identified and mapped using 50 random samples point for each class total 250 sample point for the year of 2016, 2018 and 2020. These metrics have been considered for test data on which assessment has been done using the trained machine learning (SVM) model.

Numerous quantitative measures are existing to compute the effectiveness of the trained model. Non-overlapping samples were taken from training or mutually exclusive samples for quantitative analysis and validation to calculate overall accuracy and kappa coefficient. The classified maps have to be assessed and compared with a referenced data and ground truth using an error matrix.

As shown in table 4-3, table 4-4, table 4-5 the overall accuracies for 2016, 2018, and 2020 are 85%, 89%, and 86% with the Kappa statistics of 0.81, 0.86, and 0.82, respectively. Results of user's accuracy in this study showed that in 2016 water bodies had the maximum class accuracy of 100%, and the minimum was for the bare land area (59%).

For the year 2018, user's accuracy ranged from the lowest accuracy 81% (built-up) to relatively correctly classified 100% (water bodies); whereas the corresponding range in 2020 was from 75% (built-up) to 100% (water bodies). On the other hand, results of producer's accuracy revealed that built-up area relatively correctly classified with accuracy levels of 94%, 94%, and 98% in 2016, 2018, and 2020, respectively.

Table 4-3: Error matrix of classification for 2016

	Reference (2016)							
	Classified samples	Forest	Bare land	Built-up	Vegetation	Water	Total	UA (100%)
Classified(2016)	Forest	46	0	0	1	1	48	96
	Bare land	1	27	2	16	0	46	59
	Built-up	0	5	47	0	2	54	87
	Vegetation	3	4	1	47	2	57	82
	Water	0	0	0	0	45	45	100
	Total	50	36	50	64	50	250	
	PA (100%)	92	75	94	73	90		

Overall Accuracy = 85%

Kappa statistics = 0.81

Where,

PA - producer accuracy

UA - user accuracy

Table 4-4: Error matrix of classification for 2018

		Reference (2018)						
	Classified samples	Forest	Bare land	Built-up	Vegetation	Water	Total	UA (100%)
Classified (2018)	Forest	46	0	0	1	0	47	98
	Bare land	0	45	2	4	1	52	87
	Built-up	0	5	48	0	6	59	81
	Vegetation	4	0	1	45	3	53	85
	Water	0	0	0	0	39	39	100
	Total	50	50	51	50	49	250	
	PA (100%)	92	90	94	90	80		

Overall Accuracy = 89%

Kappa statistics = 0.86

Where, PA - producer accuracy; UA - user accuracy

Table 4-5: Error matrix of classification for 2020

		Reference (2020)						
	Classified samples	Forest	Bare land	Built-up	Vegetation	Water	Total	UA (100%)
Classified (2020)	Forest	50	0	0	0	1	51	98
	Bare land	0	35	1	7	2	45	78
	Built-up	0	13	49	2	1	65	75
	Vegetation	0	2	0	41	6	49	84
	Water	0	0	0	0	40	40	100
	Total	50	50	50	50	50	250	
	PA (100%)	100	70	98	82	80		

Where, PA - producer accuracy; UA - user accuracy

Overall Accuracy = 86%

Kappa statistics = 0.82

4.4 Land Use Land Cover Change Detection

The land use land cover change in Addis Ababa city was analyzed by using classification change detection techniques and then summarized in table 4-6, table 4-7, and table 4-8. LULC change detection matrix was computed between the initial (2016) and final (2020) states was calculated to observe the shifts of land cover classes and the findings revealed that all urban centers experienced a change in the study time. As shown in the table below the changes from 2016 to 2018, from 2018 to 2020, and for the whole period from 2016 to 2020 were tabulated in a matrix. Land use land cover class which remain in their class or unchanged were represented in the diagonal matrix elements during the transition. During this time high rate of changes was detected in the built-up area.

In between 2016 and 2018, 6887.81 ha, 17110.06 ha, 2196.11 ha, 10146.67 ha, and 57.34 ha of bare land, built-up, forest, vegetation, and water bodies remained in their class respectively. However, other off-diagonal elements show the change that ensued from each LULC class to other LULC classes. Similarly, from 2018 to 2020, 6532.44 ha, 21126.71 ha, 2075.76 ha, 8068.16 ha, and 45.75 ha of bare land, built-up, forest, vegetation, and water bodies remained in their class without area conversion respectively. The major observed land use and type change during the period between 2016 and 2020. In this study time bare land, built-up, forest, vegetation, and water bodies 5032 ha, 16605.97 ha, 2131.90 ha, 8717.13 ha, and 46.64 ha were rest in their state unlike other off-diagonal matrix elements respectively.

Table 4-6: Land use/Land cover change matrix during the period 2016 – 2018

	Land Use Land Cover Change Detection Matrix (2016 – 2018)							
		2016						
	LULC	Bare land	Built-up	Forest	Vegetation	Water	Total	
		Ha.	Ha.	Ha.	Ha.	Ha.	Ha.	%
2018	Bare land	**6887.81**	1083.98	167.42	5012.77	3.93	13155.91	24.41
	Built-up	3663.48	**17110.06**	36.68	3950.65	36.01	24796.88	46.01
	Forest	98.14	2.75	**2196.11**	862.17	14.17	3173.33	5.89
	Vegetation	1378.83	91.54	871.15	**10146.67**	28.24	12516.42	23.22
	Water	10.19	19.12	11.52	159.41	**57.34**	257.57	0.47
	Total	12038.44	18307.44	3282.88	20131.24	140.10	**53900.10**	100

Table 4-7: Land use/Land cover change matrix during the period 2018 - 2020

	Land Use Land Cover Change Detection Matrix (2018 - 2020)							
		2018						
	LULC	Bare land	Built-up	Forest	Vegetation	Water	Total	
		Ha.	Ha.	Ha.	Ha.	Ha.	Ha.	%
2020	Bare land	**6532.44**	5418.48	24.72	1177.30	3.25	13156.22	24.41
	Built-up	3029.67	**21126.71**	12.49	575.46	52.48	24796.80	46.01
	Forest	219.96	52.45	**2075.76**	798.64	26.34	3173.14	5.89
	Vegetation	3166.51	700.04	563.01	**8068.16**	18.69	12516.41	23.22
	Water	36.60	29.84	5.31	140.06	**45.75**	257.56	0.48
	Total	12985.17	27327.52	2681.29	10759.61	146.54	**53900.10**	100.00

Table 4-8: Land use/Land cover change matrix during the period 2016 - 2020

	Land Use Land Cover Change Detection Matrix (2016 - 2020)							
		2016						
		Bare land	Built-up	Forest	Vegetation	Water	Total	
	LULC	Ha.	Ha.	Ha.	Ha.	Ha.	Ha.	%
2020	Bare land	**5032.0**	5922.25	29.72	1049.59	4.73	12038.29	22.33
	Built-up	1513.98	**16605.97**	0.34	154.10	32.90	18307.30	33.97
	Forest	253.42	83.13	**2131.90**	788.82	25.18	3282.44	6.09
	Vegetation	6169.72	4693.32	515.03	**8717.13**	36.79	20131.99	37.35
	Water	16.03	22.77	4.41	50.23	**46.64**	140.08	0.26
	Total	12985.15	27327.44	2681.40	10759.88	146.58	**53900.10**	100.00

As can be observed from table 4-9, in the period 2016 to 2018, bare land, built-up, forest, vegetation, and water bodies had gained 6268.10, 7686.82, 977.22, 2369.75, and 200.23 hectares of land respectively, and lost 6097.34, 10217.38, 485.29, 613.21 and 88.9 hectares of land in the same order. In the period 2018–2020, bare land (17.26%), built-up (55.82%), forest (5.48%), vegetation (21.32%), and water bodies (0.12%) were persisted without area change. During the same period, bare land, built-up, forest, vegetation, and water bodies had gained 6623.78 ha, 3670.10 ha, 1097.38 ha, 4448.25 ha, and 211.82 ha. However, 41.26%, 22.87%, 6.84%, 27.71%and 1.32% had lost in bare land, built-up, forest, vegetation, and water bodies respectively table 4-10. In the period 2016 to 2020, vegetation area was highly changed as compared to others with additional gains of 11414.86 hectares (53. 4%) and with losses of 3799.28 hectares (17.7%) to another LULC type. However, 8717.1 hectares (26.7%) remained without area change. On the other hand, bare land, built-up, forest, and water bodies lost an area of (8124.2, 8190.83, 1041.24, and 210.93 hectares respectively) and gained (7006.2, 1701.33, 1150.54 and 93.45 hectares respectively) table 4-11.

Table 4-9: Land use/Land cover change during 2016 - 2018

Land Use Land Cover Change During 2016 - 2018								
LULC Type	Persistence		Gains		Losses		Net Change	
	Ha.	%	Ha.	%	Ha.	%	Ha.	%
Bare land	6887.81	57.22	6268.10	35.81	-6097.34	-34.84	170.76	0.98
Built-up	17110.06	93.46	7686.82	43.92	-10217.38	-58.38	-2530.6	-14.46
Forest	2196.11	66.90	977.22	5.58	-485.29	-2.77	491.93	2.81
Vegetation	10146.67	50.40	2369.75	13.54	-613.21	-3.50	1756.54	10.04
Water	57.34	40.93	200.23	1.14	-88.90	-0.51	111.33	0.64
Total	36397.98	67.53	17502.12	100	-17502.12	-100	0.00	0.00

Table 4-10: Land use/Land cover change during 2018 - 2020

Land Use Land Cover Change During 2018 - 2020								
LULC Type	Persistence		Gains		Losses		Net Change	
	Ha.	%	Ha.	%	Ha.	%	Ha.	%
Bare land	6532.44	17.26	6623.78	41.27	-6623.47	-41.26	0.31	0.0019
Built-up	21126.71	55.82	3670.10	22.86	-3670.17	-22.87	-0.08	-0.0005
Forest	2075.76	5.48	1097.38	6.84	-1097.57	-6.84	-0.19	-0.0012
Vegetation	8068.16	21.32	4448.25	27.71	-4448.26	-27.71	-0.01	-0.0001
Water	45.75	0.12	211.82	1.32	-211.82	-1.32	-0.01	0.0
Total	37848.80	70.22	16051.30	100	-16051.30	-100	0.00	

Table 4-11: Land use/Land cover change during 2016 - 2020

Land Use Land Cover Change During 2016 - 2020								
LULC Type	Persistence		Gains		Losses		Net Change	
	Ha.	%	Ha.	%	Ha.	%	Ha.	%
Bare land	5032.0	15.47	7006.29	32.79105	-8124.22	-38.0232	-1117.93	-5.23
Built-up	16605.97	51.04	1701.33	7.962608	-8190.83	-38.335	-6489.50	-30.37
Forest	2131.90	6.55	1150.54	5.384814	-1041.24	-4.87326	109.30	0.51
Vegetation	8717.13	26.79	11414.86	53.42417	-3799.28	-17.7815	7615.58	35.64
Water	46.64	0.14	93.45	0.437364	-210.93	-0.98718	-117.48	-0.55
Total	32533.63	60.36	21366.47	100	-21366.47	-100	0.00	0.00

4.5 Performance Evaluation of Indices

To get the spectral profile of different land use, the band comparison of sentinel-2A image was performed. Sentinel 2A image has two NIR; namely, band 8 and 8A and two SWIR; namely, SWIR 1 and SWIR 2 bands which is more essential in urban area extraction. Band 8A (NIRnarrow) has a narrow spectral range than band 8 (NIRwide). Therefore, band 8 is intended for producing spectral profile in 10 m resolution and also for spectral built-up indices comparison using sentinel data as shown in figure 4-10.

In the extraction of built-up indices, the most challenging task is the correct differentiation between bare soil and urban areas due to the spectral similarity. Due to the complexity of soil components and soil spectra, as well as spectral signatures, overlap one another, the capability of spectral built-up indices based on Sentinel 2A were performed. Additionally, the spectral characteristics of bare land with different components and water content can differ across diverse environments and seasons.

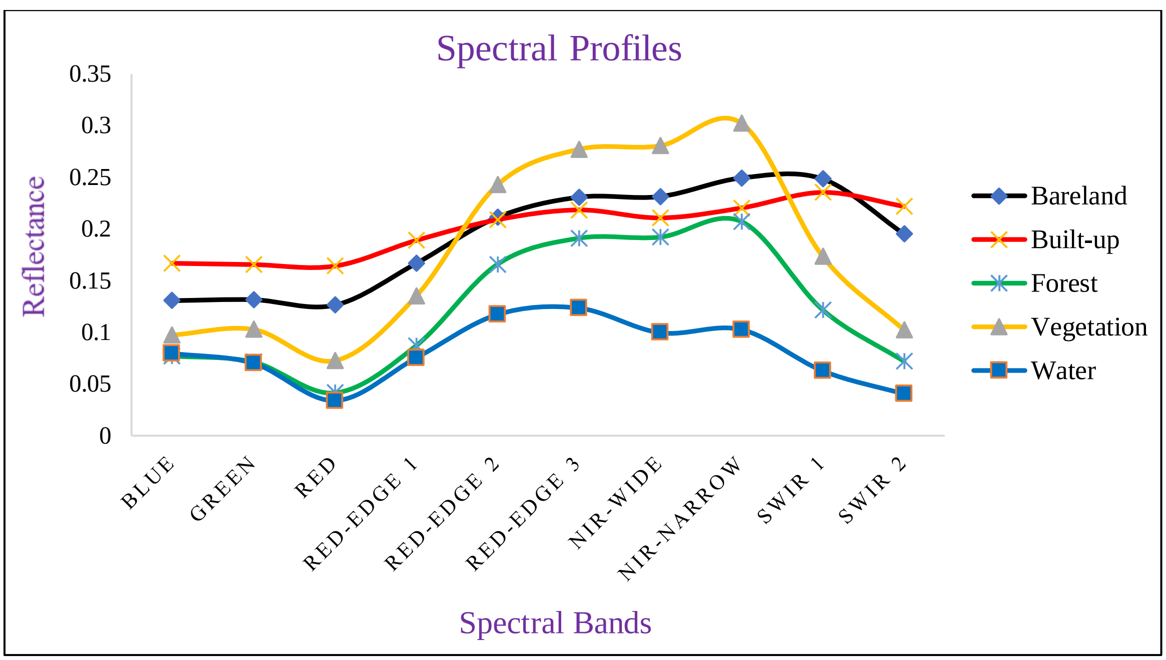

Figure 4-10: Spectral profiles of different typical LULC types

4.5.1 Comparison Based on Built-up Index

In this study, the optimal extraction of built-up surfaces using different built-up indices is carried out in the first level. An input image of the selected study site has been classified for built-up areas by calculating the value of the index. To delineate impervious surface from the pervious surface, seven spectral built-up indices were computed using pre-processed sentinel-2A MSI imagery for three different years; 2016, 2018, and 2020. In this paper, two land-use classes were mapped, which are built-up and non-built-up. To compare various spectral built-up indices, a two-step process was implemented, including computing based on a spectral formula and classifying as built-up and non-built-up area.

The non-built-up class includes forest, vegetation, bare land, and water bodies. The built-up area includes the residential area, industrial parks, parking lots, roads, and other impervious surfaces. As for all the built-up indices derived from Sentinel-2A, they all employ the NIRwide and SWIR bands. However, the ability to discriminate the impervious from the pervious surface is different as shown in figure 4-11. Visual analysis of extracted spectral indices shows that NBAI gives very good results in all three years than any other indices. Next to this index NDBI, NBI delineates built-up areas, however, the other indices (BAEI and BRBA, MBI, and UI) are not suitable to extract urban built-up in the study area.

As illustrated in Figure 4-11, the built-up indices can highlight the urban areas and separate them from other non-built-up land covers. However, detailed inspection revealed that all indices could not separate non-built-up land from the built-up areas, in most cases. The impervious surfaces, which is the region clipped with rectangle corresponds to the sample for the built-up area covered by (building, airport, and road) and other pervious surfaces (bare land and vegetation). Visual interpretation indicating that NBAI, NBDI, NBI, MBI, UI, BAEI, and BRBA can show the contrast difference between the urban area and the other land cover respectively.

- ❖ The BAEI highlights roads and buildings, however, there is high confusion between built-up and bare land which makes the index impractical to separate impervious from bare land covers.
- ❖ The BRBA highlights both roads and bare-land covers, but there is significant confusion between vegetation areas and built-up areas.

- The MBI presents an overall low contrast among the built-up and non built-up areas. Therefore, these two classes share similar intensity values.
- The NBAI can discriminate correctly between built-up and non-built-up land covers. In addition, all other non-built-up (vegetation and bare land) were identified in this index.
- The NBI differentiates impervious surfaces from pervious areas. This index reduces significantly the confusion between vegetation and built-up areas by enhancing the vegetation land covers. As can be seen in the figure below, roads were not different compared to other impervious surfaces.
- The NDBI effectively enlarges the separability contrast between built-up and non-built-up land covers, however, there some confusion between bare land and built-up.
- Like MBI, UI had the lowest potential in identifying these two land covers.

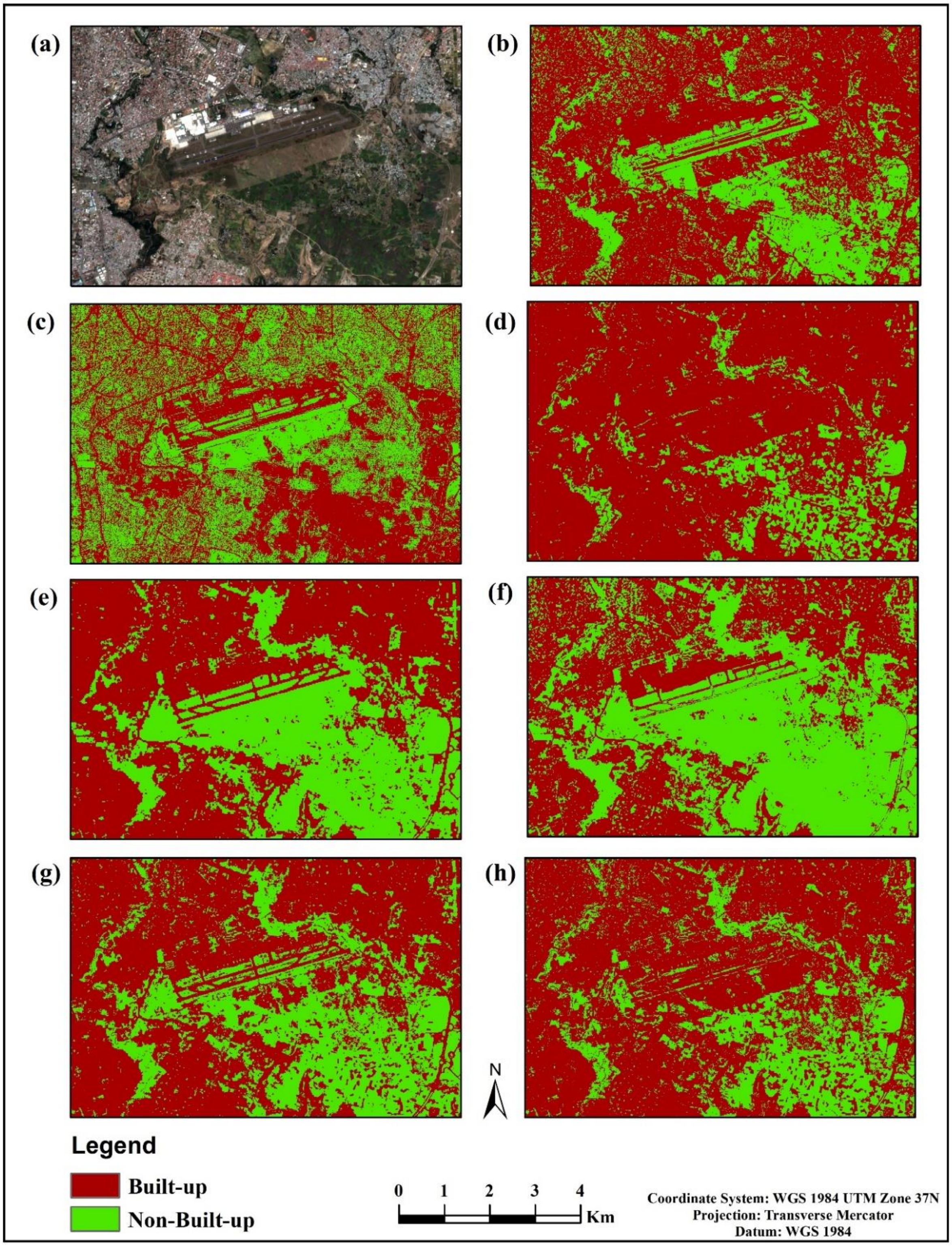

Figure 4-11: Built-up indices for 2020: (a) Sentinel-2A image (b) BAEI, (c) BRBA, (d) MBI, (e) NBAI, (f) NBI, (g) NDBI, and (h) UI

The results show signs of an infilling urban development pattern, as indicated by the gains in built-up lands in the urban center and surrounding. These changes in the landscape of Addis Ababa city are the outcomes of the continuous urbanization of the country's capital region during (2016-2020). Table 4-12 summarizes the detected extent and changes of built-up lands in the study area, which presents the spatial distribution of the detected changes for all seven indices in the figure above.

The results show that the extent of built-up land in the study area can be different depending on which index to be used. Based on the quantitative and qualitative assessment results (table 4-12; figure 4-11), the classifications of the NBAI, NBI, and NDBI were the most accurate ones. These indices show the extent and increase of built-up lands in the study area during 2016–2020. Consequently, the detected increase of built-up lands between 2016 and 2020 was from (52.8% to 56.0%), from (40% to 44.2%) and from (57.4% to 60.8%) to the corresponding built-up indices NBAI, NBI, and NDBI respectively. Based on the results of these indices, the total change of built-up lands in the study area from 2016 to 2020 was 1748.93 ha (3.3%), 2231.48 ha (4.1%), and (1836.36 ha (3.4%) for NBAI, NBI, and NDBI respectively relative to the whole landscape. However, the built-up area by BAEI (65.0%), MBI (77.5%), and UI (67.2%) is overestimated compared to others.

Table 4-12: Built-up area derived from each spectral built-up indices

	Built-up area (ha)							
	2016	%	2018	%	2020	%	change (2016-2020)	%
BAEI	33344.9	61.9	35788.9	66.4	35041.7	65.0	1696.81	3.2
BRBA	25692.4	47.7	24997.1	46.4	26342.5	48.9	650.08	1.2
MBI	41519.2	77.0	32671.6	60.6	41760.9	77.5	241.73	0.5
NBAI	28448.7	52.8	29317.1	54.4	30197.6	56.0	1748.93	3.3
NBI	21582.8	40.0	22885.7	42.5	23814.3	44.2	2231.48	4.1
NDBI	30955.5	57.4	31222.6	57.9	32791.8	60.8	1836.36	3.4
UI	34817.7	64.6	33810.1	62.7	36197	67.2	1379.33	2.6

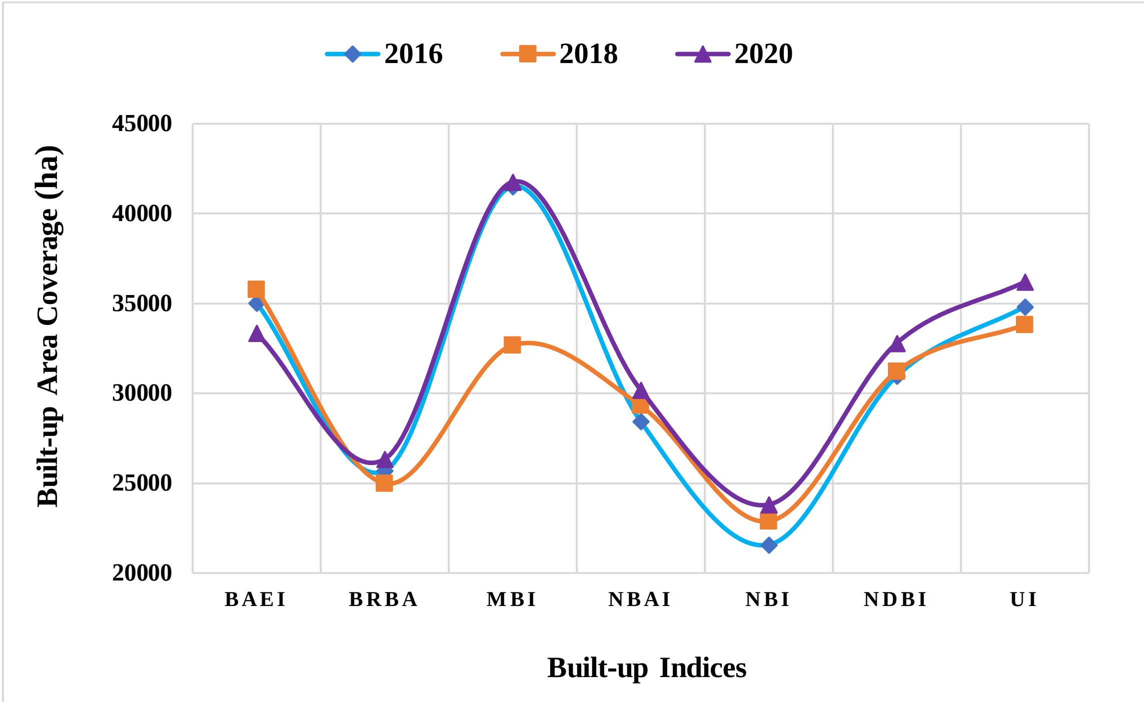

Figure 4-12: Built-up area coverage by each spectral built-up indices

4.5.2 Comparison Based on Spectral Discrimination Index

Performance of seven spectral built-up indices was evaluated by the degree of separation of highlighted built-up land covers with background land uses land covers using Spectral Discrimination Index (SDI). A value greater than one indicates a good degree of separation between built-up and non-built-up, while the poor degree of separation is indicated by lower values of SDI. Among the indices, it can be observed that, for all study periods (2016, 2018, and 2020), SDI for each built-up indices greater than 1 indicating better built-up/non-built-up pixel separability.

As described in methodology SDI was computed by using the absolute value of the mean and standard deviation of each spectral built-up indices. Based on figure 4-13, the statistics of NBAI is (1.24, 1.23, and 1.54) for 2016, 2018, and 2020 respectively. This indicates that the separation of the built-up area from other backgrounds is quite appreciable. Unlike NBAI, BRBA was low in delineating built-up from non-built-up by the value of (0.35, 0.34, and 0.2 for 2016, 2018, and 2020, respectively).

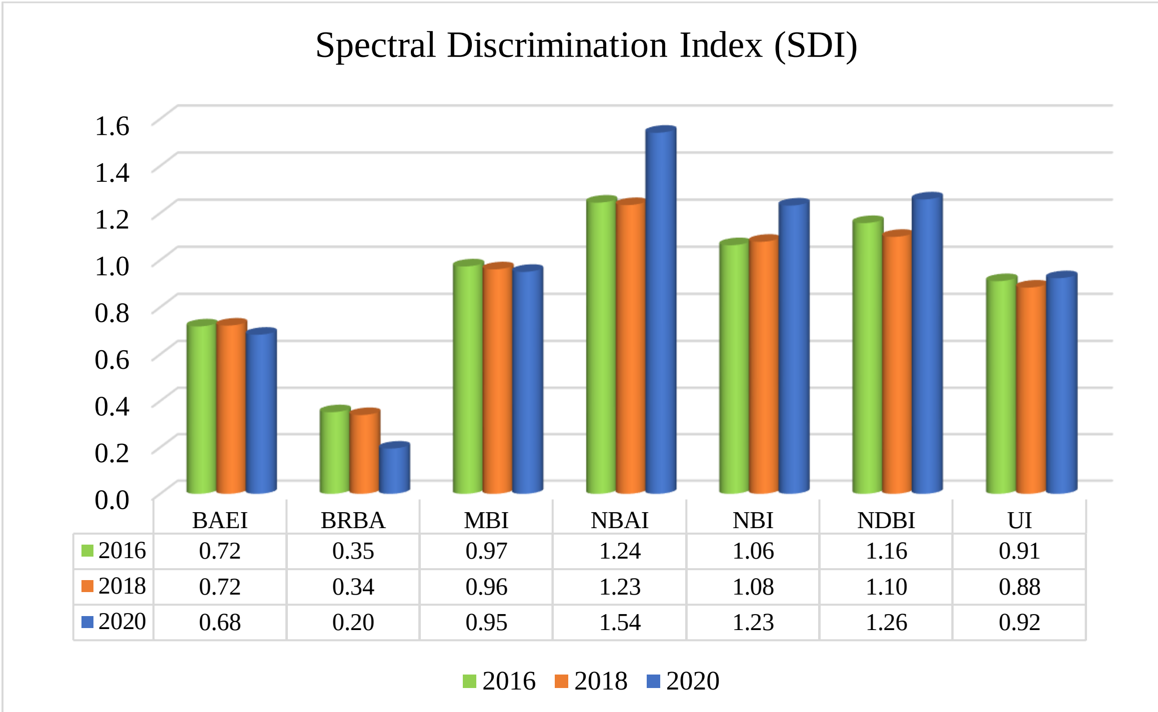

	BAEI	BRBA	MBI	NBAI	NBI	NDBI	UI
2016	0.72	0.35	0.97	1.24	1.06	1.16	0.91
2018	0.72	0.34	0.96	1.23	1.08	1.10	0.88
2020	0.68	0.20	0.95	1.54	1.23	1.26	0.92

Figure 4-13: Spectral discrimination index between built-up and non-built-up land covers

4.5.3 Comparison Based on Separability Analysis by Histogram Overlap

To analyze the discrimination capacity between built-up and non-built-up land covers by built-up indices, deep insight into their corresponding pixel value statistics is required. In addition to SDI, histograms of pixel values per land cover were produced for each built-up index from the index images as displayed in figure 4-14, figure 4-15, and figure 4-16 which can give a general idea of the discrimination capacity of built-up indices. This analysis will help to quantify at a certain point, the degree of overlapping of pixel values belonging to each class, which is a common problem for most indices. In the histograms, the point where the two classes separate was used as a threshold value.

From the resulting graphs, it is easy to note that most indices are not able to isolate only the impervious surfaces. For example, the BAEI highlights simultaneously other non-built-up areas such as bare land to some extent. Similarly, the MBI and UI moderately separate non-built-up areas from built-up. The BRBA presents the worst performance since the index mix these two land cover types. Although the ranges are varied from one index to another. Some are limited in positive range value (BAEI, BRBA, and NBI), and the others are laid from negative to positive (MBI, NBAI, NDBI, and UI). Finally, indices that have shown remarkable differences for impervious surface and non-built-up area are the NBAI, NBI, and NDBI respectively.

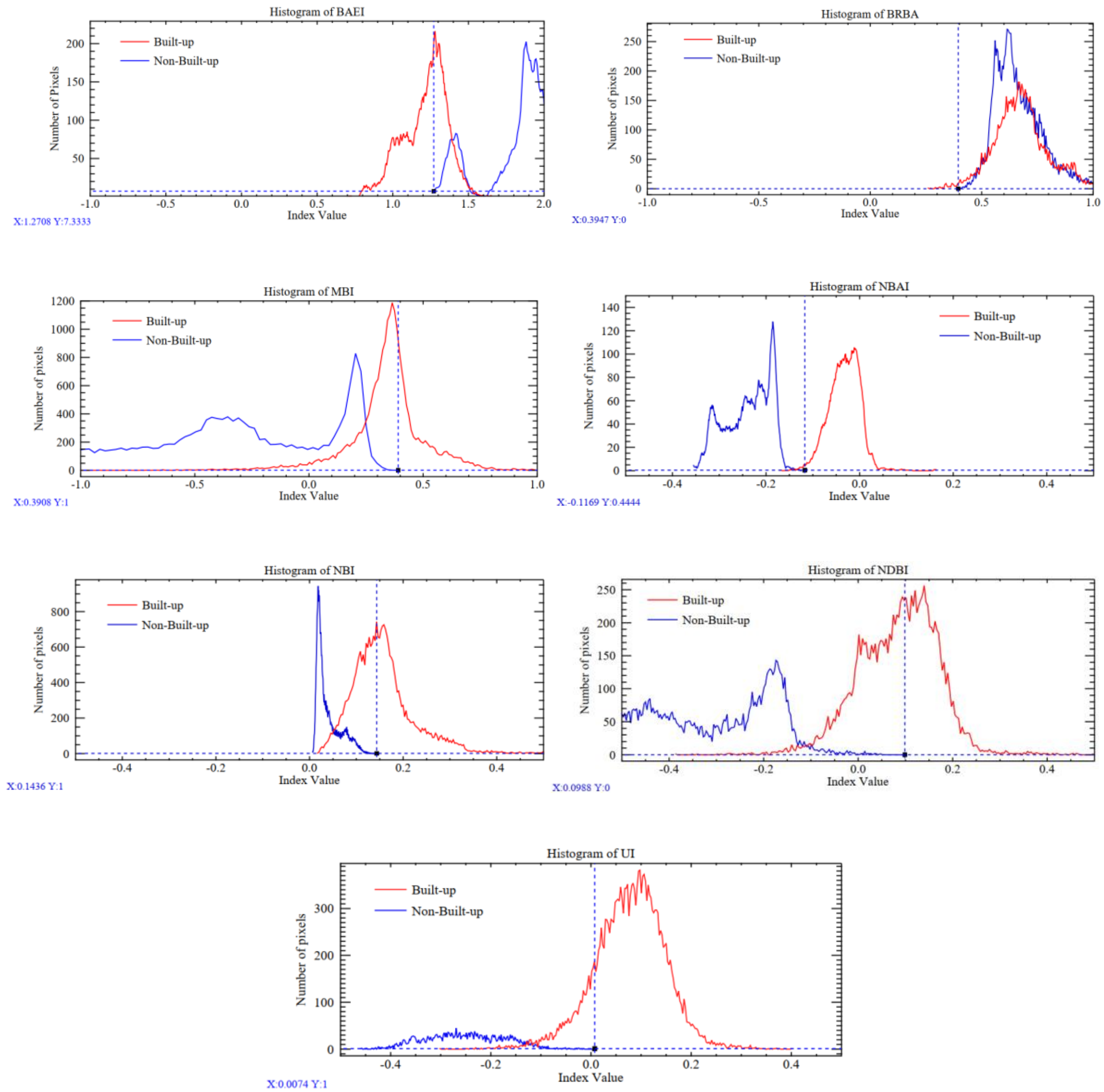

Figure 4-14: Histograms of impervious surface indices in built-up and non- built-up area in 2016

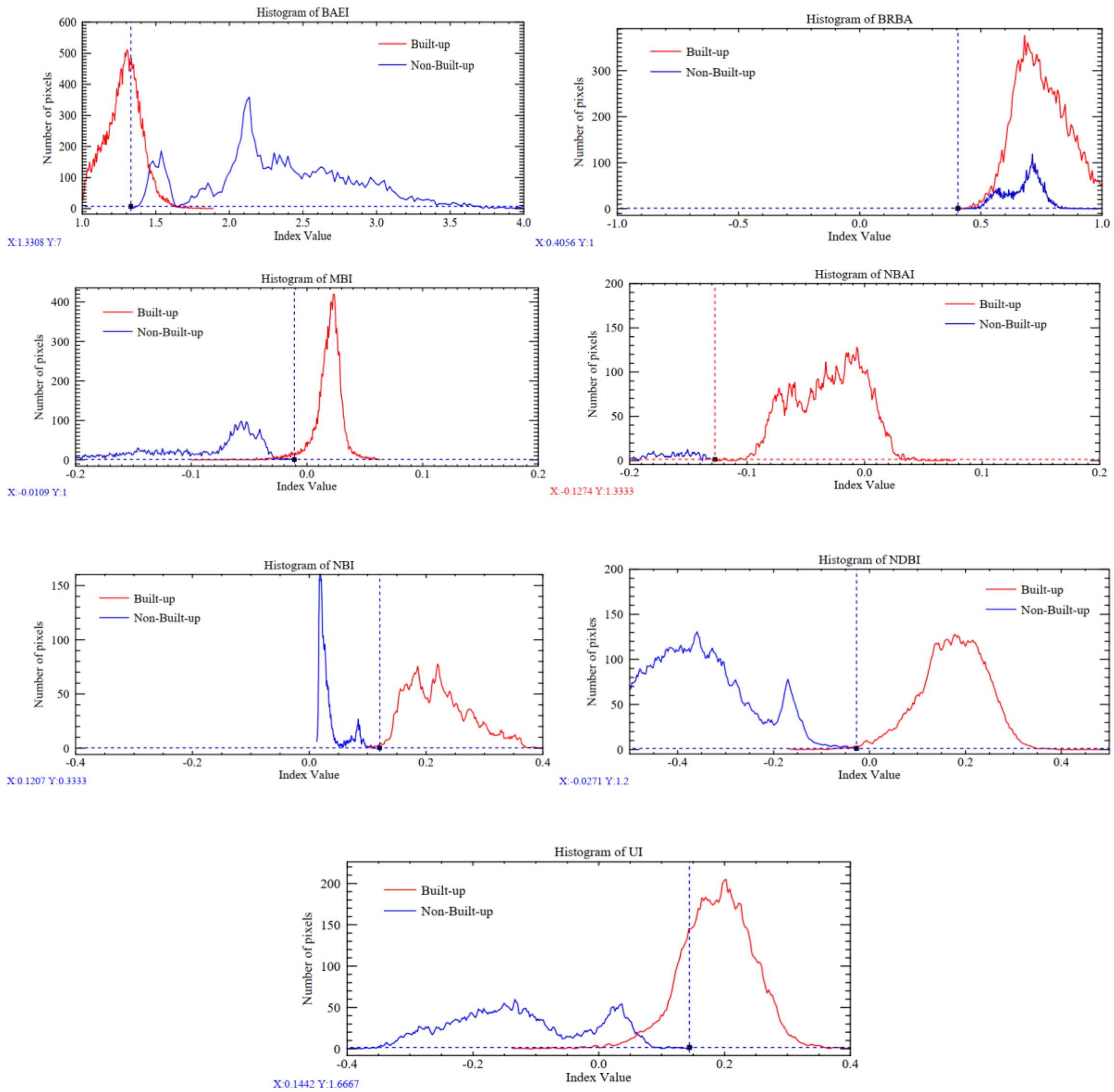

Figure 4-15: Histograms of impervious surface indices in built-up and non- built-up area in 2018

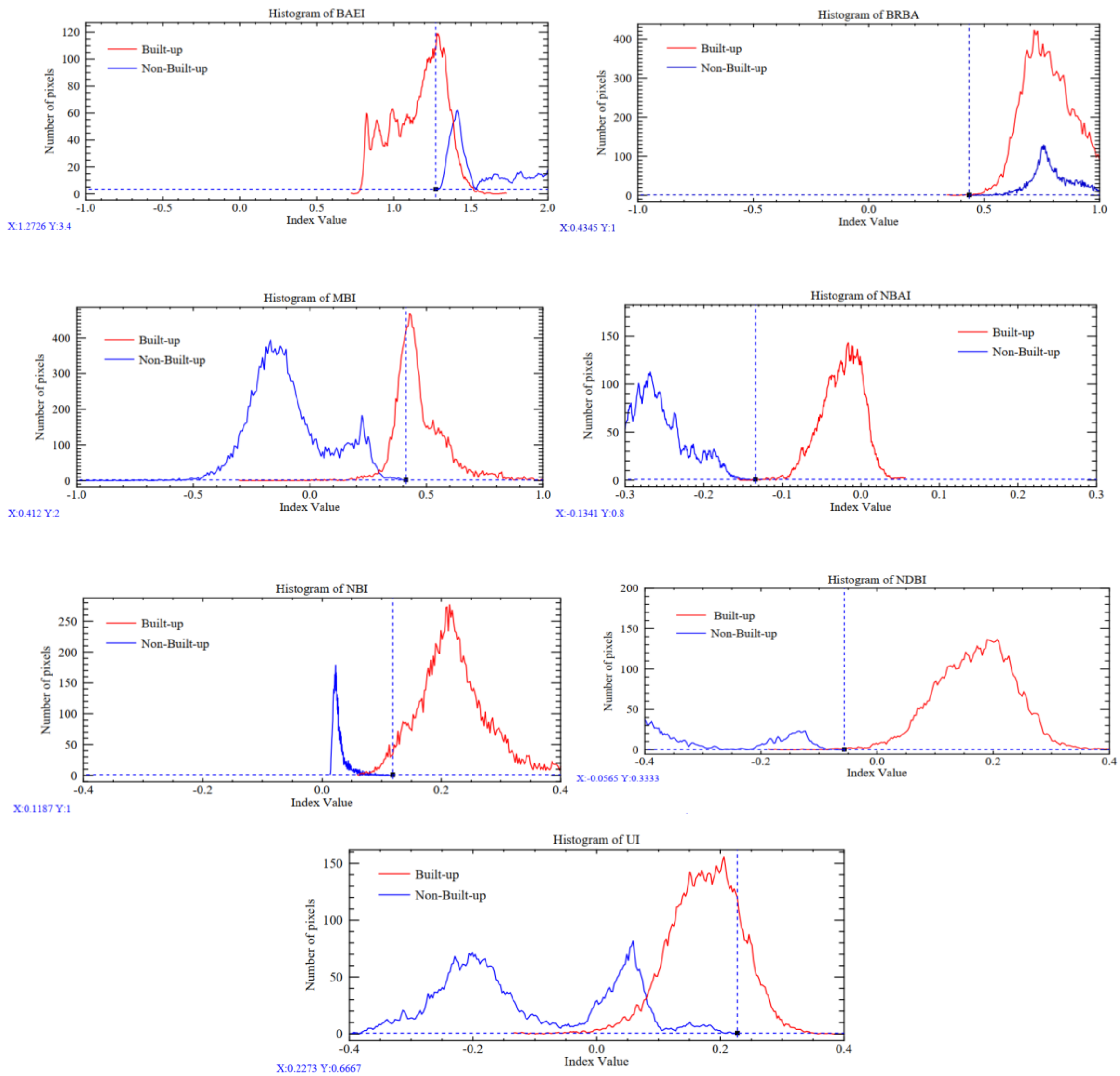

Figure 4-16: Histograms of impervious surface indices in built-up and non- built-up area in 2020

4.6 The Selection of Threshold Values

As shown in table 4-13 the threshold value was computed from each spectral built-up indices. To get this value sample pixels were taken from the computed index map for 2016, 2081, and 2020. The continuity of these indices is indicated by the value of threshold in 2016, 2081, and 2020 with similar values. From the histogram separation these three indices (NBAI, NBI, and NDBI) extracted the built-up area with the threshold value (-0.12, 0.14, and 0.098), (-0.12, 0.12, and -0.027) and (-0.13, 0.12, and -0.06) for 2016, 2018, and 2020, respectively.

Table 4-13 Threshold value for 2016, 2018 and 2020

Built-up indices	2016	2018	2020
BAEI	1.27	1.33	1.27
BRBA	0.39	0.4	0.4
MBI	0.39	-0.01	0.4
NBAI	-0.12	-0.12	-0.13
NBI	0.14	0.12	0.12
NDBI	0.098	-0.027	-0.06
UI	0.007	0.14	0.22

4.7 Quantitative Accuracy Assessment on Spectral Built-up Indices

In the comparison between a classified LULC map and a reference or ground truth map, a pixel is called an omission error (OE) when it is built up in the reference map but not in the classified map. On the other hand, a pixel is called a commission error (CE) when it is built up in the classified map but not in the reference map. To verify the robustness of the seven spectral built-up indices, quantitative assessments of the accuracy were implemented. During quantitative assessments, their respective omission error (OE), commission error (CE), overall accuracy (OA), and overall kappa coefficients (KCs) of classification utilizing built-up indices based on the confusion matrices were calculated. A total of 200 reference sample points for each spectral built-up indices were applied to assess the accuracy of all the classification results. Each reference sample was checked by an aerial photograph and google earth.

For the built-up class, (NBAI, NBI and NDBI) had the highest UA (0.92%, 0.91% and 0.85%), (0.88%, 0.88% and 0.84%), and (0.93%, 0.94% and 0.88%) for 2016, 2018 and 2020, respectively. This result indicates how a classified pixel matching with the built-up class in reality. Indeed, the results in table 4-14, table 4-15 and table 4-15 show that these indices also had the highest OAs (0.95%, 0.94%, 0.91%) and kappa value (0.9%, 0.87%, 0.81%) for 2016 , OAs (0.93%, 0.93% and 0.9%) with kappa value (0.86%, 0.85% and 0.8%) for 2018 and OAs (0.96%, 0.97% and 0.93%) with kappa value (0.92%, 0.93% and 0.86%) for 2020. Therefore, using this indices for the extraction of impervious surface for the corresponding study area is valuable. However, the OAs for BAEI, BRBA, MBI and UI in 2020 is (0.84%, 0.39%, 0.84% and 0.87%) with the kappa coefficient of (0.68%, -0.22%, 0.67% and 0.73%). This implies that there is over or under estimated built-up area when it compared with the reality and generally the result from this built-up indices is unsatisfactory.

Table 4-14: Quantitative accuracy assessment result for 2016

Built-up Indices	LULC Type	PA (%)	UA (%)	OA (%)	Kappa
BAEI	Built-up	1	0.78	0.86	0.72
	Non-Built-up	0.72	1		
BRBA	Built-up	0.57	0.65	0.63	0.26
	Non-Built-up	0.69	0.62		
MBI	Built-up	1	0.69	0.76	0.55
	Non-Built-up	0.55	1		
NBAI	Built-up	0.99	0.92	0.95	0.9
	Non-Built-up	0.91	0.99		
NBI	Built-up	0.97	0.91	0.94	0.87
	Non-Built-up	0.9	0.97		
NDBI	Built-up	0.98	0.85	0.91	0.81
	Non-Built-up	0.83	0.98		
UI	Built-up	0.98	0.78	0.85	0.70
	Non-Built-up	0.72	0.97		

Where PA- Producer Accuracy; UA- User Accuracy; OA- Overall Accuracy; Kappa- Kappa coefficient

Table 4-15: Quantitative accuracy assessment result for 2018

Built-up Indices	LULC Type	PA (%)	UA (%)	OA (%)	Kappa
BAEI	Built-up	0.99	0.83	0.89	0.78
	Non-Built-up	0.79	0.99		
BRBA	Built-up	0.46	0.52	0.52	0.03
	Non-Built-up	0.57	0.51		
MBI	Built-up	0.99	0.79	0.86	0.72
	Non-Built-up	0.73	0.99		
NBAI	Built-up	0.99	0.88	0.93	0.86
	Non-Built-up	0.87	0.99		
NBI	Built-up	0.98	0.88	0.93	0.85
	Non-Built-up	0.87	0.98		
NDBI	Built-up	0.99	0.84	0.9	0.8
	Non-Built-up	0.81	0.99		
UI	Built-up	0.99	0.79	0.86	0.72
	Non-Built-up	0.73	0.99		

Where PA- Producer Accuracy; UA- User Accuracy; OA- Overall Accuracy; Kappa- Kappa coefficient

Table 4-16: Quantitative accuracy assessment result for 2020

Built-up Indices	LULC Type	PA (%)	UA (%)	OA (%)	Kappa
BAEI	Built-up	0.89	0.81	0.84	0.68
	Non-Built-up	0.79	0.88		
BRBA	Built-up	0.4	0.39	0.39	-0.22
	Non-Built-up	0.38	0.39		
MBI	Built-up	1	0.75	0.84	0.67
	Non-Built-up	0.67	1		
NBAI	Built-up	0.99	0.93	0.96	0.92
	Non-Built-up	0.93	0.99		
NBI	Built-up	0.99	0.94	0.97	0.93
	Non-Built-up	0.94	0.99		
NDBI	Built-up	0.99	0.88	0.93	0.86
	Non-Built-up	0.87	0.99		
UI	Built-up	0.99	0.79	0.87	0.73
	Non-Built-up	0.87	0.99		

Where PA- Producer Accuracy; UA- User Accuracy; OA- Overall Accuracy; Kappa- Kappa coefficient

CHAPTER FIVE

5. DISCUSSION

5.1 Comparative Analysis of Spectral Built-up Indices

Urban areas with a high degree of homogeneity challenge the level of accuracy when they distinguish built-up areas based on spectral values by remote sensing spectral built-up indices (Ghosh et al., 2018). Some studies showed that employing the feature extraction approach into index structure may further reduce the spectral similarity between impervious surfaces and others, and thus promise more reliable impervious surface extraction (Sun et al., 2016). All spectral built-up indices cannot perfectly differentiate impervious land from pervious due to the similar spectral confusion to fully separate with the other land use and land cover classes, like bare land, dry grasslands. Based on the result, some non-built-up lands were misclassified as built-up lands, and vice versa. This is because built-up indices have failed that they all use the SWIR and NIR channels of the electromagnetic spectrum (XI et al., 2019). In this channel, bare land and dry vegetation have also similar reflectance with built-up lands and it appears in dark tones, however other land cover types appear in bright tones.

According to the studies by (Estoque & Murayama, 2015b; Kawamura, 1996; Xu, 2008; Zha et al., 2003), the main argument for using the (NIR wide and SWIR) portion of the spectrum is that built-up surface has higher reflectance in this channel compared with the NIRnarrow wavelength range. Some indices were more accurate in separating these two land use land cover classes. This study hypothesizes that the reason for spectral confusion is the mixture of other non-built-up lands with built-up lands, causing the SWIR based and NIR wide-based indices to obtain much higher producer accuracy for the built-up class. The NBAI was found to be superior to the other indices in separating built-up, roads, and airport areas with better accuracy from sentinel-2A MSI data. The use of both the first and second band of the SWIR channel, i.e. SWIR 1 and SWIR 2 in combination with visible green channels, helped the NBAI to perform better than the BAEI, BRBA NDBI, NBI, MBI, and UI, which use only either the first band, second band or NIR channel.

It can be observed that, based on their spectral profiles, the bare land has lower reflectance in the SWIR 2 channel than in the NIR channel. This feature enabled the NBAI to properly separate these bare land area and vegetation types from built-up lands, ensuing more accurate classification results. Most of the built-up surfaces have lower reflectance in visible bands (blue, green, and red) than in the NIR and SWIR bands. In the visible bands, built-up areas appear in bright tones, while other bare lands and vegetated areas appear in dark tones. However, healthy vegetation and bare land have high reflectance and appear brighter in the NIR channel. Based on the results, four indices such as MBI, NBAI, NDBI, and UI produce zero or negative values for non-built-up land covers, including forest, vegetation, bare land, and water bodies, while built-up area represented by a positive value.

In Ethiopia, much research has been conducted to observe the direct relationship between urban expansion and LULC change. Built-up areas expanded at the expense of shrinking of other non-built-up areas. Thus, this study revealed that impervious areas are expanded from 18101.88 ha to 27186.37 ha from 2016 to 2020. This study also supported by the study carried out in Addis Ababa city by (Leulsegged et al., 2012) to detect the land use and land cover change due to urbanization-induced displaced households in the peri-urban areas. And the study by (Abebe & Megento, 2016), (Admasu, 2017) to analyze the LULC dynamics of the Addis Ababa city and they conclude that there is high rate of net-loss in vegetation and agricultural land. The LULC change is not only in the capital city of the country but also in sub cities like Adama city by (Sinha & Verma, 2016), Hawassa city by (Gebeyehu, 2018), and southwest Ethiopia by (Dessu et al., 2020) showed that there was a significant increment in built-up areas, while there was a decline in green areas and open spaces.

Additionally, the result of spectral built-up indices (NBAI, NBI, and NDBI) also consistent with the findings of built-up area expansion from (28448.69 ha, 21582.83 ha, and 30955.48 ha) to (30197.62 ha, 23814.31, and 32791.84 ha) from 2016 to 2020, respectively. Thus, the previous study was also consistent with the findings of this study. The accuracy assessment is the agreement between the verified reference points or pixels and their corresponding pixels on the classified LULC maps (Estoque & Murayama, 2015a).

Here, measures used in the assessment of accuracy are discussed. Based on this, the result of quantitative accuracy assessment for classified LULC map by SVM is 85%, 89%, and 86% of overall accuracy and 0.81, 0.86, and 0.82 of kappa statistics for 2016, 2018, and 2020, respectively. The kappa coefficient is rated as almost perfect as stated by (Koch et al., 1977) and hence the classified image is found to be fit for further research. Because of the ability of SVM algorism to generalize well and it yields comparable accuracy using a much smaller training sample (Mountrakis et al., 2011). The shortcoming for the SVM approach is highly subject to the characteristics of the selected training samples and they need to set up manually, however it is suitable for small study area coverage. The highest accuracy was achieved by the NBAI, NBI, and NDBI with a kappa coefficient of (0.9, 0.87, and 0.81), (0.86, 0.85 and 0.8) and (0.92, 0.93, and 0.86) for 2016, 2018, and 2020 respectively. This result is supported by previous studies which have indicated that the NBAI, NBI, and NDBI can be used for detecting and classifying built-up lands (Jieli et al., 2008; Valdiviezo-N et al., 2018; Waqar et al., 2012; Zha et al., 2003).

Furthermore, a closer visual examination of the index and spectral discrimination index values representing bare soil and built-up surfaces has been revealed by the above indices and presents a major separability. The SDI is an index that computes the degree of separation between two land cover classes. It is calculated by considering the mean and standard deviation of the two different land covers (Pereira, 1999). The results obtained from different study times show that among the seven spectral built-up indices examined, the NBAI, NBI, and NDBI with great improvement can be used for more accurate classification of built-up lands from sentinel 2A-MSI imageries. The SDI values of these indices are greater than 1 and the overlap in histograms is the smallest. The use of this method also promotes automation, an essential process in the context of performance analysis, which was done before by (Mukherjee et al., 2021; Pandey & Tiwari, 2020; Valdiviezo-N et al., 2018).

This extraction result has been confirmed by evaluating the spectral difference from the corresponding histograms. Besides, other indices, such as BAEI, MBI, and UI, also take advantage of the feature extraction, however, these indices show an unsatisfactory result and suffer from saturation. Nonetheless, indices such as BRBA shows the least results compared to the others. This result confirms that built-up indices provide better results for months where rain or humidity is present in the study area (Valdiviezo-N et al., 2018).

CHAPTER SIX

6. CONCLUSIONS AND RECOMMENDATIONS

6.1 Conclusion

The continuous development of geospatial and remote sensing technology has seen the advance of various spectral indices to detect urban built-up lands utilizing built-up indices. Nevertheless, a comprehensive comparison between these spectral built-up indices as applied to high-resolution remote sensing satellite imageries is still lacking. Due to variation in the spectral response of different land cover features from region to region because of climatic & topographic changes, seven spectral built-up indices were assessed. The study intended to evaluate various spectral built-up indices for the extraction of impervious surfaces in Addis Ababa city using sentinel-2A MSI imagery.

In this paper, a performance comparison of these spectral built-up indices was performed in the wet season i.e. October, and the result confirms that built-up indices provide better results in wet or humid months for the study area. This is because the discrimination between bare land and the impervious surface has become more difficult for most index-based methods in dry months. According to the outcome, three indices; namely, NBAI, NBI, and NDBI are robust methods that are capable of the classification and change detection of impervious surfaces from complex urban areas. From the result, it can be concluded that the built-up area coverage of Addis Ababa city shows significant expansion from 2016 to 2020. And this result also supported by the classification output by the support vector machine classifier, however other LULC types i.e. vegetation and forest are going to be diminished.

The evaluation of these built-up indices shows a substantial agreement between spectral discrimination index, histogram overlap, and quantitative accuracy assessment. The SDI value of NBAI, NBI, and NDBI, were greater than one unlike other indices, which indicate almost perfect with the smallest histogram overlap. Similarly, the quantitative validation result was considerable in differentiating built-up and non-built-up land in between the classified LULC map by various spectral built-up indices and the machine learning algorism.

Generally, the present rising trend of urban impervious surfaces will continue in the next decades due to the dynamics of LULC in the study area. The phenomenon of urban built-up expansion always needs accurate and updated data on urban built-up areas such as the size, shape, and spatial context. The process of urbanization affects developing countries like Ethiopia unless proper environmental protection measures have been taken. From the results, it was concluded that the index-based methods are fast, easy to implement, and more effective in built-up area mapping utilizing the SWIR 1/SWIR 2 bands, in which, built-up lands have higher reflectance, allowing them to be clearly distinguished from other lands. The results are promising and the proposed approach of Sentinel-2A satellite data with robust built-up indices can allow the urban planner to understand and evaluate municipal growth for sustainable usage of the urban land system.

6.2 Recommendations

This study was dedicated to the evaluation of spectral built-up indices for impervious surface extraction using sentinel-2A MSI imageries in Addis Ababa city.

From the result of the study, the following recommendations have been suggested.

- For verification and further analysis, other studies need to be tested in the city surrounding and different geographic regions as the spectral response of the various land covers may vary spatially.

- Further application and analysis of the remaining spectral built-up indices with other threshold algorisms such as the Otsu threshold might attain enhanced results.

- It would be helpful if a high-resolution satellite images having better resolution applied for further refinement.

References

Abebe, M. T., & Megento, T. L. (2016). The city of addis ababa from 'forest city' to 'urban heat island': Assessment of urban green space dynamics. *Journal of Urban and Environmental Engineering*, *10*(2), 254–262. https://doi.org/10.4090/juee.2016.v10n2.254262

Admasu, T. (2017). *Monitoring trends of greenness and LULC (land use/land cover) change in Addis Ababa and its surrounding using MODIS time-series and LANDSAT Data*. *24*, 60. http://lup.lub.lu.se/luur/download?func=downloadFile&recordOId=8917891&fileOId=8917921

Ali, M. I., Hasim, A. H., & Abidin, M. R. (2019). *Monitoring the Built-up Area Transformation Using Urban Index and Normalized Difference Built-up Index Analysis*. *32*(5), 647–653.

Bauer, M., Loffelholz, B., & Wilson, B. (2007). *Estimating and Mapping Impervious Surface Area by Regression Analysis of Landsat Imagery*. 612–625. https://doi.org/10.1201/9781420043754.pt1

Bhatti, S. S., & Tripathi, N. K. (2014). Built-up area extraction using Landsat 8 OLI imagery. *GIScience and Remote Sensing*, *51*(4), 445–467. https://doi.org/10.1080/15481603.2014.939539

Bouhennache, R., Bouden, T., Taleb-Ahmed, A., & Cheddad, A. (2019). A new spectral index for the extraction of built-up land features from Landsat 8 satellite imagery. *Geocarto International*, *34*(14), 1531–1551. https://doi.org/10.1080/10106049.2018.1497094

Bouzekri, S., Lasbet, A. A., & Lachehab, A. (2015). A New Spectral Index for Extraction of Built-Up Area Using Landsat-8 Data. *Journal of the Indian Society of Remote Sensing*, *43*(4), 867–873. https://doi.org/10.1007/s12524-015-0460-6

Bramhe, V. S., Ghosh, S. K., & Garg, P. K. (2018). Extraction of Built-Up Area By Combining Textural Features and Spectral Indices From Landsat-8 Multispectral Image. *ISPRS - International Archives of the Photogrammetry, Remote Sensing and Spatial Information Sciences*, *XLII–5*(November), 727–733. https://doi.org/10.5194/isprs-archives-xlii-5-727-2018

Burges, C. J. C. (1998). A tutorial on support vector machines for pattern recognition. *Data Mining and Knowledge Discovery*, *2*(2), 121–167.

Campbell, J. B., & Wynne, R. H. (2011). *Introduction to remote sensing*. Guilford Press.

Carlson, T. N., & Traci Arthur, S. (2000). The impact of land use - Land cover changes due to urbanization on surface microclimate and hydrology: A satellite perspective. *Global and Planetary Change*, *25*(1–2), 49–65. https://doi.org/10.1016/S0921-8181(00)00021-7

Cavur, M., Duzgun, H. S., Kemec, S., & Demirkan, D. C. (2019). Land use and land cover classification of Sentinel 2-A: St Petersburg case study. *International Archives of the Photogrammetry, Remote Sensing and Spatial Information Sciences - ISPRS Archives*, *42*(1/W2), 13–16. https://doi.org/10.5194/isprs-archives-XLII-1-W2-13-2019

Congalton, R. G. (1991). A review of assessing the accuracy of classifications of remotely sensed data. *Remote Sensing of Environment*, *37*(1), 35–46. https://doi.org/https://doi.org/10.1016/0034-4257(91)90048-B

Copernicus, E. S. A. (2018). Copernicus open access hub. *Obtenido de Https://Scihub. Copernicus. Eu/Dhus/#/Home*.

CSA. (2013). Population Projection of Ethiopia for All Regions at Wereda Level from 2014 – 2017 (Population projection). Federal Democratic Republic of Ethiopia Central Statistical Agency, Addis Ababa, Ethiopia.

Culberg, K., & Fuhs, K. (2017). *Feature Extraction in satellite imagery using Support Vector Machines*.

Deng, C., & Wu, C. (2012). BCI: A biophysical composition index for remote sensing of urban environments. *Remote Sensing of Environment*, *127*, 247–259. https://doi.org/10.1016/j.rse.2012.09.009

Deng, C., & Wu, C. (2013). The use of single-date MODIS imagery for estimating large-scale urban impervious surface fraction with spectral mixture analysis and machine learning techniques. *ISPRS Journal of Photogrammetry and Remote Sensing*, *86*, 100–110. https://doi.org/10.1016/j.isprsjprs.2013.09.010

Deng, Y., Wu, C., Li, M., & Chen, R. (2015). RNDSI: A ratio normalized difference soil index for remote sensing of urban/suburban environments. *International Journal of Applied Earth Observation and Geoinformation*, *39*, 40–48.

Dessu, T., Korecha, D., Hunde, D., & Worku, A. (2020). Long-Term Land Use Land Cover Change in Urban Centers of Southwest Ethiopia From a Climate Change Perspective. *Frontiers in Climate*, *2*(December), 1–23. https://doi.org/10.3389/fclim.2020.577169

Estoque, R. C., & Murayama, Y. (2015a). Classification and change detection of built-up lands from Landsat-7 ETM+ and Landsat-8 OLI/TIRS imageries: A comparative assessment of various spectral indices. *Ecological Indicators*, *56*, 205–217. https://doi.org/10.1016/j.ecolind.2015.03.037

Firozjaei, M. K., Sedighi, A., Kiavarz, M., Qureshi, S., Haase, D., & Alavipanah, S. K. (2019). Automated built-up extraction index: A new technique for mapping surface built-up areas using LANDSAT 8 OLI imagery. *Remote Sensing*, *11*(17). https://doi.org/10.3390/rs11171966

Foody, G. M. (2002). *Status of land cover classification accuracy assessment*. *80*, 185–201.

Foody, G. M. (2004). Thematic map comparison. *Photogrammetric Engineering & Remote Sensing*, *70*(5), 627–633.

Gebeyehu, Y. (2018). *College of Natural and Computational Sciences College of Natural and Computational Sciences*. *March*, 2–5.

Gewali, U. B., Monteiro, S. T., & Saber, E. (2018). Machine learning based hyperspectral image analysis: A survey. *ArXiv*.

Ghosh, D. K., Mandal, A. C. H., Majumder, R., Patra, P., & Bhunia, G. S. (2018). Analysis for mapping of built-up area using remotely sensed indices - A case study of rajarhat block in Barasat sadar sub-division in west Bengal (India). *Journal of Landscape Ecology(Czech Republic)*, *11*(2), 67–76. https://doi.org/10.2478/jlecol-2018-0007

Guo, H., Huang, Q., Li, X., Sun, Z., & Zhang, Y. (2013). Spatiotemporal analysis of urban environment based on the vegetation–impervious surface–soil model. *Journal of Applied Remote Sensing*, *8*(1), 084597. https://doi.org/10.1117/1.jrs.8.084597

Guo, X., Zhang, C., Luo, W., Yang, J., & Yang, M. (2020). Urban Impervious Surface Extraction Based on Multi-features and Random Forest. *IEEE Access*, 226609–226623. https://doi.org/10.1109/ACCESS.2020.3046261

He, C., Shi, P., Xie, D., & Zhao, Y. (2010). *Improving the normalized difference built- up index to map urban built-up areas using a semiautomatic segmentation approach*. *7058*. https://doi.org/10.1080/01431161.2010.481681

Hua, L., Zhang, X., Nie, Q., Sun, F., & Tang, L. (2020). The impacts of the expansion of urban impervious surfaces on urban heat islands in a coastal city in China. *Sustainability (Switzerland)*, *12*(2). https://doi.org/10.3390/su12020475

Jensen. (2005). *• Jensen, J. R. 2005. Introductory Digital Image Processing (3*.

Jensen, J. R. (1996). Introductory digital image processing: a remote sensing perspective. Second edition. *Introductory Digital Image Processing: A Remote Sensing Perspective. Second Edition*.

Jieli, C., Manchun, L. I., Yongxue, L. I. U., Chenglei, S., & Wei, H. U. (2008). *Extract*

Residential Areas Automatically by New Built-up Index. *40701117*.

Kaufman, Y. J., & Remer, L. A. (1994). Detection of forests using mid-IR reflectance: an application for aerosol studies. *IEEE Transactions on Geoscience and Remote Sensing*, *32*(3), 672–683.

Kawakubo, F., Morato, R., Martins, M., Mataveli, G., Nepomuceno, P., & Martines, M. (2019). Quantification and Analysis of Impervious Surface Area in the Metropolitan Region of São Paulo, Brazil. *Remote Sensing*, *11*(8), 944.

Kawamura, M. (1996). Relation between social and environmental conditions in Colombo Sri Lanka and the urban index estimated by satellite remote sensing data. *Proc. 51st Annual Conference of the Japan Society of Civil Engineers*, 190–191.

Koch, G. G., Landis, J. R., Freeman, J. L., Freeman Jr, D. H., & Lehnen, R. G. (1977). A general methodology for the analysis of experiments with repeated measurement of categorical data. *Biometrics*, 133–158.

Kuc, G., & Chormański, J. (2019). *SENTINEL-2 IMAGERY FOR MAPPING AND MONITORING IMPERVIOUSNESS IN URBAN AREAS*. *XLII*, 16–17.

Latham, J. S., He, C., Alinovi, L., DiGregorio, A., & Kalensky, Z. (2002). FAO methodologies for land cover classification and mapping. In *Linking people, place, and policy* (pp. 283–316). Springer.

Leulsegged, K., Gete, Z., Dawit, A., Fitsum, H., & Andreas, H. (2012). Impact of urbanization of addis abeba city on peri-urban environment and livelihoods. *The Tenth Conference on Ethiopian Economy*, 1–30.

Liao, W., Deng, Y., Li, M., Sun, M., Yang, J., & Xu, J. (2021). Extraction and analysis of finer impervious surface classes in urban area. *Remote Sensing*, *13*(3). https://doi.org/10.3390/rs13030459

Liu, Y., Chen, J., Cheng, W., Sun, C., Zhao, S., & Pu, Y. (2014). Spatiotemporal dynamics of the urban sprawl in a typical urban agglomeration: a case study on Southern Jiangsu, China (1983–2007). *Frontiers of Earth Science*, *8*(4), 490–504. https://doi.org/10.1007/s11707-014-0423-1

Lu, D., & Weng, Q. (2007). A survey of image classification methods and techniques for improving classification performance. *International Journal of Remote Sensing*, *28*(5), 823–870. https://doi.org/10.1080/01431160600746456

Lu, Dengsheng, & Weng, Q. (2004). Spectral mixture analysis of the urban landscape in Indianapolis with Landsat ETM+ imagery. *Photogrammetric Engineering and Remote Sensing*, *70*(9), 1053–1062. https://doi.org/10.14358/PERS.70.9.1053

Lu, Dengsheng, & Weng, Q. (2009). Extraction of urban impervious surfaces from an IKONOS image. *International Journal of Remote Sensing*, *30*(5), 1297–1311. https://doi.org/10.1080/01431160802508985

Maclachlan, A., Roberts, G., Biggs, E., & Boruff, B. (2017). Subpixel land-cover classification for improved urban area estimates using landsat. *International Journal of Remote Sensing*, *38*(20), 5763–5792. https://doi.org/10.1080/01431161.2017.1346403

MacLean, M. G., & Congalton, R. G. (2012). Map accuracy assessment issues when using an object-oriented approach. *Proceedings of the American Society for Photogrammetry and Remote Sensing 2012 Annual Conference*, 1–5.

Mohapatra, R. P., & Wu, C. (2007). Subpixel imperviousness estimation with IKONOS imagery: an artificial neural network approach. In *Remote Sensing of Impervious Surfaces* (pp. 49–66). CRC Press.

Moser, C. O. N. (1996). *Confronting Crisis. A Comparative Study of Household Responses to Poverty and Vulnerability in Four Poor Urban Communities. Environmentally Sustainable Development Studies and Monographs Series No. 8.*

Mountrakis, G., Im, J., & Ogole, C. (2011). Support vector machines in remote sensing: A review. *ISPRS Journal of Photogrammetry and Remote Sensing*, *66*(3), 247–259. https://doi.org/10.1016/j.isprsjprs.2010.11.001

Mukherjee, A., Kumar, A. A., & Ramachandran, P. (2021). Development of New Index-Based Methodology for Extraction of Built-Up Area From Landsat7 Imagery: Comparison of Performance With SVM, ANN, and Existing Indices. *IEEE Transactions on Geoscience and Remote Sensing*, *59*(2), 1592–1603. https://doi.org/10.1109/TGRS.2020.2996777

Ndehedehe, C. E. (2014). Support Vector Machine Based Kernel Types in Extraction of Urban Areas in Uyo Metropolis from Remote Sensing Multispectral Image. *Researcher*, *66*(22), 105–112. http://www.sciencepub.net/researcher%5Cnhttp://www.sciencepub.net/researcher.

Osgouei, P. E., Kaya, S., & Sertel, E. (2019). *Separating Built-Up Areas from Bare Land in Mediterranean Cities Using Sentinel-2A Imagery*. 1–24. https://doi.org/10.3390/rs11030345

Pandey, D., & Tiwari, K. C. (2020). Extraction of urban built-up surfaces and its subclasses using existing built-up indices with separability analysis of spectrally mixed classes in AVIRIS-NG imagery. *Advances in Space Research*, *66*(8), 1829–1845. https://doi.org/10.1016/j.asr.2020.06.038

Parveen, S., Basheer, J., & Praveen, B. (2018). a Literature Review on Land Use Land

Cover Changes. *International Journal of Advanced Research*, *6*(7), 1–6. https://doi.org/10.21474/ijar01/7327

Pellerin, B. A. (2004). The influence of urbanization on runoff generation and stream chemistry in Massachusetts watersheds. *Department of Natural Resources*.

Pereira, J. M. C. (1999). A comparative evaluation of NOAA/AVHRR vegetation indexes for burned surface detection and mapping. *IEEE Transactions on Geoscience and Remote Sensing*, *37*(1), 217–226.

Piyoosh, A. K., & Ghosh, S. K. (2018). Development of a modified bare soil and urban index for Landsat 8 satellite data. *Geocarto International*, *33*(4), 423–442. https://doi.org/10.1080/10106049.2016.1273401

Puyravaud, J.-P. (2003). Standardizing the calculation of the annual rate of deforestation. *Forest Ecology and Management*, *177*(1–3), 593–596.

Radoux, J., Chomé, G., Jacques, D. C., Waldner, F., Bellemans, N., Matton, N., Lamarche, C., D'Andrimont, R., & Defourny, P. (2016). Sentinel-2's potential for sub-pixel landscape feature detection. *Remote Sensing*, *8*(6). https://doi.org/10.3390/rs8060488

Roberts, D. A., Gardner, M., Church, R., Ustin, S., Scheer, G., & Green, R. O. (1998). Mapping chaparral in the Santa Monica Mountains using multiple endmember spectral mixture models. *Remote Sensing of Environment*, *65*(3), 267–279. https://doi.org/10.1016/S0034-4257(98)00037-6

Rwanga, S. S., & Ndambuki, J. M. (2017). Accuracy Assessment of Land Use/Land Cover Classification Using Remote Sensing and GIS. *International Journal of Geosciences*, *08*(04), 611–622. https://doi.org/10.4236/ijg.2017.84033

Salehi, B., Zhang, Y., Zhong, M., & Dey, V. (2012). Object-based classification of urban areas using VHR imagery and height points ancillary data. *Remote Sensing*, *4*(8), 2256–2276. https://doi.org/10.3390/rs4082256

Schueler, C. F. (1987). *Remote Sensing Technology and Applications. 2*(10), 79–84. https://doi.org/10.1117/1.1509457

Semenzato, A., Pappalardo, S. E., Codato, D., Trivelloni, U., de Zorzi, S., Ferrari, S., de Marchi, M., & Massironi, M. (2020). Mapping and monitoring urban environment through sentinel-1 SAR data: A case study in the Veneto region (Italy). *ISPRS International Journal of Geo-Information*, *9*(6). https://doi.org/10.3390/ijgi9060375

Shahtahmassebi, A. R., Song, J., Zheng, Q., Blackburn, G. A., Wang, K., Huang, L. Y., Pan, Y., Moore, N., Shahtahmassebi, G., Sadrabadi Haghighi, R., & Deng, J. S. (2016). Remote sensing of impervious surface growth: A framework for quantifying urban expansion and re-densification mechanisms. *International Journal of Applied Earth Observation and Geoinformation*, *46*, 94–112. https://doi.org/10.1016/j.jag.2015.11.007

Singh, A. (1989). Review Article Digital change detection techniques using remotely-sensed data. *International Journal of Remote Sensing*, *10*(6), 989–1003. https://doi.org/10.1080/01431168908903939

Singh, H. (2019). *Practical Machine Learning and Image Processing For Facial Recognition, Object Detection, and Pattern Recognition Using Python-Himanshu Singh*. www.apress.com/978-1-4842-4148-6

Sinha, P., & Verma, N. K. (2016). *Urban Built-up Area Extraction and Change Detection of Adama Municipal Area using Time-Series Landsat Images*. *5*(8), 1886–1895.

Sinha, S., Santra, A., & Mitra, S. S. (2020a). Semi-automated impervious feature extraction using built-up indices developed from space-borne optical and SAR remotely sensed sensors. *Advances in Space Research*, *66*(6), 1372–1385. https://doi.org/10.1016/j.asr.2020.05.040

Smits, P. C., Dellepiane, S. G., & Schowengerdt, R. A. (1999). Quality assessment of image classification algorithms for land-cover mapping: a review and a proposal for a cost-based approach. *International Journal of Remote Sensing*, *20*(8), 1461–1486.

Stathakis, D., Perakis, K., & Savin, I. (2012). Efficient segmentation of urban areas by the VIBI. *International Journal of Remote Sensing*, *33*(20), 6361–6377. https://doi.org/10.1080/01431161.2012.687842

Sukawattanavijit, C., Chen, J., & Zhang, H. (2017). GA-SVM Algorithm for Improving Land-Cover Classification Using SAR and Optical Remote Sensing Data. *IEEE Geoscience and Remote Sensing Letters*, *14*(3), 284–288. https://doi.org/10.1109/LGRS.2016.2628406

Sun, G., Chen, X., Jia, X., Yao, Y., & Wang, Z. (2016). Combinational Build-Up Index (CBI) for Effective Impervious Surface Mapping in Urban Areas. *IEEE Journal of Selected Topics in Applied Earth Observations and Remote Sensing*, *9*(5), 2081–2092. https://doi.org/10.1109/JSTARS.2015.2478914

Thapa, R. B., & Murayama, Y. (2011). Urban growth modeling of Kathmandu metropolitan region, Nepal. *Computers, Environment and Urban Systems*, *35*(1), 25–34. https://doi.org/10.1016/j.compenvurbsys.2010.07.005

United Nations. (2018). World Urbanization Prospects 2018. In *Department of Economic and Social Affairs. World Population Prospects 2018*. https://population.un.org/wup/

United Nations, & Nations, U. (2014). *World Urbanization Prospects: The 2014 Revision,* *CD-ROM Edition*. 1–20.

Valdiviezo-N, J. C., Téllez-Quiñones, A., Salazar-Garibay, A., & López-Caloca, A. A. (2018). Built-up index methods and their applications for urban extraction from Sentinel 2A satellite data: discussion. *Journal of the Optical Society of America A*, *35*(1), 35. https://doi.org/10.1364/josaa.35.000035

Vigneshwaran, S., & Kumar, S. V. (2018). *EXTRACTION OF BUILT-UP AREA USING HIGH RESOLUTION SENTINEL-2A AND GOOGLE SATELLITE IMAGERY*. *XLII*(September), 3–5.

Walker, B. K., Ph, D., & Foster, G. (2009). *Accuracy Assessment and Monitoring for NOAA Florida Keys mapping*. *1*, 1–32.

Waqar, M. M., Mirza, J. F., Mumtaz, R., & Hussain, E. (2012). Development of New Indices for Extraction of Built-Up Area & Bare Soil. *Open Access Scientific Reports*, *1*(1), 1–4. https://doi.org/10.4172/scientificreports.13

Weng, F., & Pu, R. (2013). Mapping and assessing of urban impervious areas using multiple endmember spectral mixture analysis: A case study in the city of Tampa, Florida. *Geocarto International*, *28*(7), 594–615. https://doi.org/10.1080/10106049.2013.764355

Weng, Qihao. (2012a). Remote sensing of impervious surfaces in the urban areas: Requirements, methods, and trends. *Remote Sensing of Environment*, *117*, 34–49. https://doi.org/10.1016/j.rse.2011.02.030

Weng, QIHAO. (2001). Modeling urban growth effects on surface runoff with the integration of remote sensing and GIS. *Environmental Management*, *28*(6), 737–748. https://doi.org/10.1007/s002670010258

Wu, C. (2004). Normalized spectral mixture analysis for monitoring urban composition using ETM+ imagery. *Remote Sensing of Environment*, *93*(4), 480–492. https://doi.org/10.1016/j.rse.2004.08.003

Wu, C., & Murray, A. T. (2003). Estimating impervious surface distribution by spectral mixture analysis. *Remote Sensing of Environment*, *84*(4), 493–505.

Xi, Y., Thinh, N. X., & Li, C. (2019). Preliminary comparative assessment of various spectral indices for built-up land derived from Landsat-8 OLI and Sentinel-2A MSI imageries. *European Journal of Remote Sensing*, *52*(01), 240–252. https://doi.org/10.1080/22797254.2019.1584737

XI, Y., Thinh, N. X., & LI, C. (2019). Preliminary comparative assessment of various spectral indices for built-up land derived from Landsat-8 OLI and Sentinel-2A MSI imageries. *European Journal of Remote Sensing*, *52*(1), 240–252.

https://doi.org/10.1080/22797254.2019.1584737

Xu, H. (2008). A new index for delineating built-up land features in satellite imagery. *International Journal of Remote Sensing*, *29*(14), 4269–4276. https://doi.org/10.1080/01431160802039957

Xu, Hanqiu. (2007). Extraction of urban built-up land features from landsat imagery using a thematic-oriented index combination technique. *Photogrammetric Engineering and Remote Sensing*, *73*(12), 1381–1391. https://doi.org/10.14358/PERS.73.12.1381

Xu, Hanqiu. (2010). Analysis of impervious surface and its impact on Urban heat environment using the normalized difference impervious surface index (NDISI). *Photogrammetric Engineering and Remote Sensing*, *76*(5), 557–565. https://doi.org/10.14358/PERS.76.5.557

Xu, Hanqiu, Huang, S., & Zhang, T. (2013). Built-up land mapping capabilities of the ASTER and Landsat ETM+ sensors in coastal areas of southeastern China. *Advances in Space Research*, *52*(8), 1437–1449. https://doi.org/10.1016/j.asr.2013.07.026

Yang, L., Huang, C., Homer, C. G., Wylie, B. K., & Coan, M. J. (2003). An approach for mapping large-area impervious surfaces: Synergistic use of Landsat-7 ETM+ and high spatial resolution imagery. *Canadian Journal of Remote Sensing*, *29*(2), 230–240. https://doi.org/10.5589/m02-098

Yu, X., & Lu, C. (2014). Urban percent impervious surface and its relationship with land surface temperature in Yantai City, China. *IOP Conference Series: Earth and Environmental Science*, *17*(1). https://doi.org/10.1088/1755-1315/17/1/012163

Zha, Y., J. Gao, and S. Ni. 2003. "Use of normalized difference built-up index in automatically mapping urban areas from TM imagery." *International Journal of Remote Sensing* 24, no. 3: 583-594.

Zhang, H. K., Roy, D. P., Yan, L., Li, Z., Huang, H., Vermote, E., Skakun, S., & Roger, J. C. (2018). Characterization of Sentinel-2A and Landsat-8 top of atmosphere, surface, and nadir BRDF adjusted reflectance and NDVI differences. *Remote Sensing of Environment*, *215*(October 2017), 482–494. https://doi.org/10.1016/j.rse.2018.04.031

Zhang, H., Li, Y., & Gao, X. (2009). Potential impacts of land-use on climate variability and extremes. *Advances in Atmospheric Sciences*, *26*(5), 840–854.

Zhang, X., Xiao, P., & Feng, X. (2013). Impervious surface extraction from high-resolution satellite image using pixel- and object-based hybrid analysis. *International Journal of Remote Sensing*, *34*(12), 4449–4465. https://doi.org/10.1080/01431161.2013.779044